The Fatigue Performance of Angle Cross-Frame Members in Bridges

by

Geoffrey Scott McDonald

and

Karl H. Frank

The University of Texas at Austin
Ferguson Structural Engineering Laboratory

Conducted for the
American Institute for Iron and Steel

Report FSEL No: 09-1
December 2009

Acknowledgements

We greatly appreciate the financial support from the American Institute for Iron and Steel that made this research project possible. The support of the project director, Alex Wilson is also very much appreciated. The specimens for the project were donated by Hirschfeld Industries.

Table of Contents

List of Tables

List of Figures

CHAPTER 1

Introduction

This study investigated the fatigue performance of welded angle cross-frame connections and the factors affecting the fatigue life of these members. The type of cross-frame used in this analysis is one of three typical cross-frame connection details. Other connection details include using WT or Channel sections as cross-frame braces, however, angle cross-frames are the most common connection detail and will be the only cross section considered in this research.

1.1 BACKGROUND INFORMATION

Cross-frames are elements in bridges that enhance both the lateral and torsional stiffness of bridge girders. Providing the cross frames is the primary method of improving the lateral torsional buckling capacity of steel girder systems during construction. Cross frames are primarily comprised of angles that are typically welded to connection plates to form a truss between two adjacent girders. The connection plates are then welded or bolted to the girder. Typical K-frame and X-frame design details taken from the AASHTO/NSBA Steel Bridge Collaboration of Guidelines for Design Details can be seen in Figure 1 and Figure 2. The connection detail, taken from the same document can be seen in Figure 3. It is important to note that only one of the angle legs is welded to the connection plate which will cause a shear lag effect and reduce the effective area of the angle at the weld.

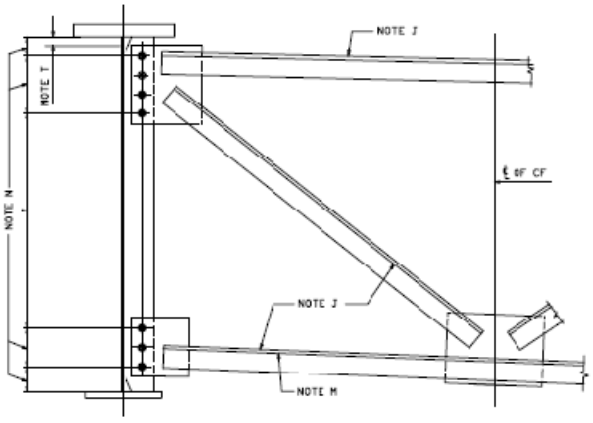

Figure 1. Standard K-Frame Design Detail (AASHTO/NSBA, 2006)

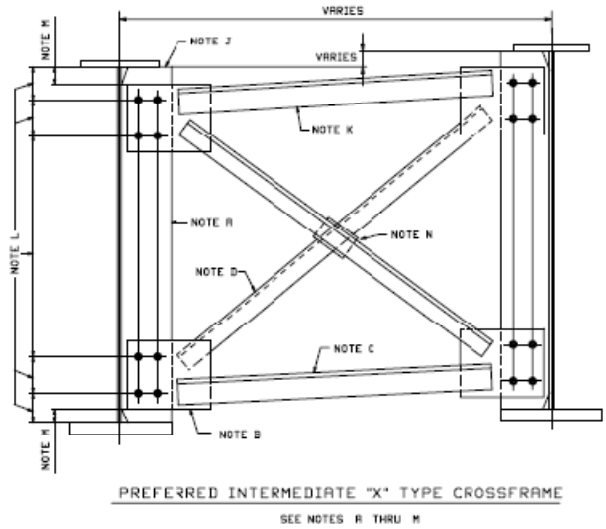

Figure 2. Standard X-Frame Detail (AASHTO/NSBA, 2006)

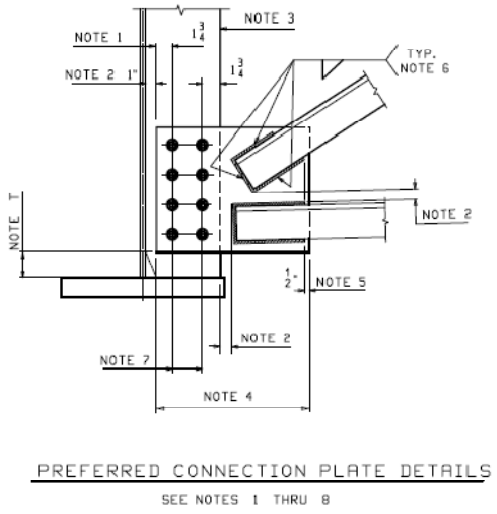

Figure 3. Standard Cross-Frame Connection Detail (AASHTO/NSBA, 2006)

AASHTO includes strength requirements for cross-frames to withstand the lateral loads caused by wind forces. These are the primary forces for which cross-frames are designed. According to Section 10.20.2.2 of the AASHTO Bridge Design Specification (AASHTO, 2007) the maximum horizontal force (FD) in the transverse diaphragms and cross frames is obtained from the following:

$$FD = 1.14 * W * S_d$$

Cross-frame members are also needed for lateral stiffness during the construction process before the concrete deck is poured. Section 10.2.3 of the NCHRP Recommended Specifications for Steel Curved-Girder Bridges (NCHRP, 1998) recommends this for box girders during construction:

> External bracing at other than support points is usually not necessary. If analysis shows that the boxes will rotate excessively when the deck is placed, temporary external bracing may be desirable.

Currently other forces are not required to be considered in the design of cross-frames. The NCHRP Project 12-26, Guide Specifications for Distribution of Loads for Highway Bridges, did not consider cross-frames in live load distribution(NCHRP, 1998). Research conducted and reported in Field Measurements of Intermediate External Diaphragms on a Trapezoidal Steel Box Girder Bridge determined live load ranges for two (Cheplak, 2001). These loads may not be designed for, but that does not mean that they are not experienced by the members. These stresses caused by these loads may not be enough to yield members, but could potentially damage the members by fatigue cracking.

Cross-frame members may be designed using the AASHTO specification, but many DOT's have prescribed methods for cross-frame design and construction (Helwig 2006). In order to remain conservative, the DOT's prescribed methods often yield much stiffer elements which in turn attract larger live loads. TxDOT currently has three recommended standard angle sizes for cross-frame design in section 2.6.1 of its Steel Bridge Design Recommendation (TxDOT, 2007):

> Equal leg angles are often more cost-effective than unequal leg angles. Fabricators discourage back-to-back angles used as cross-frame members. Some common angle sizes for diaphragms are L3.5 x 3.5 x 3/8, L4 x 4 x 3/8, and L5 x 5 x 1/2.

If the stress concentrations are very high then many of the loads that are not considered in the design of cross-frame members may become very significant and a better understanding of the interaction between girders and their cross-frame members will be required.

1.2 MOTIVATION FOR RESEARCH

Cross-frames are considered load carrying members in curved girder bridges and must be designed for fatigue. Currently AASHTO has no comparable category of fatigue for these types of members and without experimentation and analysis a realistic fatigue design cannot be achieved. A category E detail has been recommended by the LRFD Design Manual for Highway Bridge Superstructures (Grubb, Corven, Wilson, Bouscher, & Volle, 2007) based upon the fatigue category for shear on the throat of a fillet weld. However, this approach does not take into account the geometric effects of the angle. In order to determine a more realistic fatigue life for welded angles, a better understanding of the angle geometry and its effect upon the stress concentration must be acquired.

Previous fatigue research has been performed on similar details, but no fatigue testing of the connection of interest has been performed that could be found by the author. Fatigue testing of welded channel connections and welded angle connections were performed by Wilbur M. Wilson at University of Illinois (Wilbur M. Wilson, Walter H. Bruckner, John E. Duberg, Howard C. Beede, 1944). These connections are similar enough to be compared with the connection detail in question, but cannot be substituted due to important differences. The detail of the Wilson angle connection and channel connection are shown in Figure 4 and Figure 5 respectively.

The Wilson angle connection was built up using 7 5/8 in. long ½ by 7 in. wide plates with a 0.5 in. thickness and a 16 in. long 2 ½ x 2 x ¼ in. angle. The angle was cut so that the attached leg tapered from its full length to the thickness of the angle along the weld. All welds were ¼ in. fillet welds and the length of the weld that runs longitudinally was 4 in. This weld detail is very different from the weld detail used in most cross-frame angle connections.

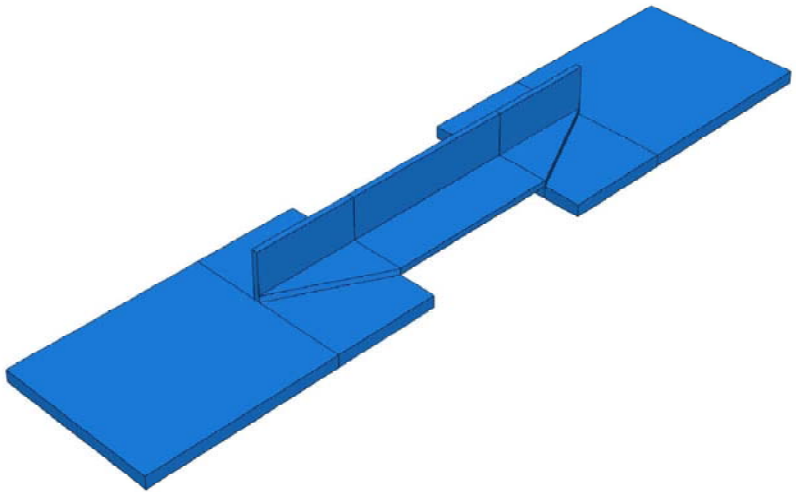

Figure 4. Wilson Angle Connection

The Wilson channel connection was built up using 7 ¼ in. long ½ by 7 in. plates and a 16 in. long 3 x 4.1 in. channel. The sides and ends of the channel were welded with 3/16 in. fillet welds and the length of the longitudinal weld was 4 in. long. This weld detail is much more similar to the detail used for cross-frame connections, but the channel eliminates the in-plane eccentricity.

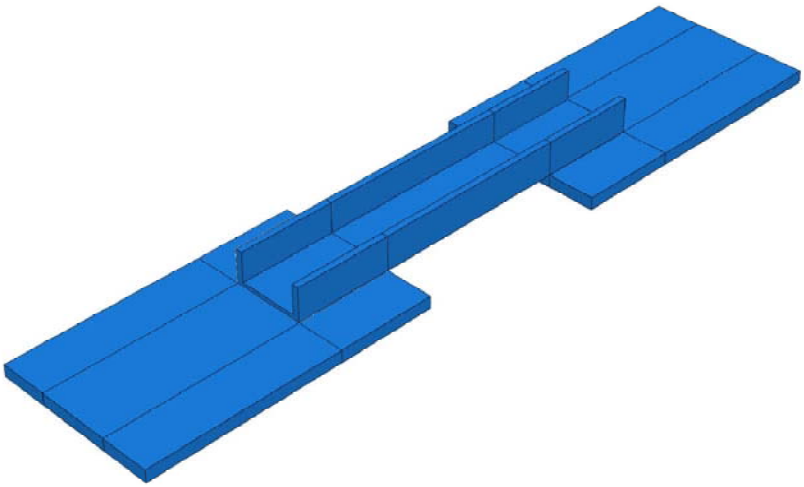

Figure 5. Wilson Channel Connection

Fatigue design has primarily focused on the fatigue of the typical girder details but has failed to address the fatigue life of other members. Fatigue cracking will occur wherever relatively high stress ranges in cyclical loading occur which can occur in noncritical members, and cracking in the welded angles of a cross-frame may spread into the connection plate and then into the bridge girder causing an unexpected brittle failure. It is therefore imperative to understand the fatigue life of cross-frame members in order to design them against this type of failure.

1.3 SCOPE AND OBJECTIVES

The American Iron and Steel Institute (AISI) funded this project in order to determine the fatigue life of angle cross-frame members. This project is a part of many projects currently being conducted to understand angle cross-frame members and their behavior. The goal of this research was to achieve a better understanding of the fatigue life for cross-frame members and to be able to determine the stress concentration factor from the geometric properties of the specimen. Fatigue tests were performed on thirty different cross-frame specimens along with six static tests of similar details. Finite element analyses were conducted for each of the details tested as well as many more details in a parametrical study to determine the effects of each geometric property upon the stress concentration factor. Although no theoretical equation for the stress concentration was found, certain guidelines were developed to estimate the local stresses at the weld toe in the angle which can be used to provide an estimate of fatigue performance that considers the geometry of the angle and the connection.

CHAPTER 2

Test Specimens and Testing Procedure

2.1 DESCRIPTION OF SPECIMENS

The general specimen detail is that of an angle welded to two plates which represent the connections between the angle and the gusset plate or, in the case of an X type cross-frame shown in Figure 6, the transverse angle.

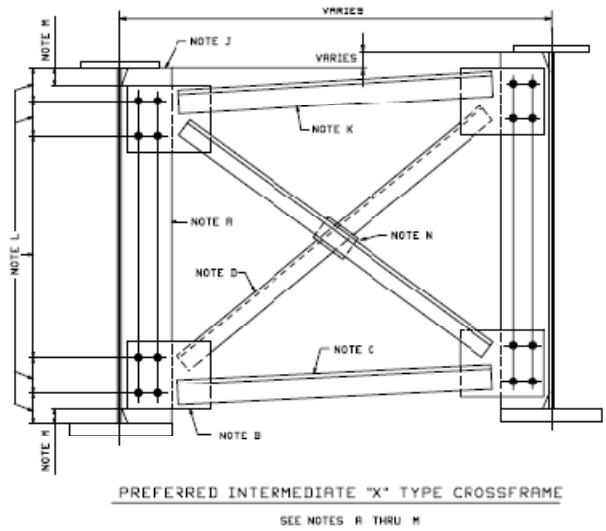

Figure 6. Welded Angle Detail with Weld Locations (AASHTO/NSBA, 2006)

The detail of a basic specimen was shown in Figure 7. It is comprised of a single angle welded to two end plates which were gripped by the test machine tested in uniaxial tension. The welds used to connect the angle to the end plates were 5/16 in. fillet welds. The lengths of the angles in the test specimen were shorter than a typical cross-frame detail used in practice in order fit the specimens in the test machine. Also, the end plates were thicker than typical plates used in practice to ensure that the cracking occurred in the angle as opposed to the plates.

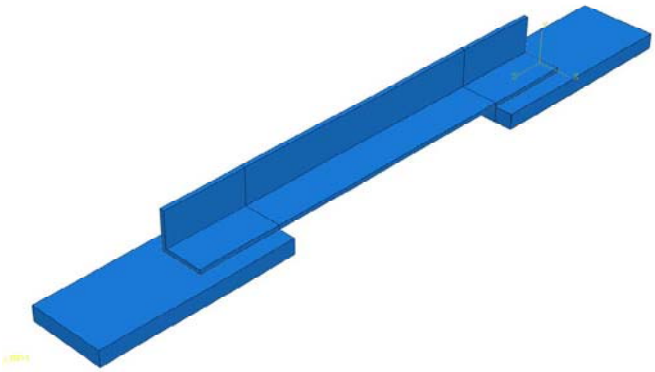

Figure 7. General Specimen Detail

A total of 36 angle specimens were provided by Hirschfeld Steel for testing in this project. Six different specimen details were used for the fatigue testing, consisting of two different angle geometries. The two angle geometries used were an equal leg 4 x 4 x 3/8inch angle and an unequal leg 5 x 3 x 3/8 inch angle. Twelve of the twenty four unequal length angles were attached to the end plate by the long leg and the other twelve were attached by the short leg. The other twelve angle specimens had equal length angles. Six specimens of each of the preceding categories used equal length welds while the other six used balanced welds to connect the plates to the angle. The welds were designed based upon the ultimate strength of the angle so that the strength of the weld was equal to the strength of the angle.

The balanced welds were designed by aligning the centroid of the weld group with the centroid of the angle. The method used to balance the weld is presented in the LRFD Design Manual for Highway Bridge Superstructures (Grubb, Corven, Wilson, Bouscher, & Volle, 2007). This procedure can also be found in most steel design textbooks. This was done by taking moments about a point and setting the resultant moment to zero. First, the strength of the transverse end weld was calculated by multiplying the factored resistance R_r by the effective throat dimension T_E and the end weld length L_{w2}= the width of the leg attached to the end plate:

$$R_r = \varphi\, 0.8\, F_y$$

$$T_E = \frac{5}{16} * \sqrt{2}$$

$$F_{2s} = R_r * t_e * L_{w2}$$

The force required in the weld connecting the lower leg in Figure 1, F_{1s} , can be found by summing moments about the upper edge of the angle weld:

$$F_1 = \frac{T_u * y}{d} - \frac{F_2}{2}$$

The force required by the bottom weld F_{3s} is equal to the summation of the forces in the longitudinal direction:

$$F_{3s} = T_u - F_{1s} - F_{2s}$$

The welds are referred to as the back or front weld in this report. The front weld is the weld on the bottom in Figure 8 and the back weld is the weld at the top of the figure along the edge where the two legs of the angle intersect.

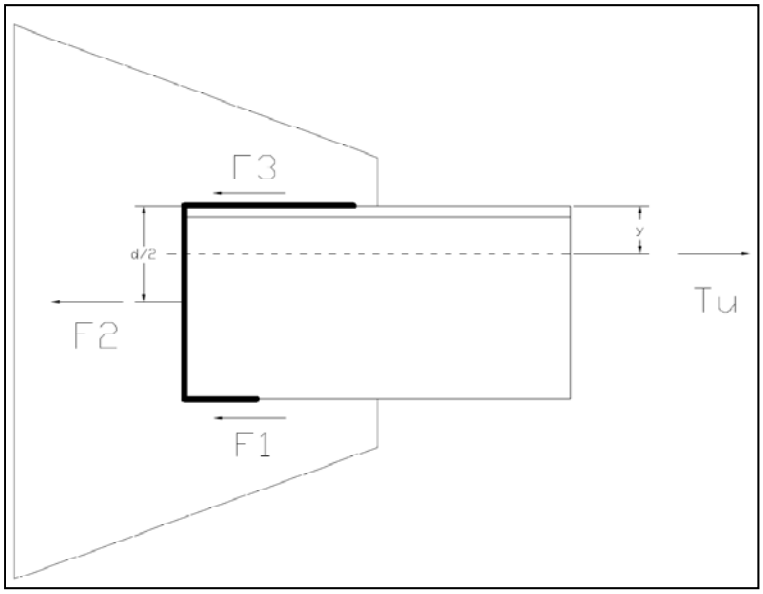

Figure 8. Weld Balancing Example

A summary of the specimens included in the testing program is given in Table 1. The first column of the table is the label assigned to the specimen. Table 2 contains detailed dimensions of the end plates, specimen lengths, and the weld lengths of each type of specimen. Due to the differences in weld length between the equal length weld detail and the balanced weld detail, different angle lengths and plate lengths were used for each type of specimen. The specimen geometries are shown in Figure 9 through Figure 14.

Name	Angle	Outstanding Leg	Balanced Weld
44E	4" x 4" x 3/8"	4"	No
44B	4" x 4" x 3/8"	4"	Yes
53SE	5" x 3" x 3/8"	3"	No
53SB	5" x 3" x 3/8"	3"	Yes
53LE	5" x 3" x 3/8"	5"	No
53LB	5" x 3" x 3/8"	5"	Yes

Table 1. Angle Specimen Overview

	Outstanding Leg	Inside Leg	Angle Thickness	Angle Length	Plate Length	Plate Thickness	Plate Width	Back Weld	Front Weld
44E	4	4	3/8	39 1/2	24	1 1/2	7 1/8	7 1/4	7 1/4
44B	4	4	3/8	47	24	1 1/2	7 1/8	11 1/2	4 3/4
53LE	5	3	3/8	40 1/2	24	1 1/2	7 1/8	7 1/4	7 1/4
53LB	5	3	3/8	50	24	1 1/2	7 1/8	9 1/2	5 3/4
53SE	3	5	3/8	38 1/4	24	1 1/2	7 1/8	7 1/4	7 1/4
53SB	3	5	3/8	44	18	1 1/2	7 1/8	12 1/2	3 3/4

Table 2. Specimen Details

Figure 9. 44E Detail

Figure 10. 44B Detail

Figure 11. 53LE Detail

Figure 12. 53LB Detail

Figure 13. 53SE Detail

Figure 14. 53SB Detail

2.2 TESTING PROCEDURE

2.2.1 Test Configurations

2.2.1.1 Single-Angle Test Configuration

The first test configuration was a single specimen with the connection plates gripped at each end. This configuration is shown in Figure 15. Specimen 44E1 was tested using this method. All the static tension tests were also performed using a single specimen in the test machine. However, the problem with configuration 1 is that the eccentricity of the angle resulted in a moment on the grips of the machine that could lead to damage of the test machine. As a result a second test configuration that is outlined in the next section was utilized for much of the testing.

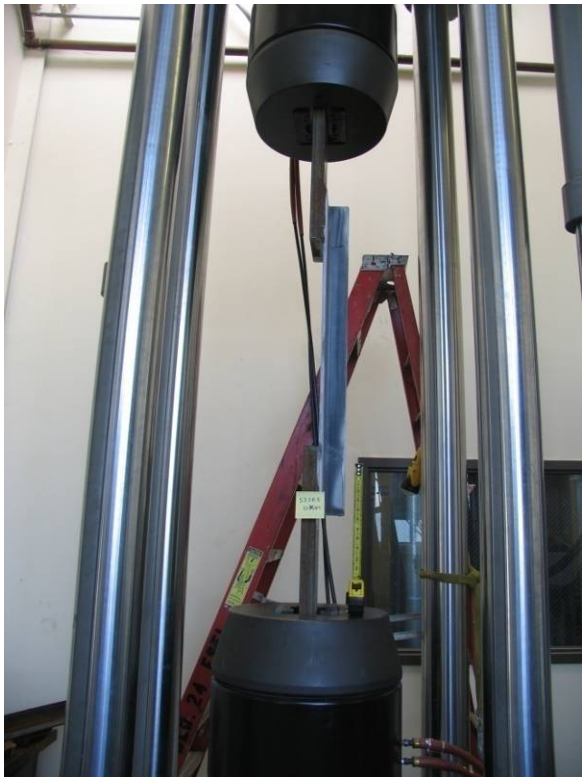

Figure 15. 1st Test Configuration

2.2.1.2 Double-Angle Test Configuration without Spacers

The second test configuration had two identical test specimens placed back to back in order to minimize the out-of-plane bending of the connection plates that may lead to damage of the testing machine. Figure 16 depicts the layout and the resultant center of gravity of this configuration.

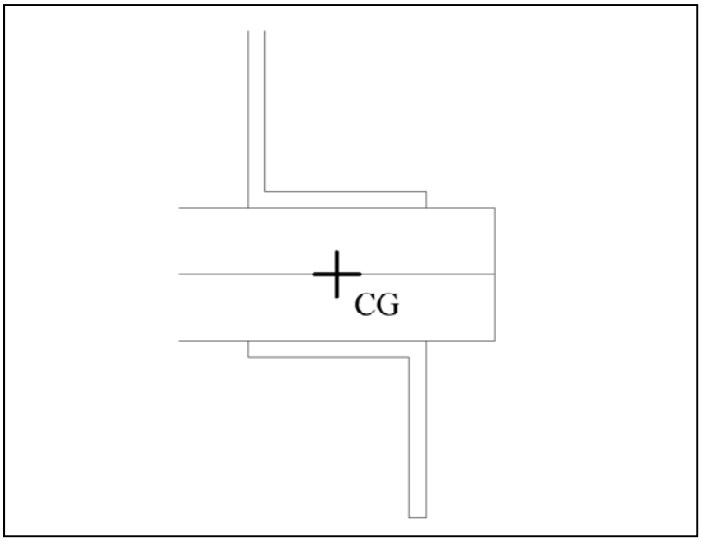

Figure 16. Double-Specimen Configuration Top View

However, this configuration resulted in variable contact pressure between the two plates which changed the force distribution in the angles. The eccentricity of the angles caused the end plates to bend in towards each other. Initially, a small gap existed at the end of the plates due to distortion caused by welding. The gap is shown in Figure 20. As the specimen was loaded, the gap was closed which caused a change in the stress distribution of the specimens. The effect of this was determined by attaching strain gauges to various specimens on the outstanding leg as shown in Figure 18. Load was then applied to in both the single-specimen configuration and double-specimen configuration without spacers. In the first test configuration, the specimens exhibited a linear relationship between the applied load and the strain in the angle, but in the second test configuration as the applied load increased the strain did not increase linearly when the plates came in contact. Figure 18 shows the recordings of the same strain gauge during the two different tests. As the specimen was loaded in the single-specimen configuration the strain became negative, indicating compression, while the same specimen tested with a companion specimen to produce the double-specimen configuration, the strain was positive, indicating tension. These strains were taken from the outside face of the outstanding leg of the angle at the location shown in Figure 19. Specimens 44E3, 44E4, 44E5, and 44E6 were tested in the double-specimen configuration without spacers.

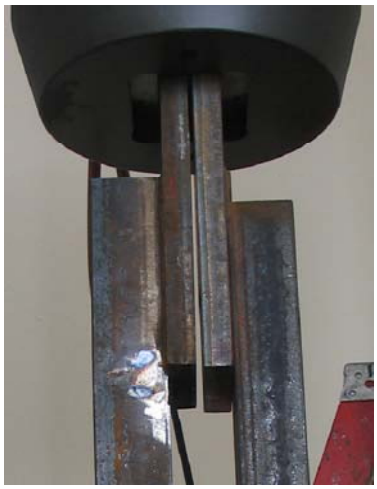

Figure 17. 3rd Test Configuration Close-Up

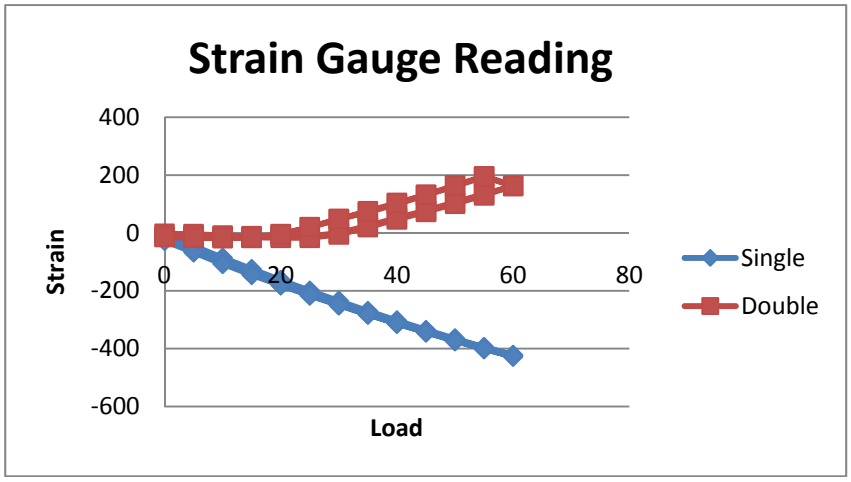

Figure 18. Strain Gauge Reading

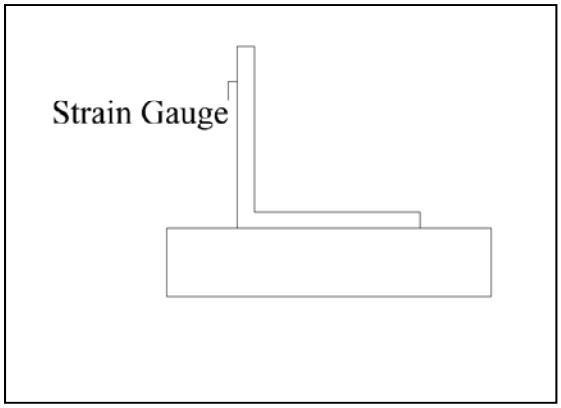

Figure 19. Strain Gauge Location

2.2.1.3 Double-Angle Test Configuration with Spacers

The third test configuration was very similar to the second configuration except that a spacer was placed in between the two plates in order to prevent the contact between the end plates beyond the grip. Various values of the spacer plate thickness were used in order to ensure that the plates did not touch. The gap can be seen between the two end plates at the top of the specimen in Figure 19. Specimens 44B1, 44B2, 44B3, 44B4, 53LE1, 53LE2, 53LE3, 53LE4, 53SE1, 53SE2, 53SE3, and 53SE6 were tested using this method.

Figure 20. 3rd Test Configuration

2.2.1.4 Double-Angle Test Configuration with Bolted Connection

Some of the end plates of the specimens were not long enough to fit into the grips so another design was needed to test them. The fourth test configuration utilized thicker plate spacers that were bolted to both specimens and gripped in the machine themselves. This configuration is shown in Figure 21. . Specimens 53LB1, 53LB2, 53LB3, 53LB4, 53SB1, 53SB4, 53SB5, and 53SB6 were tested using this method.

Figure 21. 4th Test Configuration

A summary of the test configurations and stress range (S_r) and minimum stress used for each fatigue test is listed in Table 3.

Angle	Sr	Min Stress
44e1	12	4
44e3	12	4
44e4	8	4
44e5	12	4
44e6	8	4
44b1	12	4
44b2	12	4
44b3	8	4
44b4	8	4
53Le1	12	4
53Le2	12	4
53Le3	8	4
53Le4	8	4
53Lb1	8	4
53Lb2	8	4
53Lb3	12	4
53Lb4	12	4
53Se1	8	4
53Se2	11	4
53Se3	11	4
53Se6	8	4
53Sb1	8	4
53Sb4	12	4
53Sb5	12	4
53Sb6	8	4

Table 3. Test Summary

2.2.2 Fatigue Tests

The fatigue testing was conducted by cyclically loading the specimens using a constant amplitude stress variation between two tensile stresses until a crack the specimen reached a certain level and the number of cycles was then recorded as the fatigue life of the specimen. Instead of completely fracturing the specimen, the test was stopped when a crack at least 1 inch long was observed. Figure 22 show a cracked specimen after testing. Cracking generally occurred at the ends of the front fillet welds at both end of the test specimen. Figure 23 shows a close up of the crack. The crack length of this specimen reached approximately 2 inches before the test was stopped.

Figure 22. Cracked Specimen

Figure 23. Close-Up of Cracked Specimen

A minimum nominal stress of 4 ksi was used for all tests. Two different nominal stress ranges of 8 ksi and 12 ksi were used for each specimen design in order to compare the performance of the connection and angle geometries at the same stress levels. All nominal stress ranges were calculated by dividing the change in load by the nominal gross area of the angle. Tests were run using load control at a frequency range between 2 and 3 Hz. The limitation of the testing frequency was determined by the stability of the testing machine. An MTS closed loop machine with a 550 kip capacity was utilized in the tests. The machine has been shown previously in Figures 15, 19, and 21.. Displacement limits and error limits were specified using the machines monitoring software to stop testing if the specimen had a visible crack or if the machine became unstable. Records of testing were recorded frequently to ensure that the test

was running smoothly and to have a separate hard copy of the results. When one of the specimens cracked it was either replaced with an identical specimen or repaired and the testing continued until the second specimen failed.

2.2.3 Static Tests

The static testing for the specimens were also conducted using the same 550 kip testing machine. Load control was used to slowly strain the specimen until the specimen started to yield and then displacement control was used to bring the specimen to failure. The dynamic yield, the static yield and the ultimate strength of each specimen were recorded.

Tensile tests of coupons taken from the angles were conducted in a similar manner as the static testing except that a smaller closed loop MTS machine with a maximum load capacity of 22 kips was used. The coupon dimensions and tolerances were determined according to the requirements for longitudinal flat tension tests prescribed in ASTM A370. The dimensions of the coupons tested are shown in Figure 24.

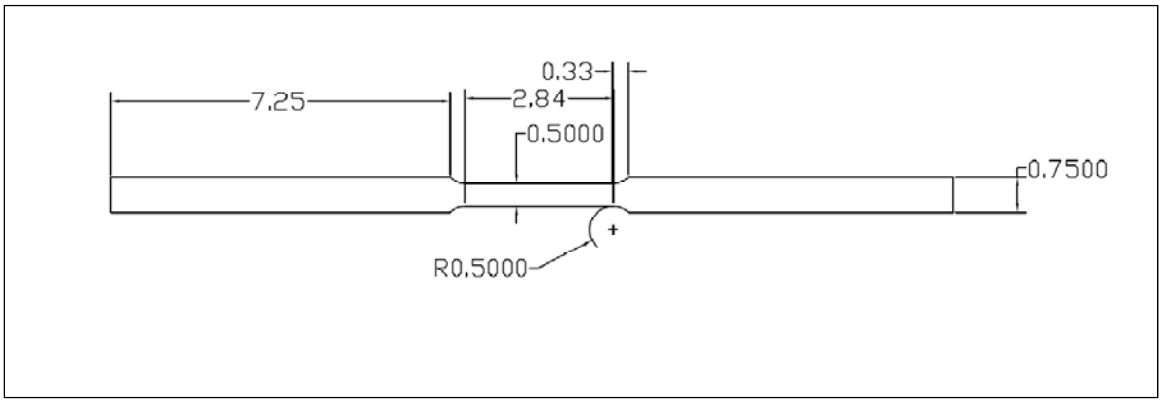

Figure 24. Coupon Dimensions

Each coupon was either taken from the midsection of the inside leg or the outstanding leg. A figure of the coupon locations is depicted in Figure 25. The dynamic yield, the static yield and the ultimate strength of the tensile specimens were recorded from these tests.

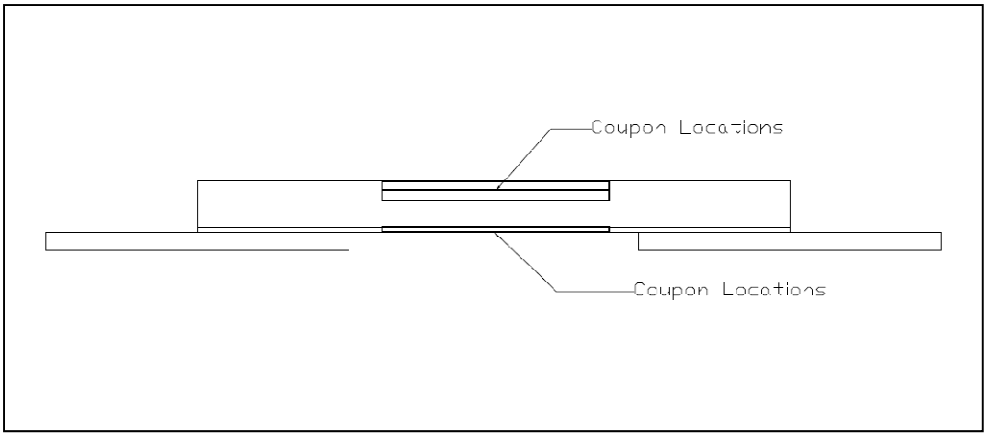

Figure 25. Coupon Locations

2.2.4 Full Size Specimen Tests

Static tests on full sized specimens and tensile tests of coupons were performed to determine the ultimate strength of each detail. The shear lag of each specimen was calculated by dividing the maximum load in the tests by the nominal strength of the specimen, which was calculated by multiplying the gross area of the angles by the tensile strength as determined from the tensile coupon tests. The static tests were performed on a single angle specimen using test configuration 1 and loading the specimen monotonically until failure. As the specimen started to yield the loading method was changed from load control to displacement control in order to ensure that the plasticity of each specimen could be observed. Figure 26 through Figure 28 show the load deformation curves for the tests. Table 4 gives the value of the maximum load and displacement of each test. The 53SE specimen had the highest strength but least elongation while the 44B specimen had the largest elongation. The difference in specimen length among the different geometry influences the elongation values.

Specimen	Max Load	Max Displacement
44E	204	2.54
44B	219	4.34
53LE	192	1.76
53LB	163*	1.34
53SE	211	1.72
53SB	181*	1.35

Table 4. Static Test Results

*End connection failed before reaching tensile capacity of angle

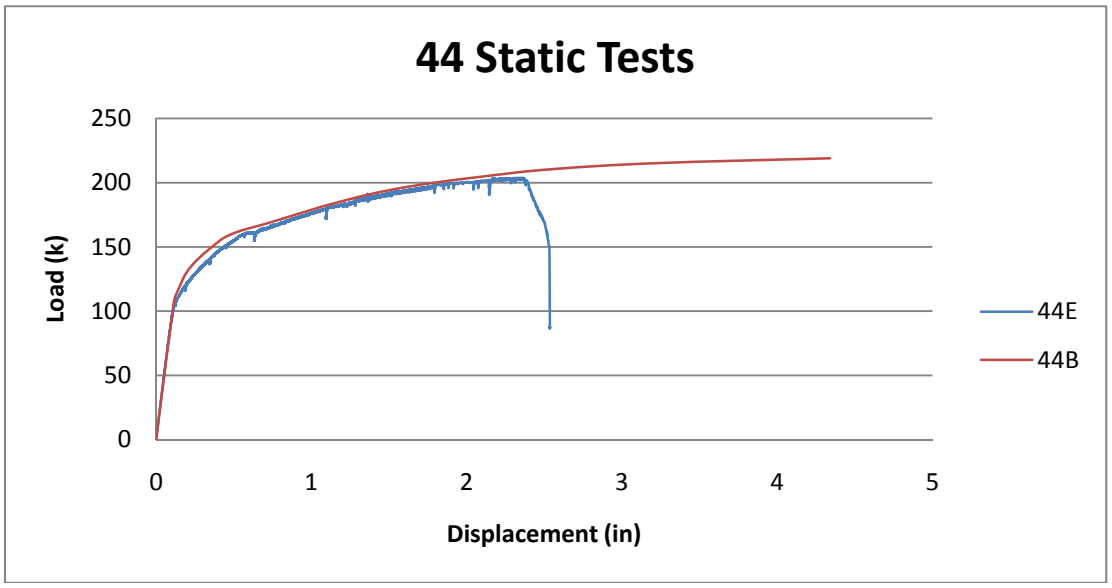

Figure 26. 44 Static Tests

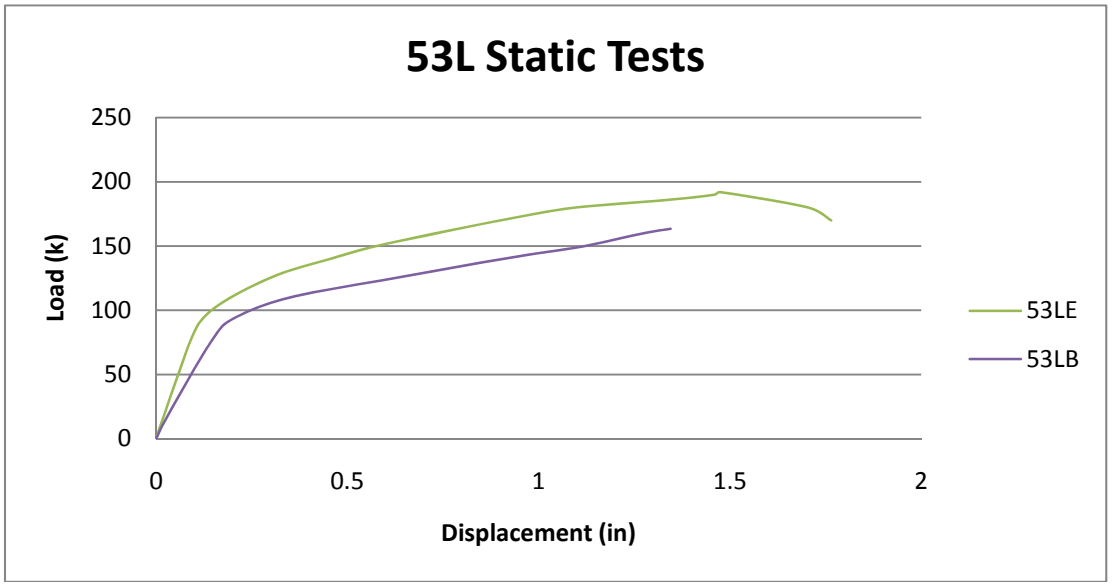

Figure 27. 53L Static Tests

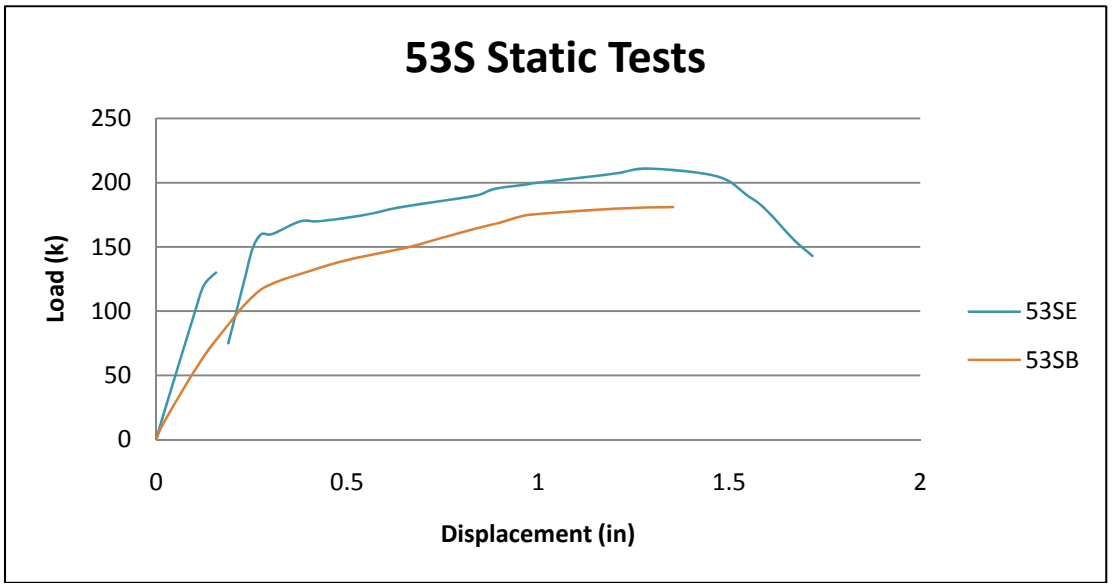

Figure 28. 53S Static Tests

It is important to note that specimens 53LB and 53SB were not long enough to be placed in the grips so extra plates were welded on to lengthen the specimen. Each plate had an identical plate welded all the way around a few inches offset from the original plate. However, these welds were not strong enough and failed before reaching the fracture strength of the angle in both specimens. Figure 29 through Figure 31 shows the specimen before testing and failed specimen.

Figure 29. Undeformed Specimen

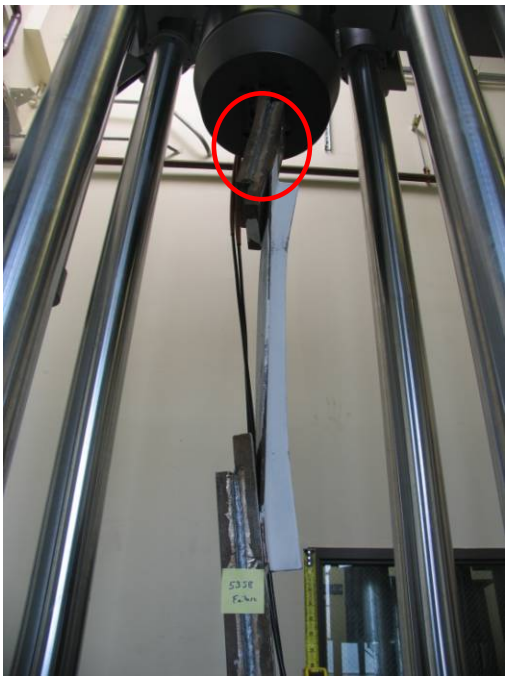

Figure 30. Failed Specimen (failure is circled)

Figure 31. Close-up of Failed Specimen

Specimens 44E, 44B, 53LE, 53SE all failed with a fracture of the weld and fracture of the angle. It is difficult to determine which of the two failures the ultimate cause of the failure was because both fractures occurred nearly simultaneously. Figure 32 and Figure 33 below show the typical failures of static test specimens.

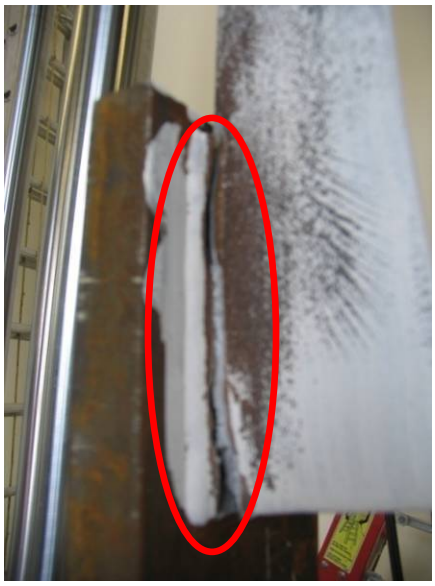

Figure 32. Typical Static Failure of Weld

Figure 33. Typical Static Failure of Angle

Tensile coupons were also tested to check the actual yield and ultimate strength of the steel as well as to check the shear lag equations used in the AISC steel design manual. The loading method used for specimens 1 through 8 was load control until the specimen started to yield and then displacement control until fracture, while the loading method for specimens 9 through 12 was solely load control until fracture. The loading rate for the second group of tests was approximately 0.1 kips/sec. The results for the tensile coupon tests are presented in Table 5. The second round of testing was performed because the tensile strength of the steel in the 44E angles and the tensile strength of the steel in the 44B angles appeared different. The coupons cut

for the second group of tensile tests were taken from the actual statically tested specimen in order to get more accurate results than the first group of tests. According to the results, the two of the 44B angles had higher tensile strengths than the 44E angles. The ultimate strength is higher for the second group of tests compared to the first group, but this is probably due to the higher loading rate. The 53 angles have higher tensile strengths which are to be expected in unequal length angles.

Angle	Weld	Ultimate Strength (kips)	Ultimate Stress (ksi)
4X4	Equal	14.5	72.4
4X4 *	Equal	16.1	87.7
4X4	Balanced	14.9	76.6
4X4 *	Balanced	17.4	97.7
5X3	Equal	15.6	80.8
5X3	Balanced	15.6	80.6

Table 5. Coupon Test Results

The results of the static tests and the tensile tests are listed in Table 6. The nominal stress was computed by dividing the maximum static load by the area of the angle. The tensile stress was computed by taking the average maximum tensile coupon load and dividing it by the area of the coupon and the shear lag was calculated by taking the dividing the nominal stress by the tensile stress. The effective area and ultimate strength of each specimen was then computed using the AISC Specification(AASHTO, 2007) and compared to the true ultimate strength. The longer weld length was used for the AISC calculations when determining the shear lag in specimens with balanced welds. If the AISC specification provisions is accurate, the ratio of the calculated ultimate strength to the actual ultimate strength should be equal to one. Angles 53SB and 53LB both have values above unity due to the low ultimate strengths caused by the weld failure of connecting the end plates to the extension plates and are not representative of a shear lag effect. The shear lag values for specimens 44E and 44B are very close to unity which does not make sense physically although the specimens from the second test resulted in a much lower shear lag value. However, these specimens proved to have a higher calculated ultimate strength than measured ultimate strength, but may be attributed to the high loading rate. The true shear lag is probably closer to the results of the second test because the tensile strength was calculated using the steel from the static test specimen.

For example, the maximum load for the static test of specimen 53LE was 192 kips. This was divided by the gross area of the angle to find a nominal stress of 67.1ksi. The tensile strength of the steel taken from the specimen in the coupon test was 80.6 ksi. The nominal stress divided by the tensile strength yields a value of 0.83 which represents the shear lag factor for this specimen. Using the method described in the AISC Manual, x is computed as the out of plane eccentricity of the angle and is 1.6 for this specimen. l is the length of the longer weld or 7.5 in. A_e is found by multiplying the factor 1-x/l by the gross area of the angle which is equal to 2.25 in2. The final ratio represents the calculated ultimate load of the tensile strength times the effective area over the ultimate load found during the static test. A value of 1 indicates that the

calculated shear lag is correct. A value less than 1 indicates that the effective area is smaller than it should be and a value greater than 1 indicates that the effective area is too large. When the effective area is too small this indicates that the estimated shear lag effect is too large and when the effective area is too large the estimated shear lag effect is too small.

Specimen	Max Load	Nominal Stress (ksi)	Tensile Strength (ksi)	Shear Lag	x	l	1-x/l	Ae	Fu*Ae/Pu
44E	204	71.23	72.35	0.98	1.13	7.25	0.84	2.41	0.86
44E Test 2	204	71.23	87.66	0.81	1.13	7.25	0.84	2.41	1.04
44B	219	76.57	76.59	1	1.13	11.25	0.9	2.57	0.9
44B Test 2	219	76.57	97.68	0.78	1.13	11.25	0.9	2.57	1.15
53LE	192	67.13	80.69	0.83	1.6	7.5	0.79	2.25	0.95
53LB *	163.4	57.13	80.69	0.71	1.6	12.5	0.87	2.49	1.23
53SE	211	73.78	80.69	0.91	0.854	7	0.88	2.51	0.96
53SB *	181	63.29	80.69	0.78	0.854	9.5	0.91	2.6	1.16

Table 6. Shear Lag Calculations

CHAPTER 3

Test Results

3.1 Test Results Overview

When the fatigue specimen had a significant sized crack (greater than approximately 1 inch), the test was considered complete. The number of cycles and nominal stress range calculated by dividing the load range by the measured gross are of each specimen was recorded.

The relationship between the stress range, S_r, and the number of cycles, N, for steel can be described as:

$$N = Sr^{-3} * A$$

where A is proportional to the stress concentration factor as well as crack geometry and other factors. The AASHTO code has various fatigue categories with respective A factors that represent common details and their fatigue performance. The number of the cycles was plotted against the stress range along with the AASHTO category lines on an S-N curve in Figure 34. The category lines indicate the relative fatigue performance of the other common details and also provide a way to compare the relative fatigue performance of the various angle details. In general, the balanced weld details performed better than the equal length weld details. Each balanced weld detail for the same geometry was typically performed one category better than the equal length detail. A summary of all angle fatigue tests conducted is provided in Table 7 complete with A-value calculations. The location of failure in each specimen was also included. A failure in the front denotes a crack in the angle at the toe of the weld farthest from the outstanding leg, while a failure in the back denotes a crack in the angle at the toe of the weld closest to the outstanding leg and an end failure denotes a crack in the transverse weld along the edge of the angle. It is important to note that the 53LB specimens failed at the end of the angle instead of in the front or back of the angle where the failure was expected. Each failure can be seen below in Figure 35 through Figure 37.

Angle	Sr	N	A	Failure
44e1	12	231,174	4.E+08	Front
44e3	12	602,830	1.E+09	Front
44e4	8	2,158,038	1.E+09	Front
44e5	12	382,325	7.E+08	Front
44e6	8	2,278,038	1.E+09	Front
44b1	12	997,143	2.E+09	Back
44b2	12	1,025,453	2.E+09	Back
44b3	8	2,924,774	1.E+09	Back
44b4	8	3,801,386	2.E+09	Back
53Le1	12	300,052	5.E+08	Back
53Le2	12	318,805	6.E+08	Front
53Le3	8	1,655,604	8.E+08	Back
53Le4	8	2,314,378	1.E+09	Front
53Lb1	8	3,080,034	2.E+09	End
53Lb2	8	3,080,034	2.E+09	End
53Lb3	12	505,290	9.E+08	End
53Lb4	12	505,290	9.E+08	End
53Se1	8	1,104,311	6.E+08	Front
53Se2	11	824,273	1.E+09	Front
53Se3	11	310,191	4.E+08	Front
53Se6	8	1,070,376	5.E+08	Front
53Sb1	8	1,764,362	9.E+08	Front
53Sb4	12	963,607	2.E+09	Front
53Sb5	12	963,607	2.E+09	Front
53Sb6	8	1,764,362	9.E+08	Front

Table 7. Angle Fatigue Summary

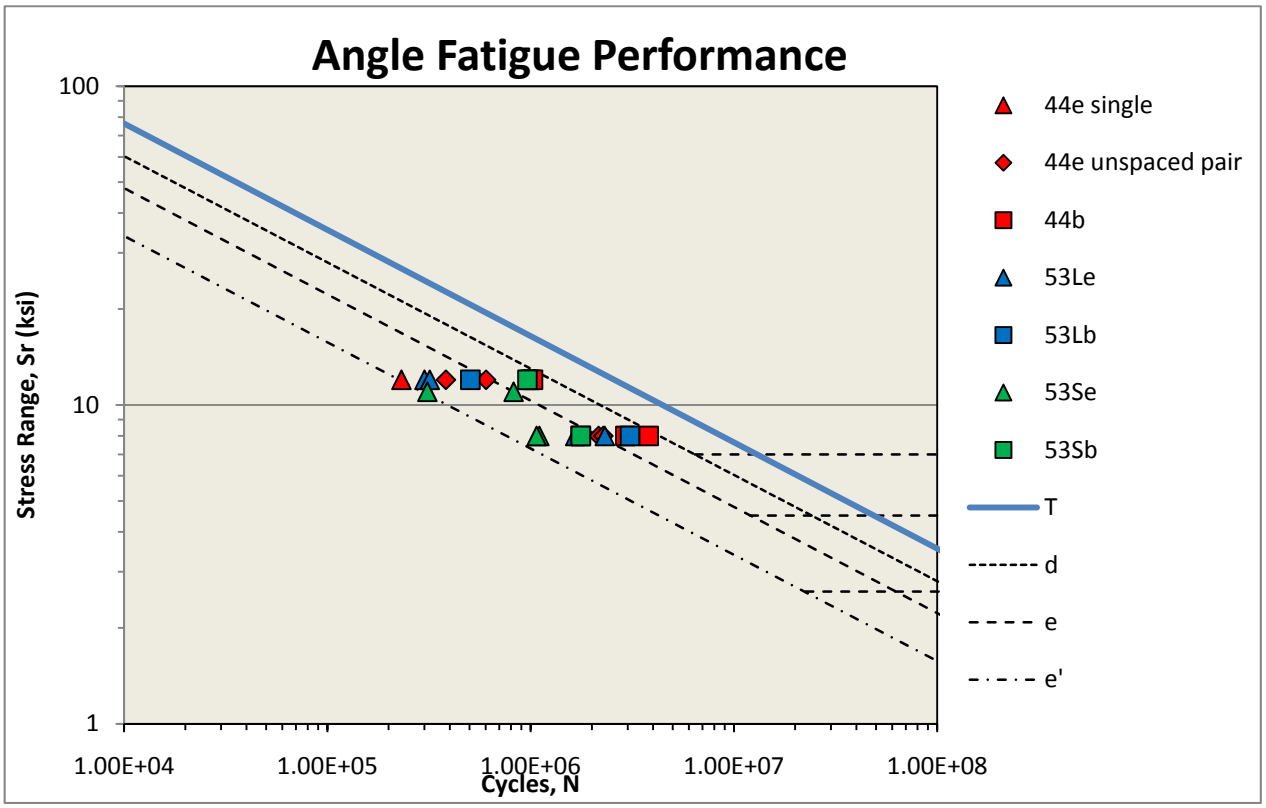

Figure 34. Angle Fatigue Performance

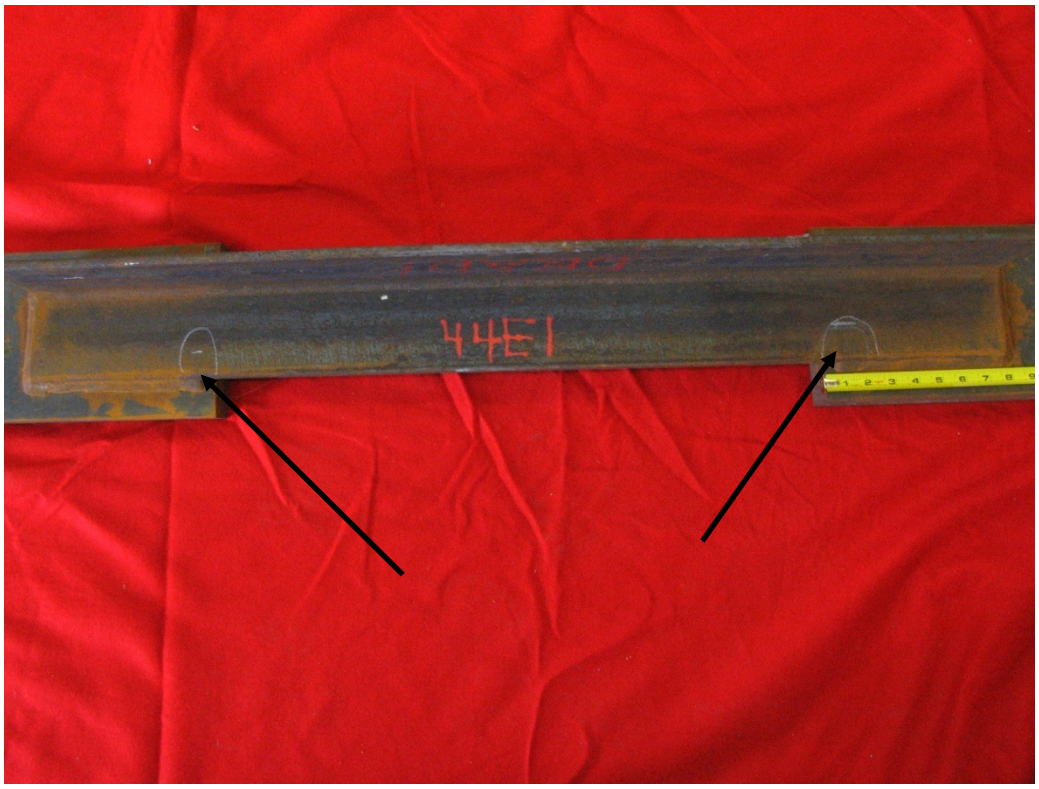

Figure 35. Front Failure Location

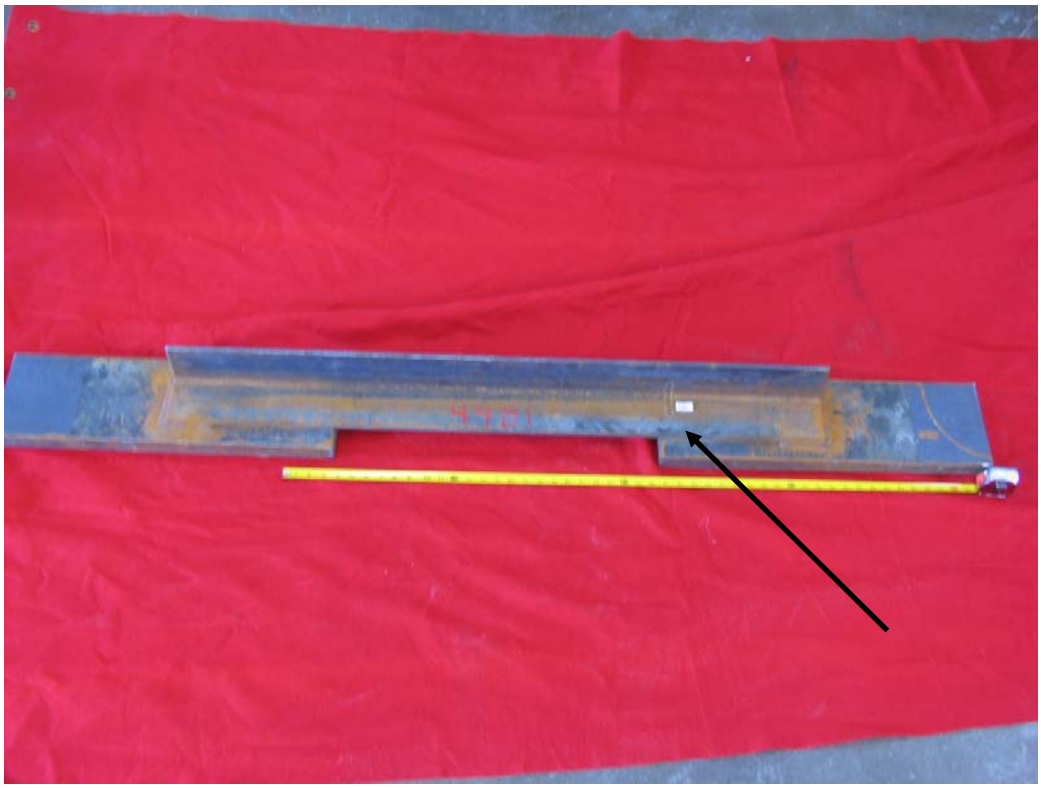

Figure 36. Back Failure Location

Figure 37. End Failure Location

3.2 4X4 ANGLE FATIGUE PERFORMANCE

Fatigue performances of the equal leg 4x4 angles, or 44 angles, are shown in Figure 43. The 44 angle with equal length welds, or 44E angle, that was tested using the single-angle test configuration barely fell into the E' category, but the 44 angles tested using the double-angle test configuration without spacers were almost an E category detail. The reason for the discrepancy is due to the fact that the angles tested using test setup 2 had a reduced stress range because of the contact pressure between the plates. The 44 angles with balanced welds, or 44B angles, fell right in the middle of an E category detail. Figure 38 through Figure 42 show typical failures of both the 44 angles with equal length welds and the 44 angles with balanced welds.

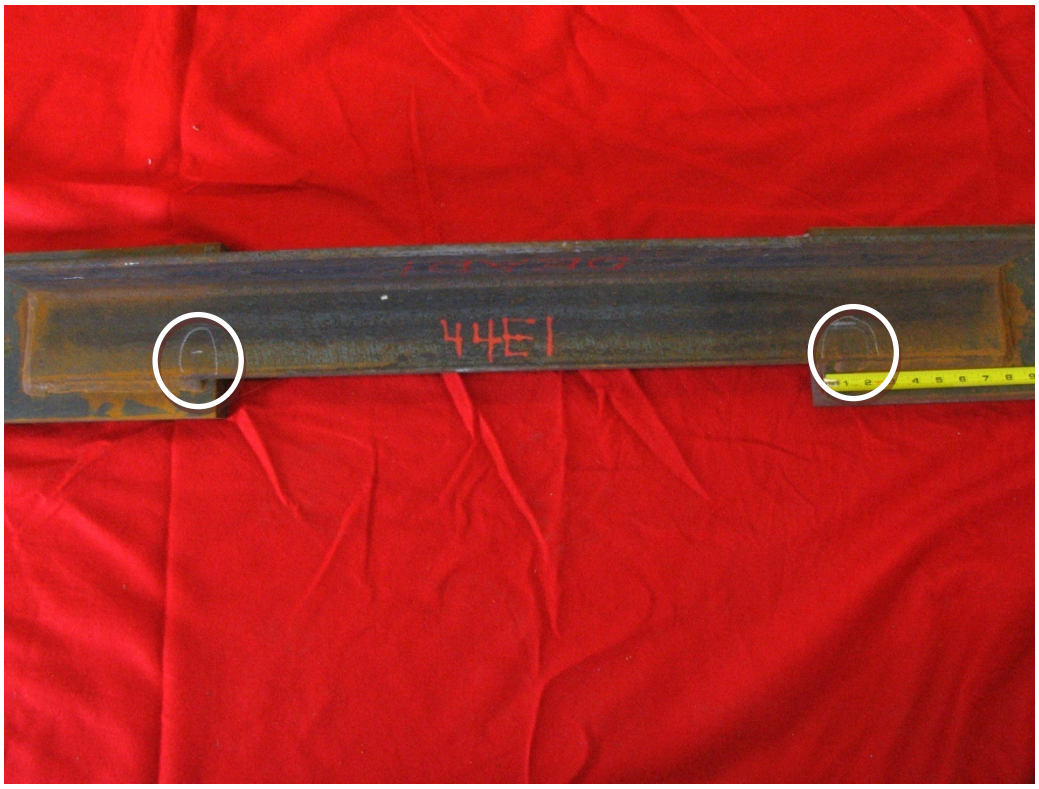

Figure 38. 44E Angle Failure

Figure 39. 44E Angle Failure Close-Up

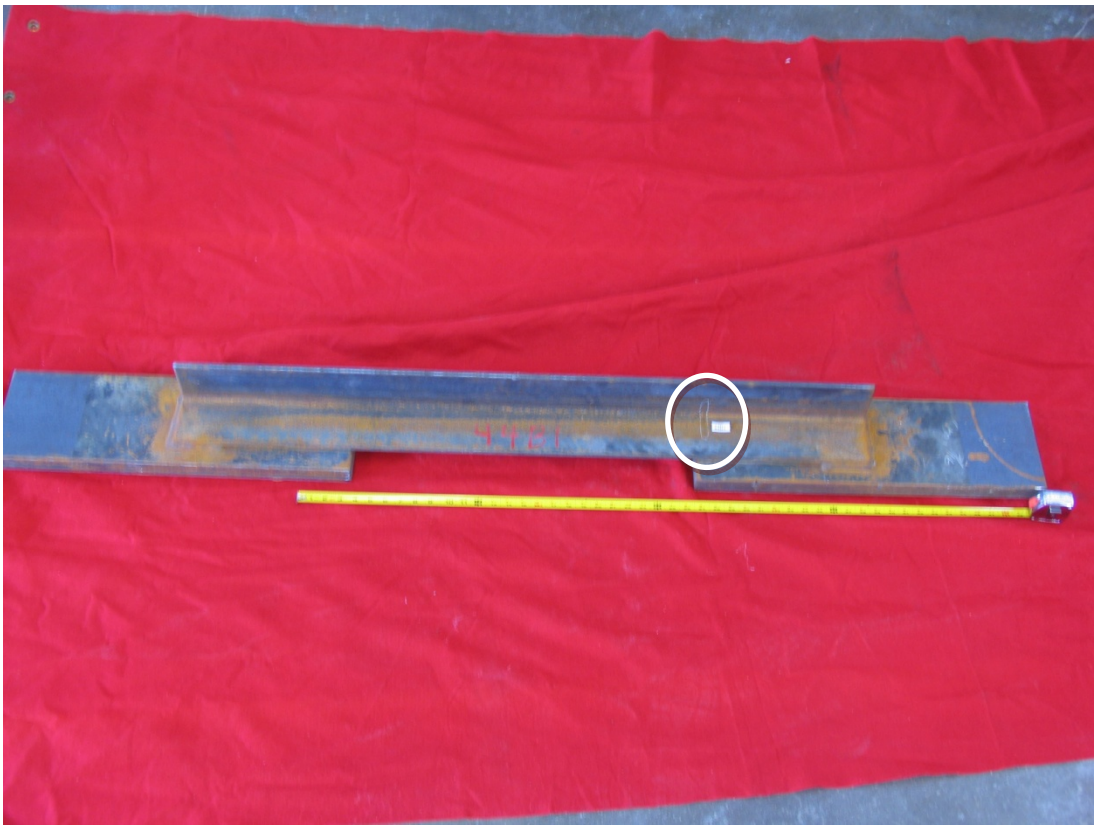

Figure 40. 44B Angle Failure

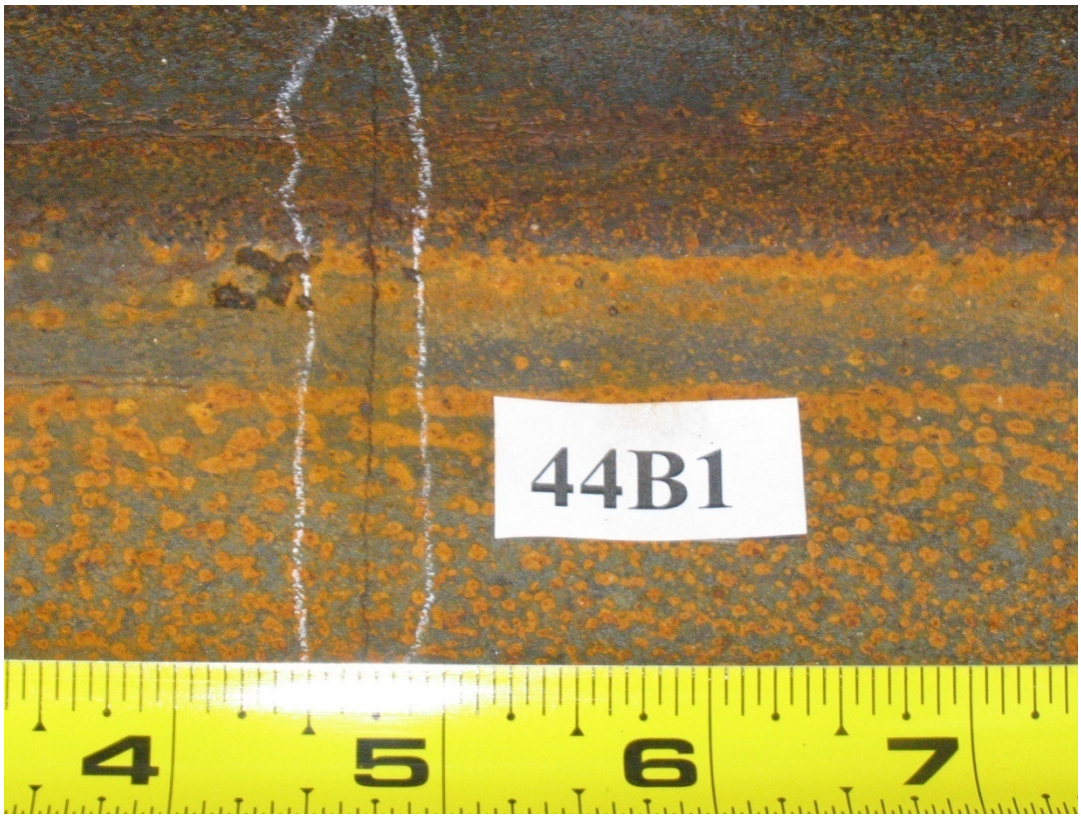

Figure 41. 44B Angle Failure Close-Up

Figure 42. 44B Angle Failure Backside Close-Up

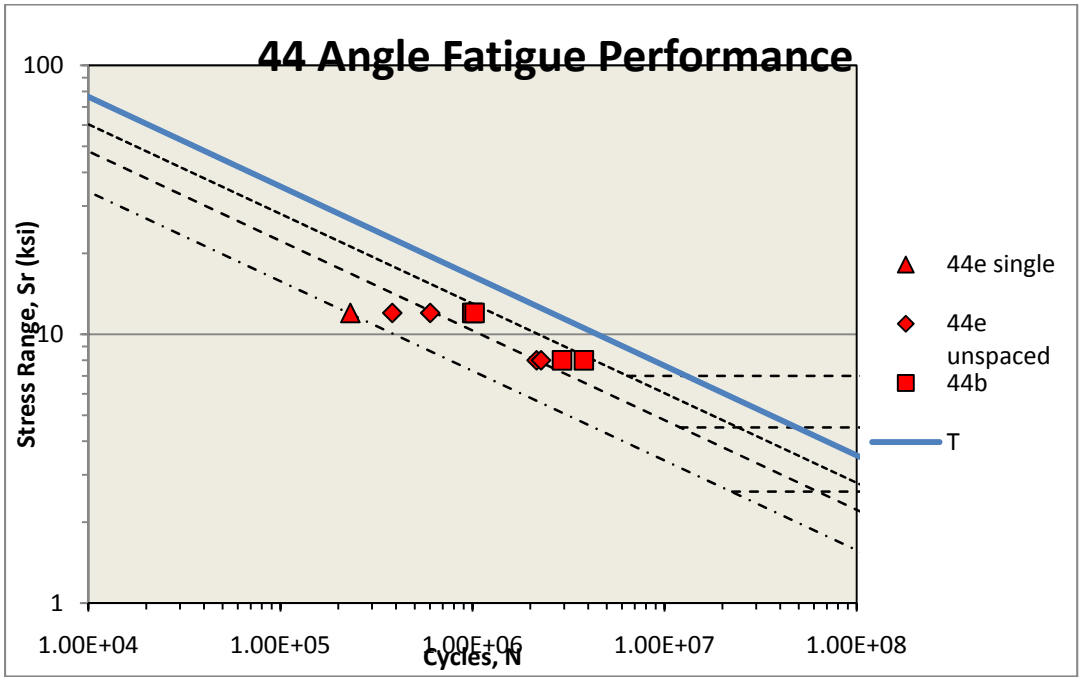

Figure 43. 44 Angle Fatigue Performance

3.3 5x3 Short Leg Outstanding Angle Fatigue Performance

Fatigue performances of the unequal leg 5x3 angles with the short leg outstanding, or 53S angles, are provided in Figure 44. The 53S specimens with equal length welds fell into the category E' while the specimens with balanced welds fell into category E. The 53S specimens with equal length welds were tested at a slightly lower stress range of 11 ksi because the connection plates came in contact with each other at higher stresses. This should have no effect upon the fatigue performance of the specimen. There was some substantial scatter for the equal length welded specimens tested at 11 ksi. One specimen was on the low end of the E' category while the other specimen was almost an E category detail. There was no visible explanation of this discrepancy but can probably be attributed to a variation in initial flaw size.

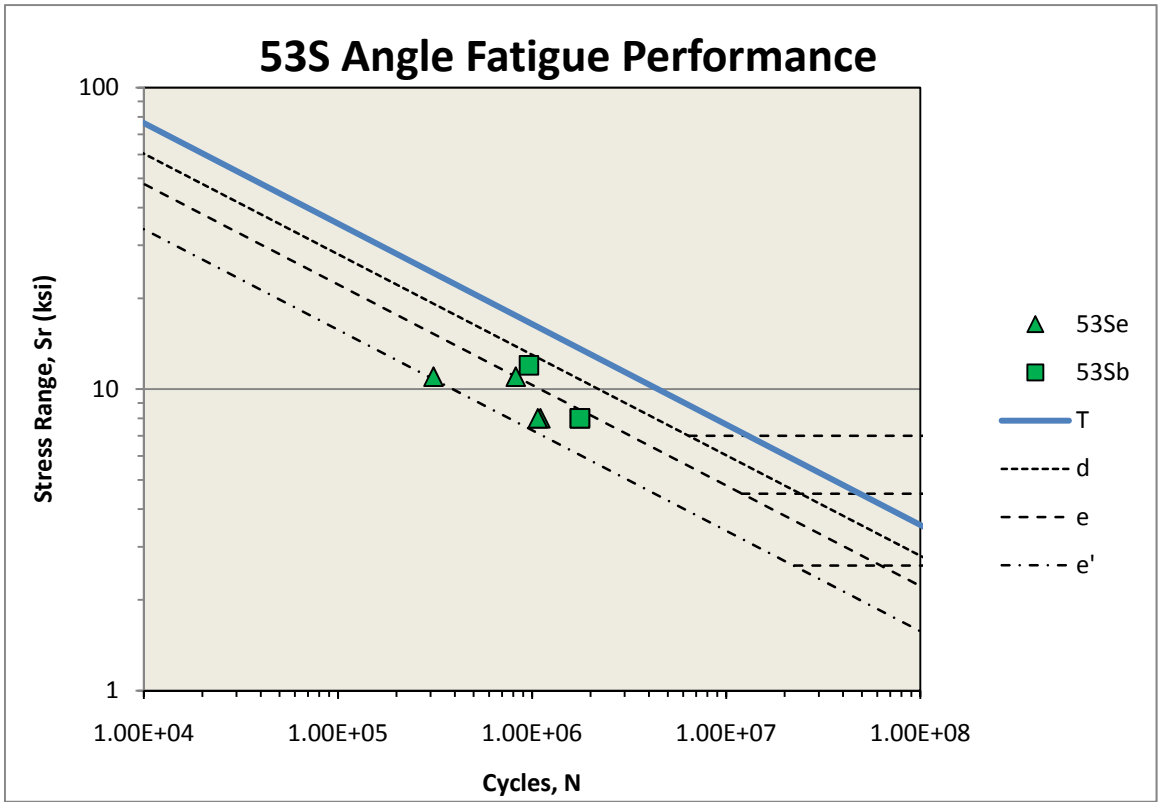

Figure 44. 53S Angle Fatigue Performance

Figure 45. 53SE Angle Failure

Figure 46. 53SE Angle Failure Close-Up

Figure 47. 53SB Failure

Figure 48. 53SB Failure Close-Up

3.4 5x3 Long Leg Outstanding Angle Fatigue Performance

Fatigue performances of the unequal leg 5x3 angles with the long leg outstanding, or 53L angles, are graphed in Figure 44. The 53L specimens with equal length welds fell in category E' and the specimens with balanced welds fell in category E. The 53LB specimens all failed at the end of the angle because the connection plates were relatively short which caused high shears to form near the end of the angle. This fatigue performance is probably not indicative of similar details with longer plate lengths.

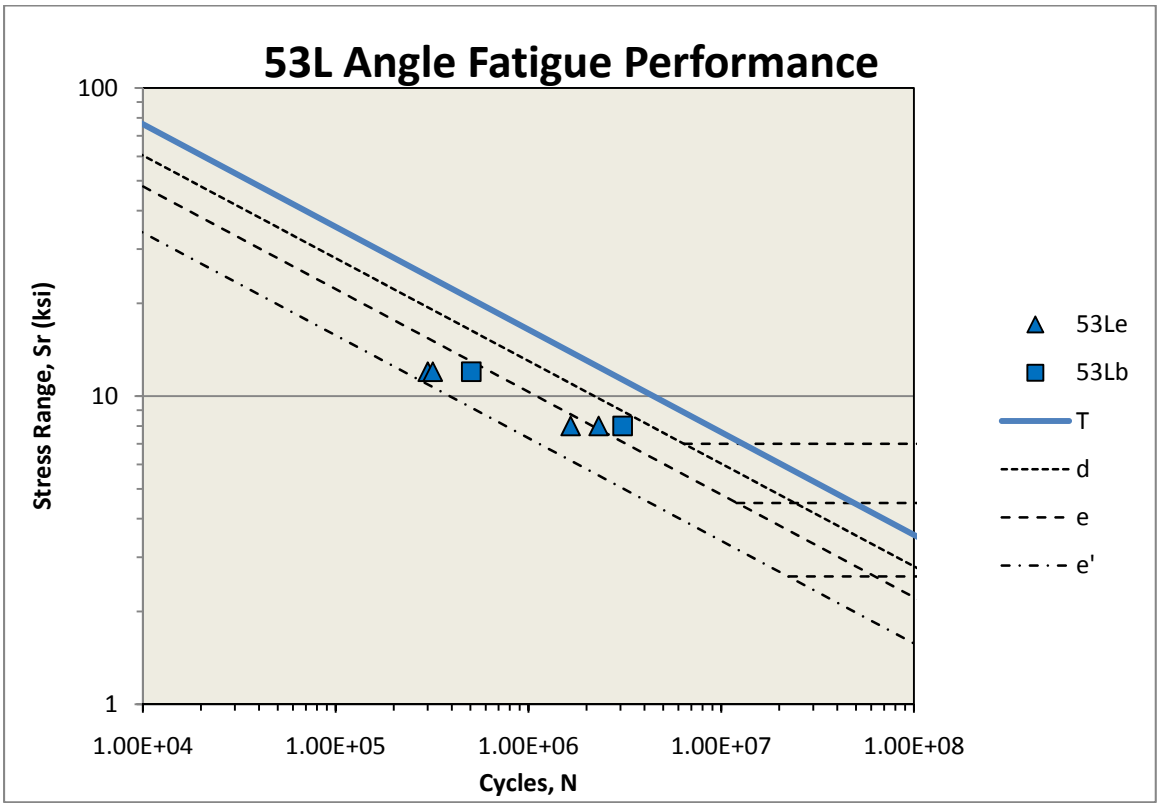

Figure 49. 53L Angle Fatigue Performance

Figure 50. 53LE Angle Failure

Figure 51. 53LE Angle Failure Close-Up

Figure 52. 53LB Angle failure

Figure 53. 53LB Angle Failure Close-Up

3.5 TEST DATA ANALYSIS

In the previous section, the nominal stresses were compared with the fatigue lives for each specimen detail. Because the nominal areas for each angle geometry are the same, the relative fatigue performances can be compared. The difference in fatigue performance for each detail is attributed to the difference in stress concentration and initial flaw size. If the stress concentration can be accurately approximated then the fatigue performance of each detail could be compared according to this value. Taking the maximum elastic membrane and bending stresses at the toe of the angle without accounting for shear lag or end plate flexibility has been proposed as one such method. The membrane and bending stresses at a horizontal distance x and vertical distance y from the origin depicted below in Figure 54 can be calculated using the equation below:

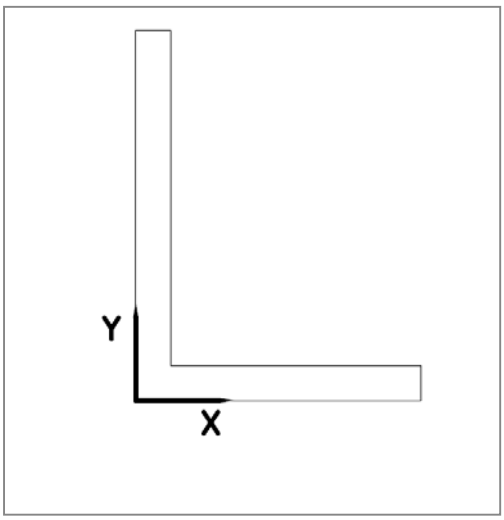

Figure 54. Diagram for Stress Calculations

$$\sigma = \frac{P}{A} + \frac{M_x * I_x}{{I_x}^2 - {I_{xy}}^2} * \left(y - \frac{I_{xy} * x}{I_y}\right) + \frac{M_y * I_y}{{I_y}^2 - {I_{xy}}^2} * \left(x - \frac{I_{xy} * y}{I_x}\right)$$

The moments M_x and M_y are calculated by multiplying the load by the eccentricity between the centroid of the weld group and the angle in the y-direction and x-direction respectively. The values I_x, I_y, and I_{xy} are properties of the angles that are calculated using their nominal geometries.

The calculated elastic stresses for each detail can then be plotted against the fatigue life of the specimens. If the stresses calculated are accurate then the new plot should have less scatter, because the variations in stress due to geometry should be accounted for. However, in Figure 55, it is clear that adjusting the fatigue performance to account for the elastic membrane and bending stresses increases the scatter of the data. This indicates that other effects that have not been accounted for are significant factors in determining the fatigue performance.

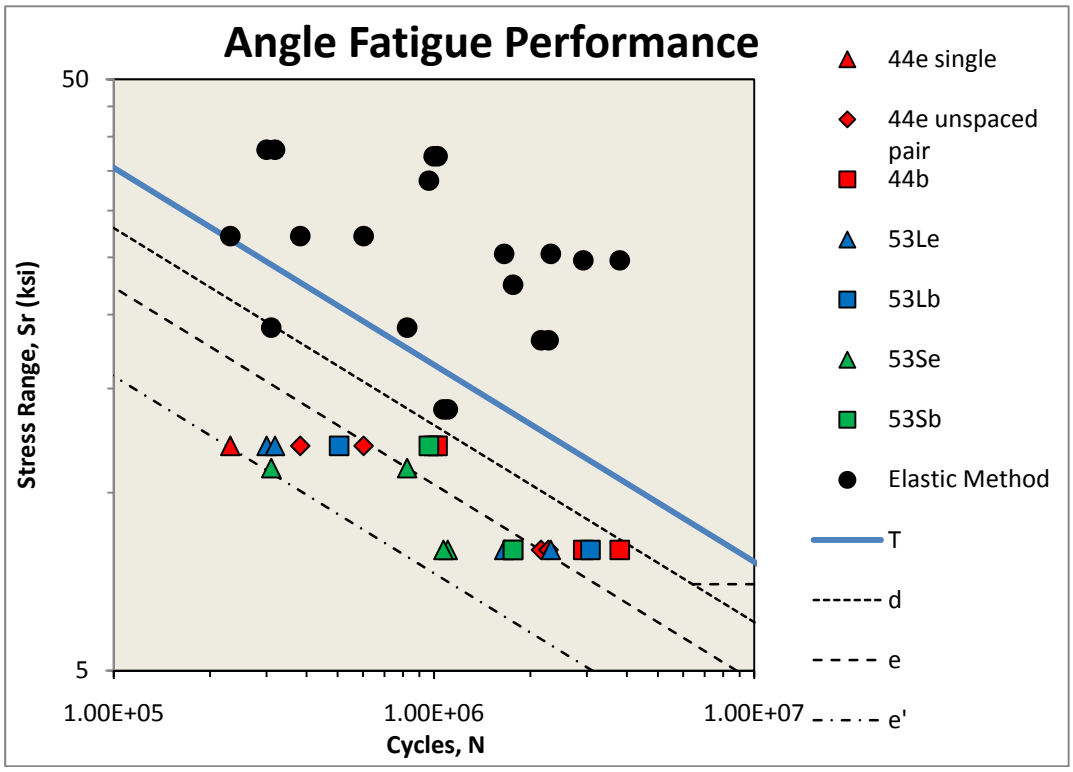

Figure 55. Adjusted S-N Data Using Elastic Method

Another possible way to adjust the stresses is to use the reduced area derived for shear lag calculations instead of the nominal stress. The effective area can be calculated by reducing the nominal area A by the factor 1-x/l where x is the eccentricity of the angle in the y direction and l is the length of the longest longitudinal weld. The stress is then calculated as the load over the effective area. Figure 56 shows the S-N data adjusted for shear lag. It is difficult to visually determine whether the scatter of the data was reduced so statistic methods were applied to evaluate the accuracy of the method. The slope of the line should be equal to negative three, because that value is constant for steel. The equation of the line was calculated by minimizing the sum of the squares. The multivariable linear regression with a fixed slope of negative 3 yields the equation:

$$N = 1.52 * 10^9 * {S_r}^{-3}$$

The r value for this trend line is equal to 0.71 which is much better than 0.55 that was found for the initial data. The shear lag adjustment decreases the scatter and gives a better approximation of the stress concentration than the nominal stress.

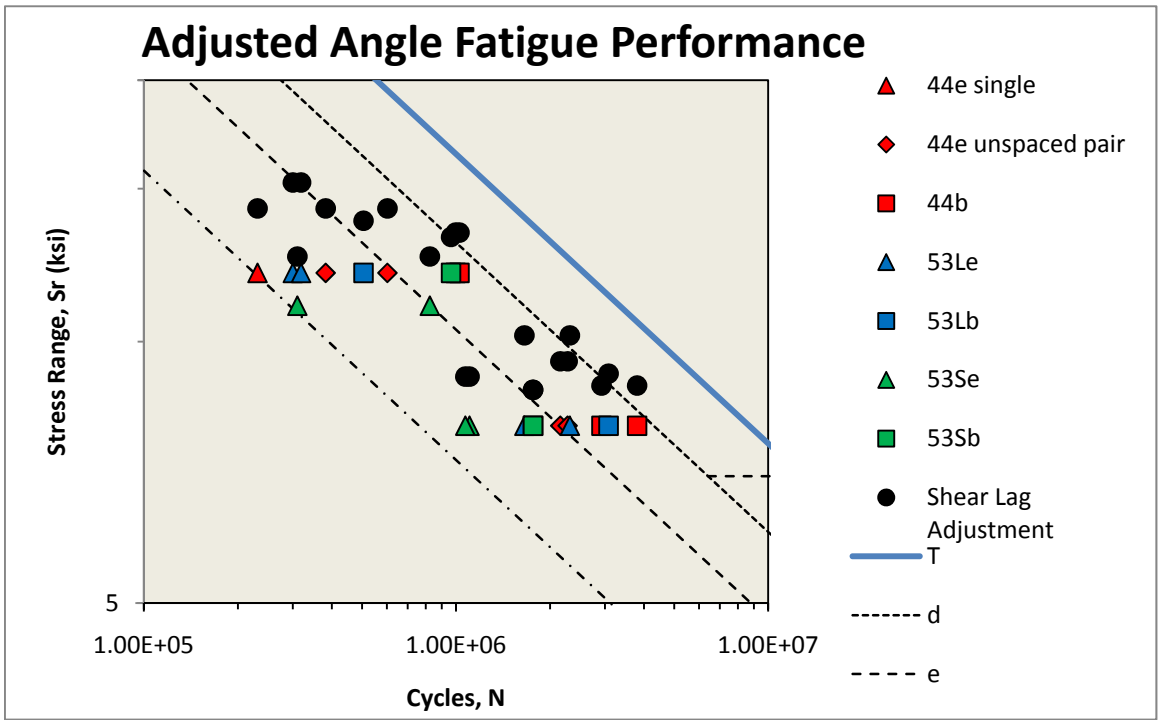

Figure 56. Adjusted S-N Curve for Shear Lag

3.6 WILSON CONNECTION RESULTS

The Wilson connection fatigue results taken from Munse's Fatigue of Welded Structures (Munse, 1964) are provided in Table 8. These fatigue results are plotted with the angle fatigue performance below in Figure 57. Most of the Wilson data has a very similar performance compared with the angle tested in this study. Most are category E or E' with one falling into category C. However, the dimensions of the Wilson connections have many differences with the angles tested in this study and cannot be directly compared. The hot spot stresses calculated using finite element methods will be compared later on in Chapter 6.

Detail	Nominal Stress Range (ksi)	Cycles	A
Angle	10	2572000	2.57E+09
Angle	10.1	5177000	5.33E+09
Angle	16	507800	2.08E+09
Angle	12.8	511800	1.07E+09
Angle	12.8	555000	1.16E+09
Angle	16	494000	2.02E+09
Angle	19.3	56400	4.05E+08
Angle	19.3	34300	2.47E+08
Channel	25	55900	8.73E+08
Channel	25	41800	6.53E+08
Channel	20	47500	3.80E+08
Channel	20	68600	5.49E+08
Channel	10	1137100	1.14E+09
Channel	10	1688100	1.69E+09
Channel	18	108400	6.32E+08
Channel	12.8	1011400	2.12E+09

Table 8. Wilson Connection Results

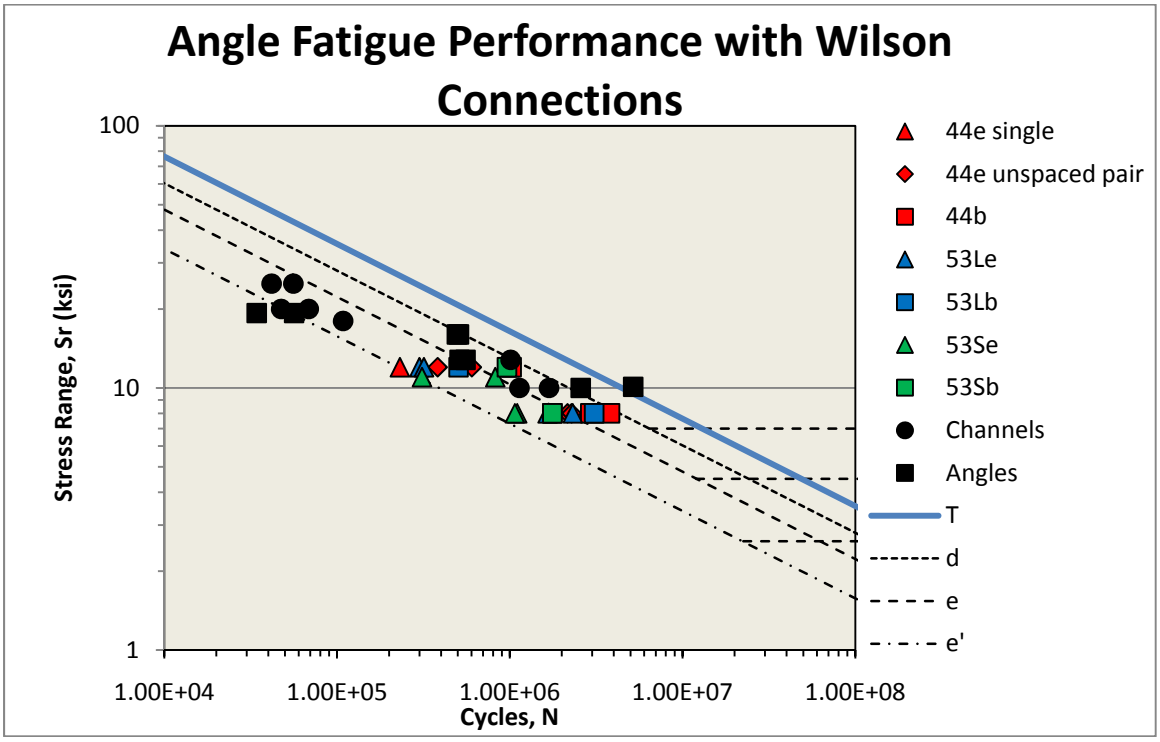

Figure 57. Angle Fatigue Performance with Wilson Connections

3.7 TESTING SUMMARY

The results of the fatigue testing remain inconclusive in determining any superior performance between the various angle geometries. The 4x4 angles with balanced welds performed the best out of the balanced details, but the 4x4 equal with length welds had the poorest performance out of the equal length weld details. Also, the 5x3 angles with the long leg outstanding and balanced welds performed better than the 5x3 angles with the short leg outstanding and balanced welds at 8 ksi stress range, but performed worse at 12 ksi. This indicates that there is a lot of scatter which is probably due to the variance in initial flaw size.
The angle details with balanced welds consistently performed better than their equal length welded counterparts. However, due to the variation of other factors such as angle length and plate length in the balanced welds, it is not conclusive whether the increase in fatigue performance is due to the balancing of the welds, other geometric variations or both.

Calculating the maximum elastic membrane and bending stresses resulted in an increase of scatter in the data which indicates that the method is not adequate in approximating the stress concentration. Using the shear lag adjustment decreases the scatter of the data which indicates that the shear lag does account for some of the stress concentration. However, the data does not produce any discernable pattern that could be used to develop a design guideline.

CHAPTER 4

Discussion of FEM Modeling

4.1 FEM Modeling Overview

The fatigue lives of the specimens that we tested have been determined, but they are not representative of every type of angle cross-frame design possible. In order to be able to investigate the effects of various geometric parameters on the fatigue life, a finite element model was developed using ABAQUS (2006) to find the stress concentrations at the toe of the weld. In order to ensure that the finite element model reflected real world results the data taken from the model was compared with the fatigue test results. Each specimen detail was analyzed using ABAQUS and the stress concentrations at the weld toe where the specimen cracked were calculated. Then, fatigue testing data was plotted using the hot spot stress, or the stress concentration factor multiplied by the nominal stress, instead of the nominal stress. The data was then analyzed to see if there was a reduction in scatter by the inclusion of the geometric stress concentration, while the remaining scatter in the data can be attributed to variations in initial flaw size and weld profile geometry.

There are many details to consider when creating a finite element model such as element type, mesh density, level of geometric variables considered, and the extrapolation methods to be utilized in estimating the hot spot stress. After extensive preliminary investigation, an optimum finite element modeling method was determined for the requirements of this project.

Each part was created using the dimensions taken from the fatigue specimens and then assembled. The plate lengths were reduced by the amount that was gripped by the test machine. Then, the welded connections were modeled by tying all of the degrees of freedom between to the angle and the plates where the weld would be. The assembled model of the 4x4 angle with equal length welds can be seen below in Figure 58.

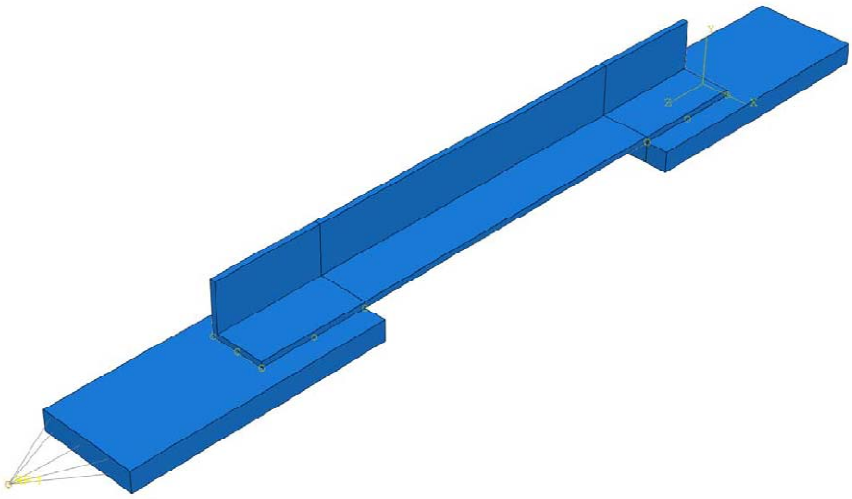

Figure 58. 44E Model with Interactions

The boundary conditions and loading were then modeled to simulate the testing machine's interaction with the specimen. The face of one end plate was held completely fixed where every degree of freedom was fixed, while the face of the other end plate was restricted to movement in the longitudinal direction. The moving face was coupled to a reference point so that there would be no relative rotation between the points along the face. A unit pressure was then applied to the moveable face to simulate the uniform loading from the grips of the machine. Figure 59 shows the model of the 4x4 angle with equal length welds with the boundary conditions and loads applied.

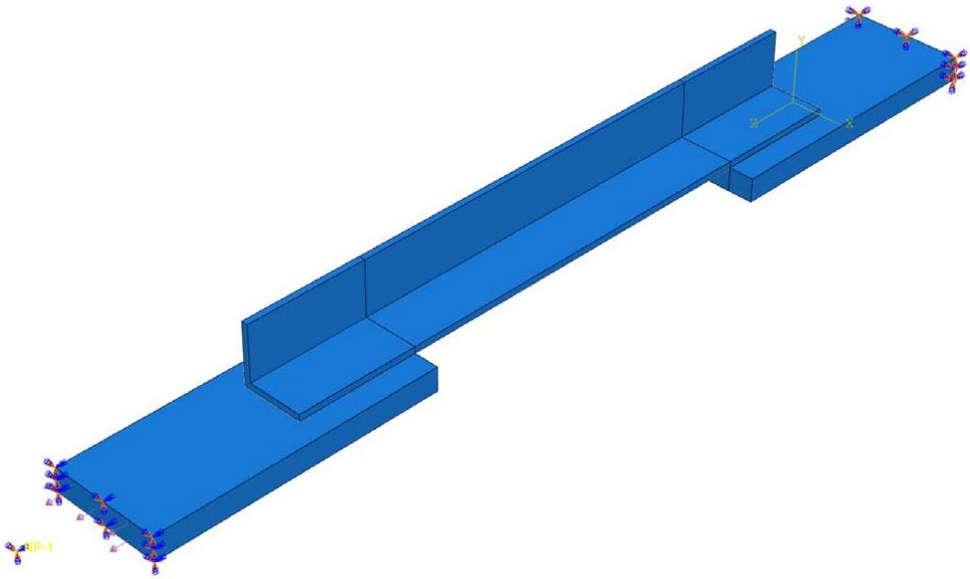

Figure 59. 44E Model with Boundary Conditions

Figure 60 below shows the model with the mesh applied to the assembly. Linear reduced integration solid elements were used for the majority of models. A mesh size of ¼ the thickness of the angle was used for the angle, while a mesh size of 0.5 in. was used for the end plate.

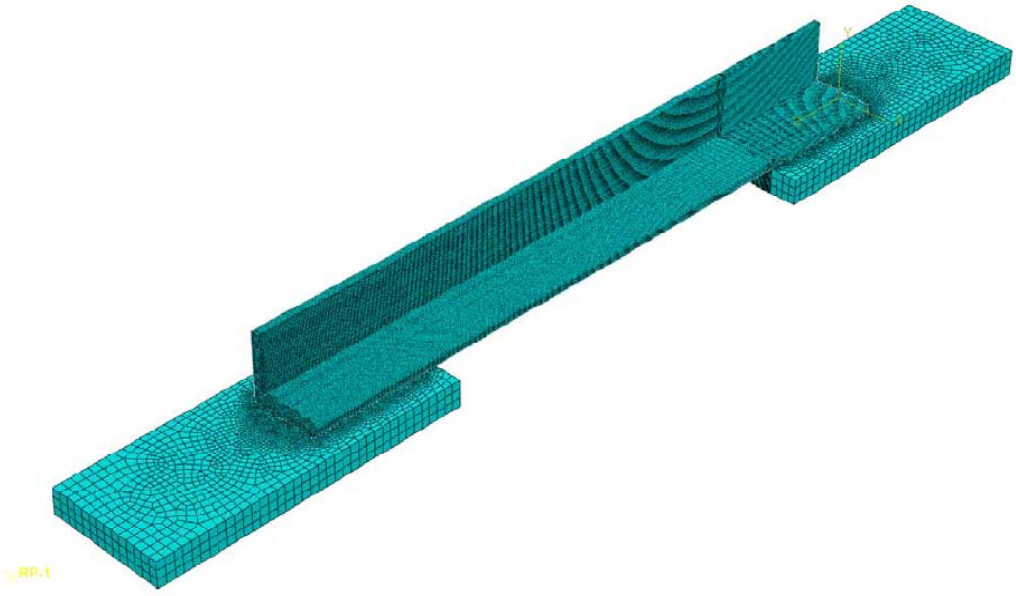

Figure 60. 44E Model with Mesh

4.2 MODELING METHODS

4.2.1 Element Type

The best method of modeling of the angle system was explored. The ABAQUS documentation recommended using solid quadratic reduced integration (C3D20) elements for stress concentration analyses so they were initially considered. However, quadratic reduced integration requires much more computational power than linear reduced integration, so the effect of changing the element type to linear reduced integration was investigated. A test model using the 4x4 angle with equal length weld specimen dimensions was analyzed using linear reduced integration, quadratic reduced integration and linear full integration and the stress concentrations were compared. A graphical representation of the stress concentration factor, SCF, calculations computed using the DNV method is provided in Figure 61.

The difference between the three different methods is negligible so the linear reduced integration elements using edge nodes were used for modeling of the angles and the gusset plate for all subsequent modeling.

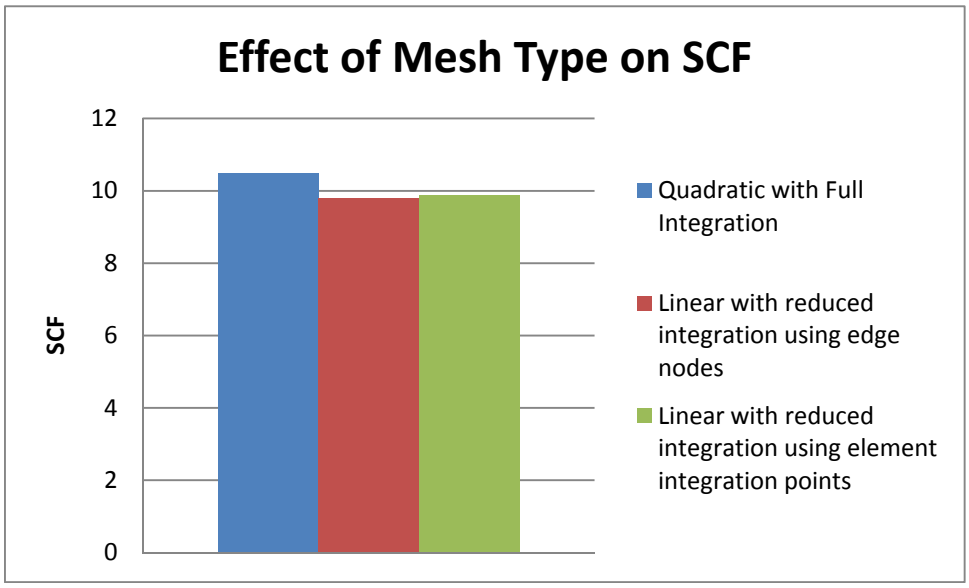

Figure 61. Stress Concentrations of Various Mesh Integration Methods

4.2.2 Effect of Modeling Weld

The geometry of the weld was also considered in the finite element modeling. Modeling the weld geometry is a much more complicated process than specifying that concurrent nodes of the angle and plate have the same displacement at the weld. There will be slightly different forces since the weld actually transfers forces through the entire area of the weld, so the effects of modeling the weld geometry on the stress concentration were investigated. The same 4x4 angle with equal length welds was modeled with the weld geometry and without the weld geometry. Figure 62 shows the 4x4 angle with weld geometry model and Figure 63 shows a more detailed view of the weld mesh. The weld geometry required tetrahedron shaped elements so 4-node linear reduced integration tetrahedron elements were used for that portion of the mode. The stress distribution near the weld toe and the stress concentration for the two geometries are shown in Figure 64 and Figure 65, respectively. The stress at the weld toe was calculated using the DNV method, which is described later. Modeling the weld geometry did not have a significant effect upon the stress concentration and therefore was not considered in the subsequent finite element models.

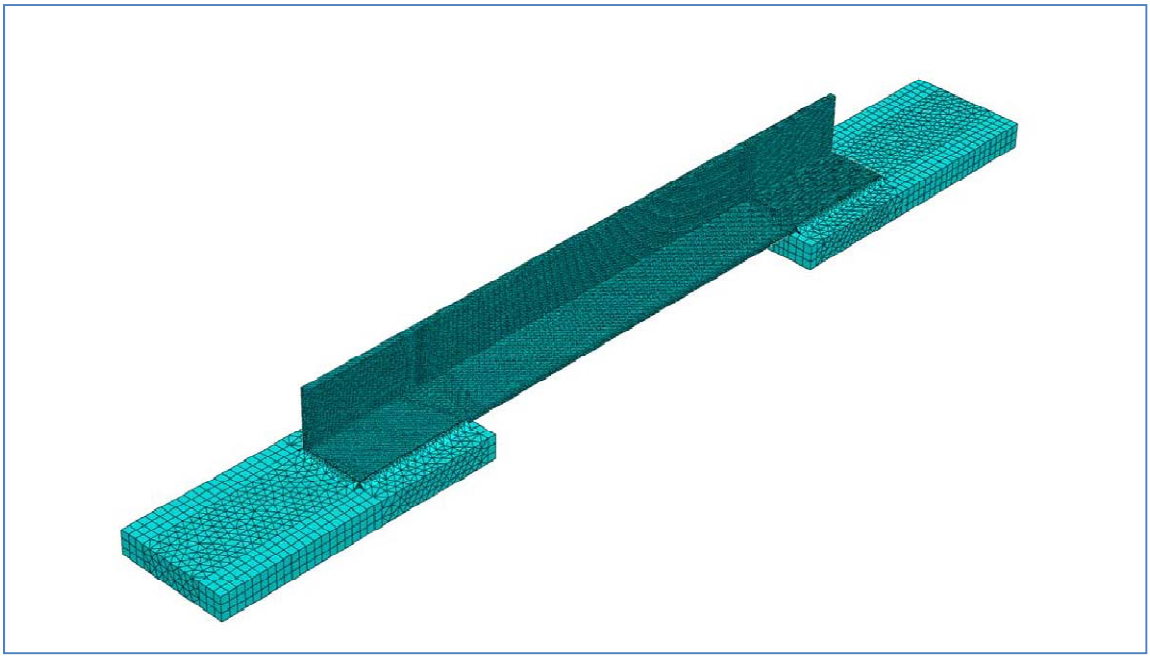

Figure 62. Mesh of 4x4 Angle with Weld Geometry

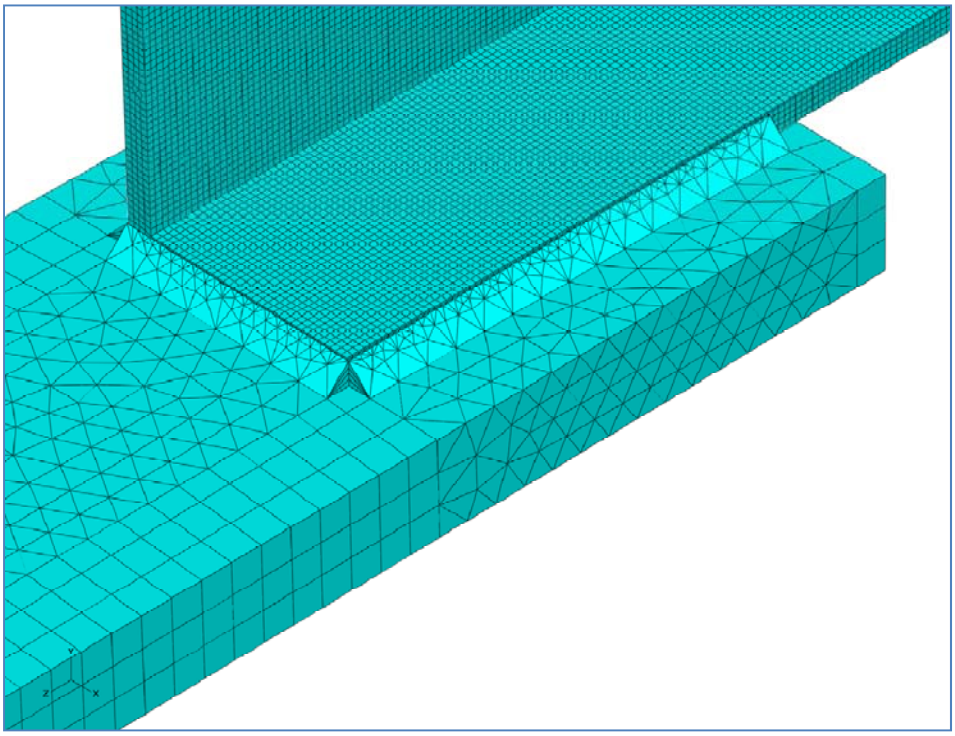

Figure 63. Weld Geometry Close-Up

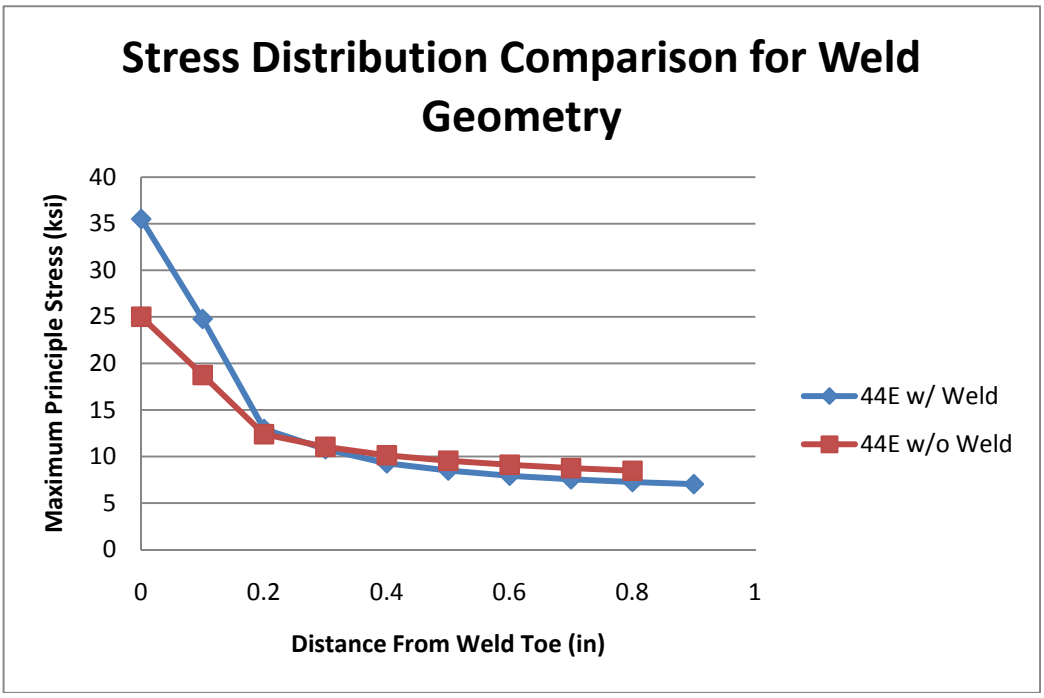

Figure 64. Stress Distribution Comparison for Weld Geometry

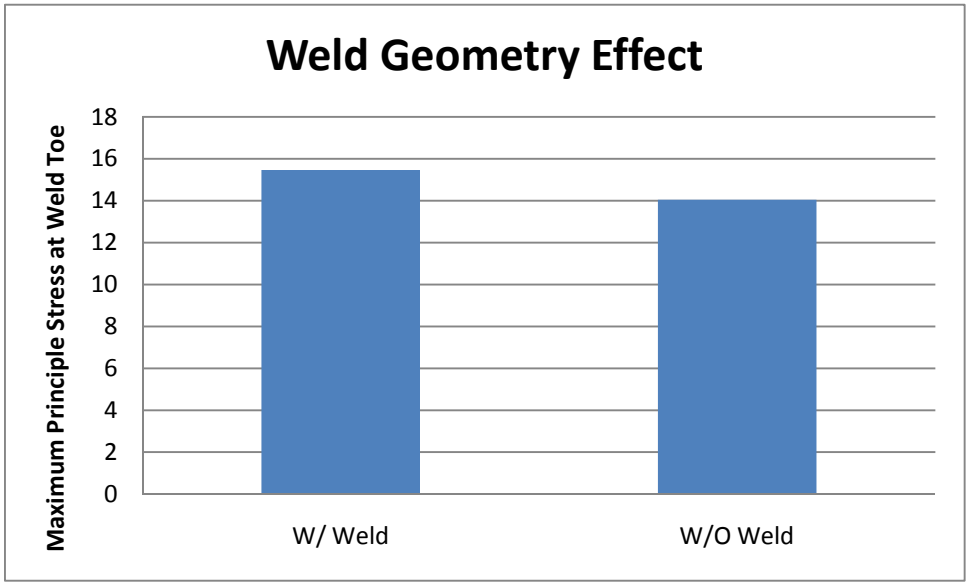

Figure 65. Stress Concentration for Varying Weld Geometries

4.2.3 Evaluation of Hot Spot Extrapolation Methods

Finite element models will return a very high stress at geometric discontinuities such as the right angle formed between end of the angle and the plate surface. The stress at these locations will increase as the element size is decreased. Extrapolation schemes have been

developed which employ extrapolation of the stress remote from the weld in attempts to eliminate the sensitivity of the hot spot stress with element size. The hot spot stress is defined as the intercept of the straight line at distance of zero which is lower than the stress estimated from the finite element solution. Three different methods were considered in determining the hot spot stress at the weld toe. These were the Dong method, the DNV method, and the AWS method.

4.2.3.1 AWS Method

The AWS method linearly extrapolates the maximum principal stresses taken at points along the longitudinal edge a certain distance away from the stress singularity. The method requires the distances of the points from the stress singularity to be 0.4 times the thickness and 1 times the thickness of the angle (Niemi, Fricke, & Maddox, 2006). AWS meshing requirements are shown in Figure 66. Also, the AWS method requires a fine mesh with at least two elements through the thickness.

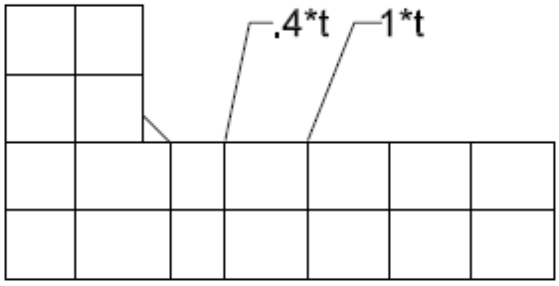

Figure 66. Mesh used for AWS Method

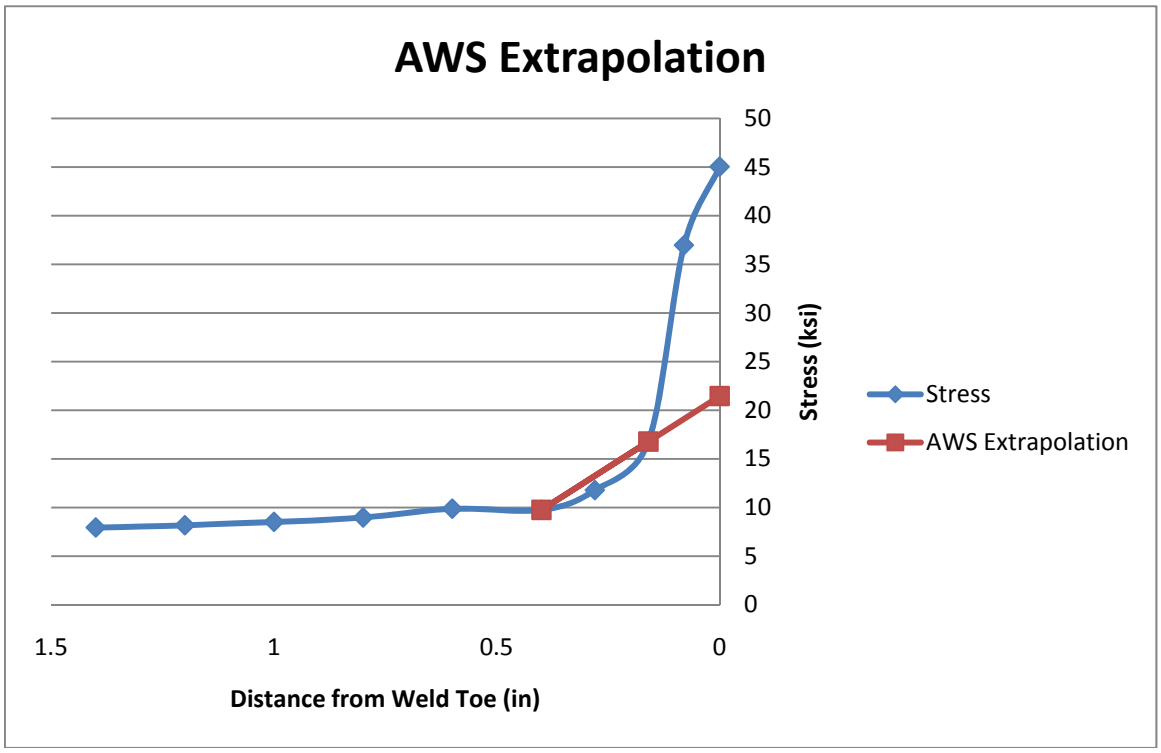

Figure 67. AWS Extrapolation Method

4.2.3.2 DNV Method

The DNV method is very similar to the AWS method because this method also linearly extrapolates the maximum principal stresses taken at points along the longitudinal edge a certain distance away from the stress singularity. However, the DNV method required the distances to be 0.5 times the thickness and 1.5 times the thickness and only requires one element through the thickness. The meshing requirements for the DNV method are provided in Figure 68. A graphical representation of the application of the DNV method is shown in Figure 69.

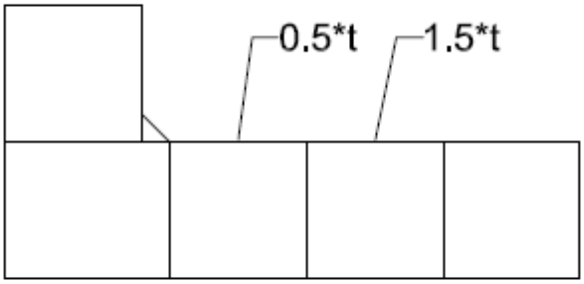

Figure 68. Mesh used for DNV Method

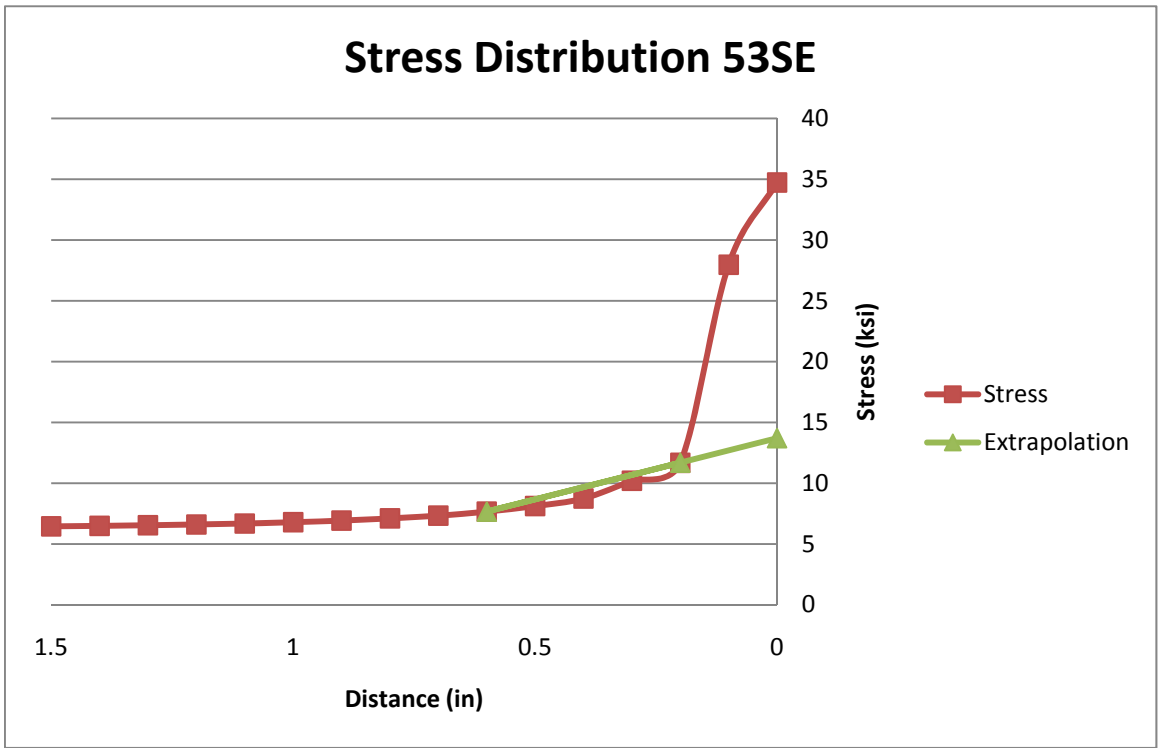

Figure 69. DNV Extrapolation Method

4.2.3.3 Dong Method

The Dong method takes a much different approach to finding the stress concentration by taking the nominal stresses in the longitudinal direction and shear stresses in the transverse direction at multiple points through the thickness of the angle at certain distances away from the stress singularity and applying equilibrium. Dong asserts that the method is mesh insensitive so that the stresses computed from any sized mesh can be compared to the stresses computed using any other mesh. A graphical representation of the application of the Dong method (Dong, 2001) can be seen below in Figure 70 through Figure 72. The shear stresses, the bending stresses and the membrane stresses are computed using a finite element modeling program at a distance delta away from the weld toe. A structure subjected to uniaxial bending will have a stress distribution depicted in Figure 71, but can be approximated as the stress distribution in Figure 72. The relationship between the stresses along line B and the Stresses along line A can be found by equilibrium.

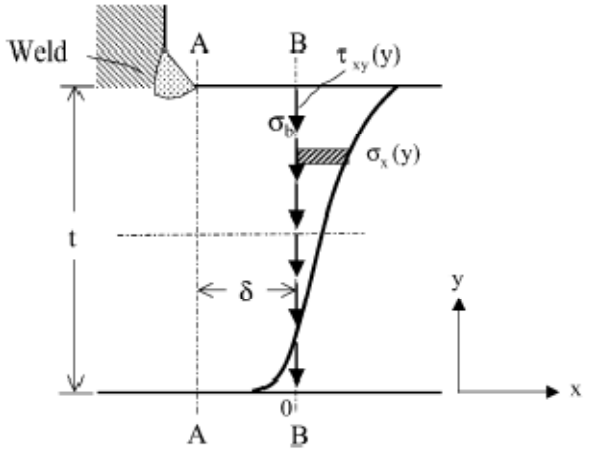

Figure 70. Finite Element Shear and Longitudinal Stress (Dong, 2001)

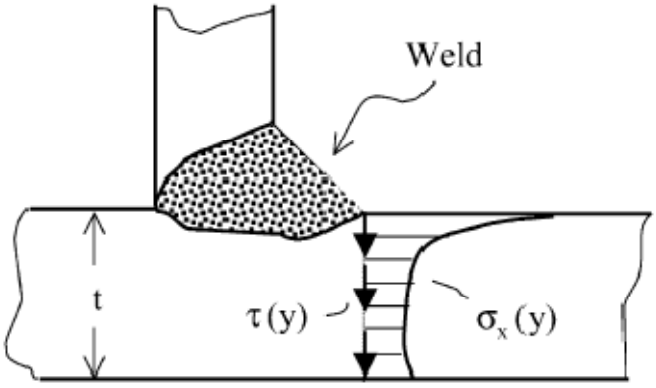

Figure 71. True Stresses at Weld Toe (Dong, 2001)

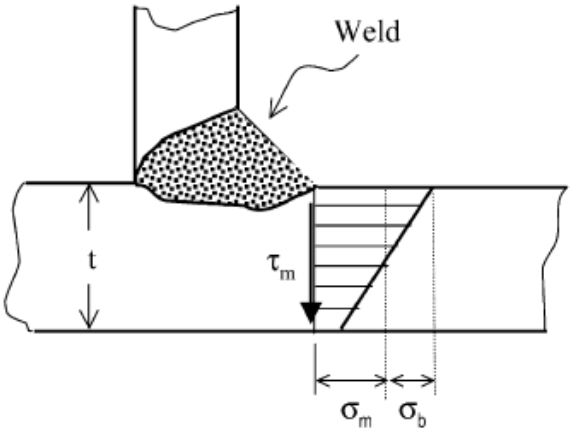

Figure 72. Approximate Stress at Weld Toe (Dong, 2001)

4.2.3.4 Comparison

The same model of 4x4 angle specimen with equal length welds were analyzed using each method with the same element type, linear reduced integration elements, but different meshing schemes per the requirements of the method. The stress concentrations were then compared to determine whether the there was any significant difference between the various methods. Also, different mesh sizes and distances from the weld toe were utilized for the Dong method because there is no distance that is specified in the procedure (Dong, 2001).

The AWS method and DNV method are very similar because they both utilize a linear extrapolation of the maximum principle stress. However, the stress distributions are very different. The DNV method gives a much smoother curve than the AWS method due to the uniform mesh size. The results of the stress concentration comparisons, between the AWS and DNV methods for two specimens are shown in Figure 73. These methods are supposed to take the bending and membrane stresses where there is no nonlinearity due to the geometry and extrapolates those stresses to the weld toe, but the AWS method seems to be picking up some of the nonlinearity. The 44E model used the same dimensions as a 4x4 angle with equal length welds while the LLO model used the same dimensions except that the outstanding leg was increased to be 6 inches.

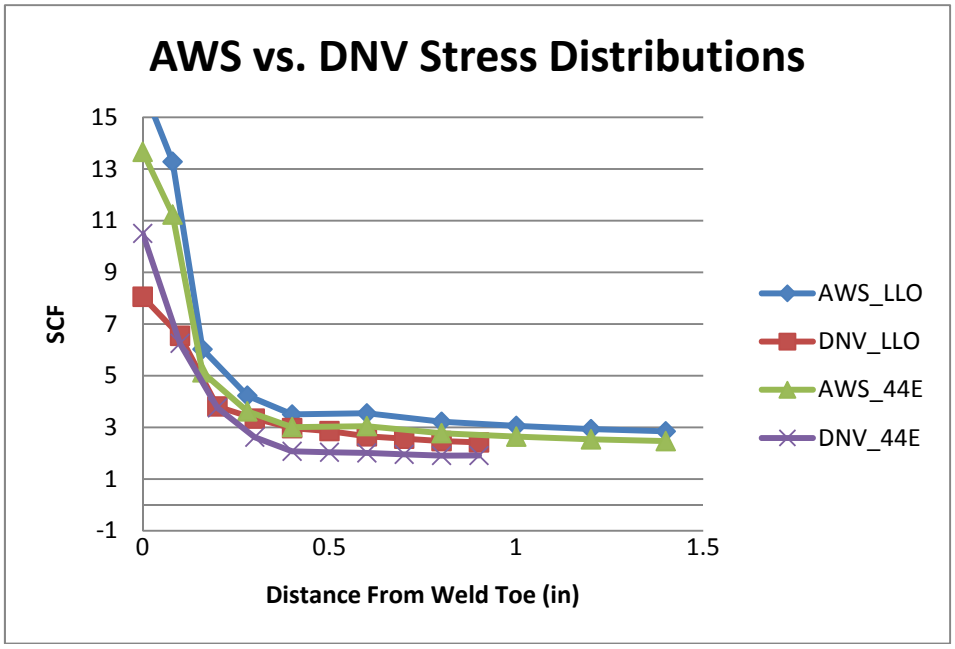

Figure 73. AWS and DNV Stress Distribution Comparison

The Dong method showed some distance sensitivity. This may be due to the fact that the stress is not uniform through the width of the angle. Also, Dong's method assumes that there is only one axis of bending and does not incorporate the bending about the second axis. The results of the stress concentration comparisons for the Dong method can be seen below in Figure 74. For reference, the stress concentration calculated using the DNV method and the same mesh size has been plotted. The Dong method and the DNV method have very similar stress concentration

factors when the Dong method is applied close to the weld toe, but the SCF for the Dong method becomes much lower farther away from the weld toe.

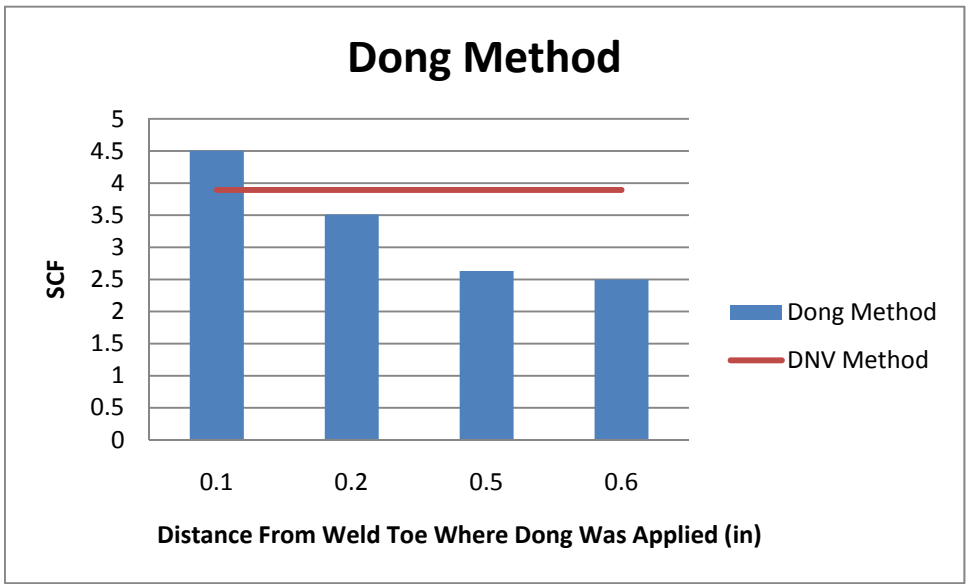

Figure 74. Dong Method Stress Concentration Comparison

4.2.4 Influence of Element Size – DNV Method

The DNV method appeared to be the best method to use because of the ease of use and the low computing time while still remaining accurate so it was used for the stress concentration computation for all of the subsequent finite element models. However, using a mesh equal to the thickness of angle with linear, reduced integration elements does not fully capture bending stresses so the decision was made to find an optimum mesh size that captured bending and provided consistent results. The DNV method was applied to different mesh sizes for the specimen geometry and the calculated stress concentrations compared. A graphical comparison of the differing stress concentrations can be seen below in Figure 75.

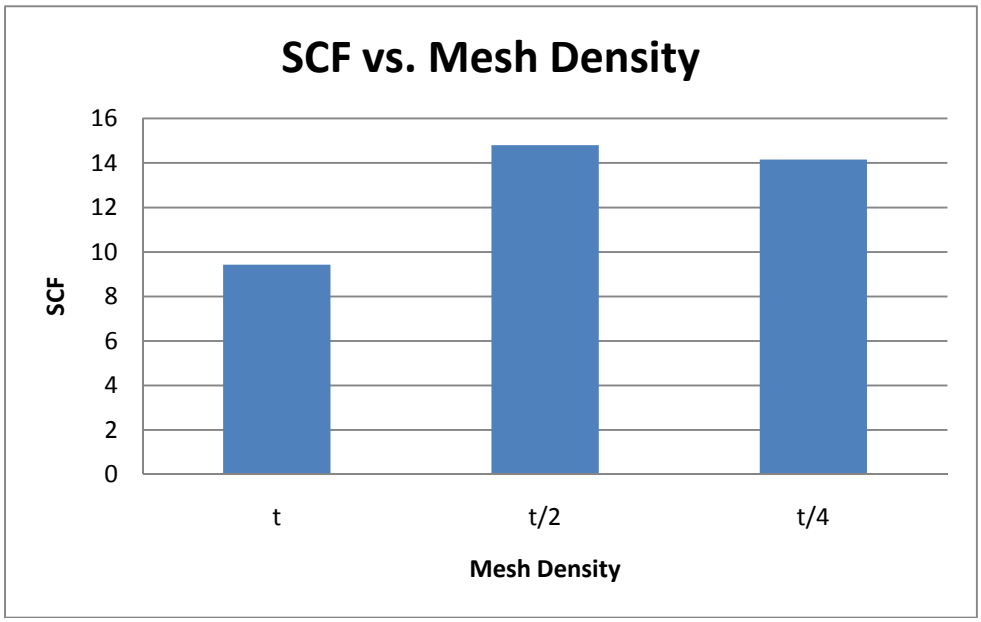

Figure 75. DNV Stress Concentrations for Varying Mesh Density

Figure 76 shows the stress distributions and extrapolations for three different mesh densities, *t*, *t*/2 and *t*/4. The stresses reported at the weld toe for the *t*/4 and *t*/2 mesh densities are approximately 35 and 14 respectively, but because the stresses reported away from the weld toe are very similar the hot spot stress is nearly the same. A mesh density of t would not be a good choice because the hot spot stress varies greatly from the hot spot stress found using a mesh density of t/2. It was decided that the most accurate yet economic results were calculated using a mesh thickness of 0.25 times the thickness of the angle. It is important to note that the DNV method is mesh-sensitive and that each model must use the same mesh density to provide comparable results.

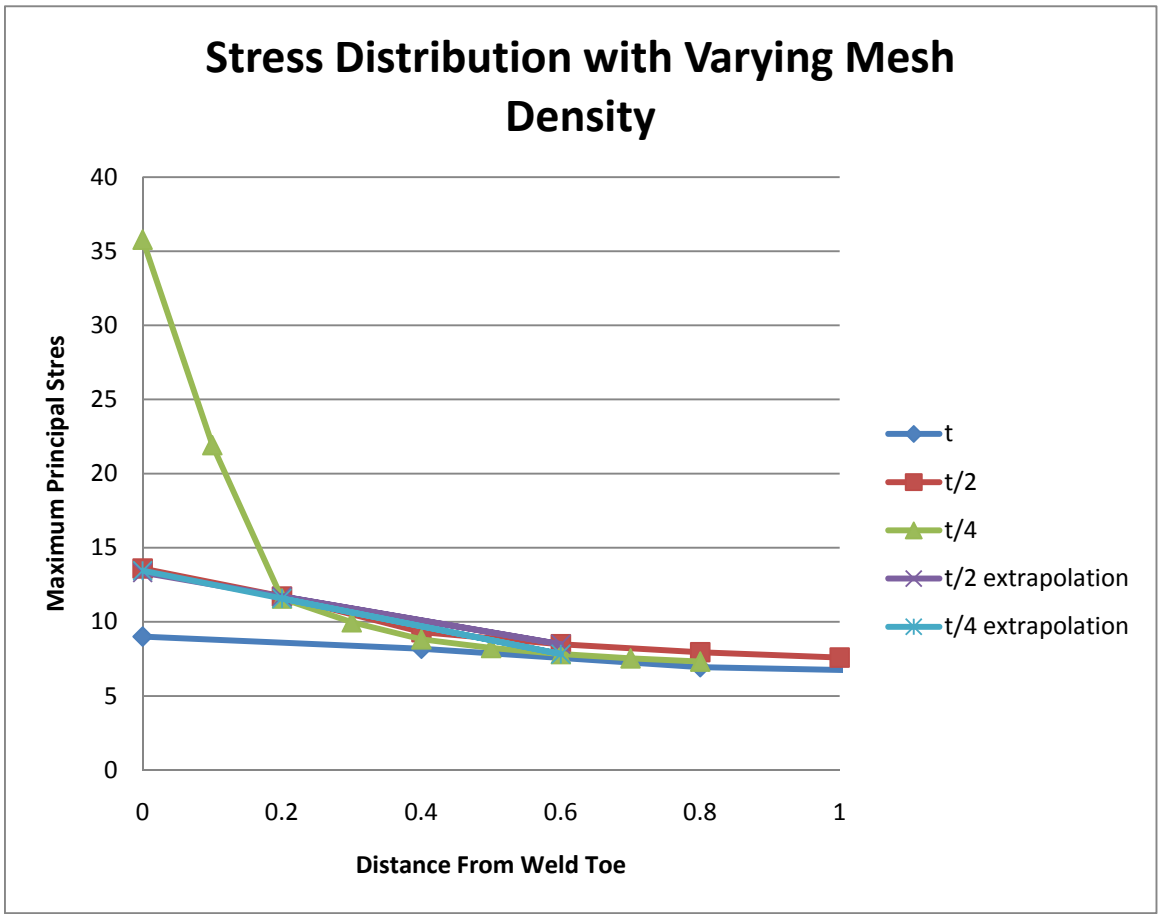

Figure 76. Maximum Principle Stress Distribution for Varying Mesh Density

4.2.5 Hotspot Location

The location of the highest reported stress in ABAQUS was not always the location of the highest stress concentration as determined by the DNV method. As shown in Figure 77, the higher membrane and bending stress occurs at the location which does not have the largest extrapolated hot spot stress. The largest elemental stresses occurred at the toe of the weld on the back side of the angle while the largest extrapolated stress is at the weld toe at the front of the angle. Therefore, in this report the hot spot stress was calculated at the weld toe in both the back and the front of the angle, and the higher stress extrapolated stress was used to calculate the stress concentration factor.

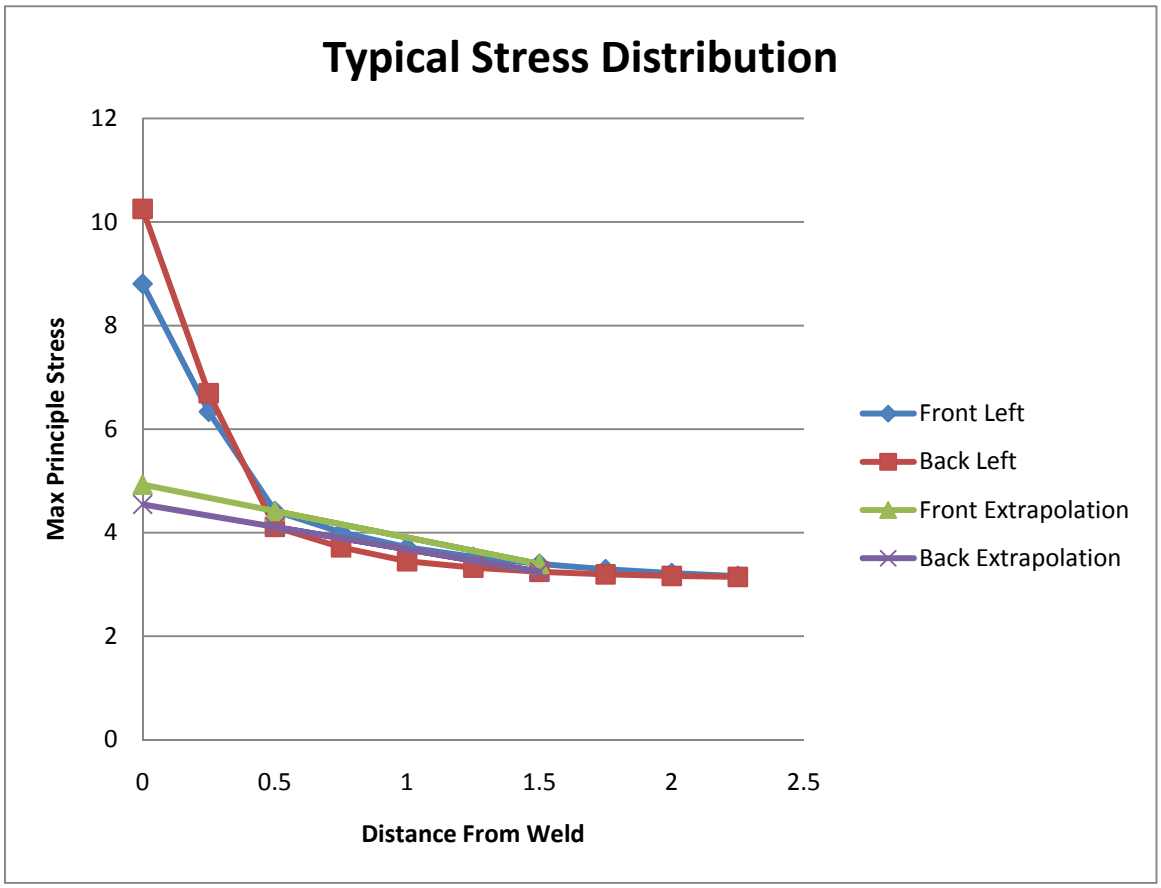

Figure 77. Stress Distribution Comparison between Front and Back Welds

The results of the analysis are shown in Figure 78. The maximum principle stress which was used for the extrapolation calculations is plotted on the mesh. The extrapolation of the stresses will be covered in more detail later in the chapter.

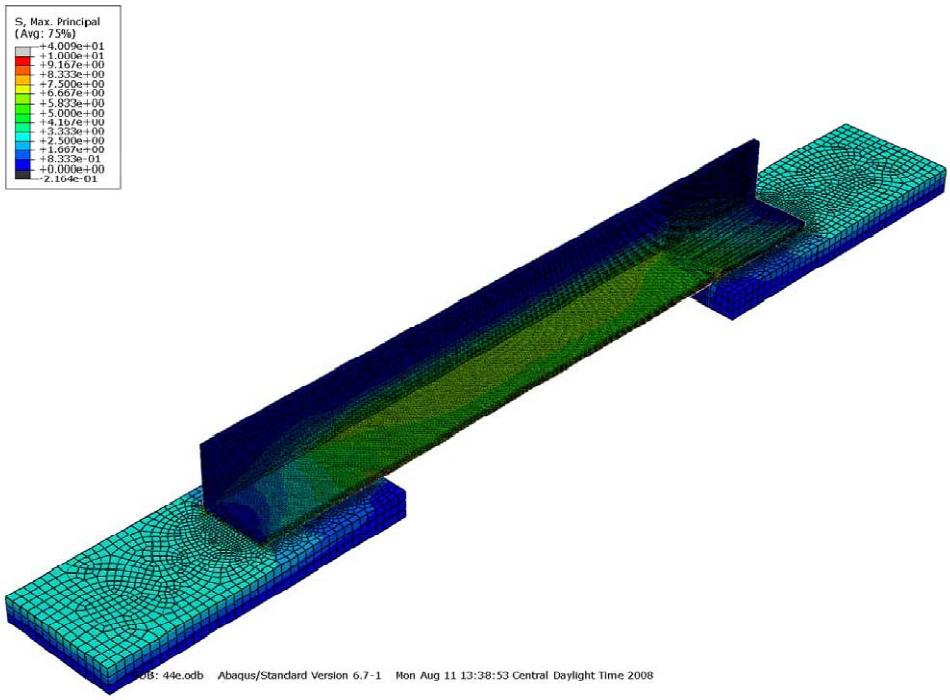

Figure 78. 44E Model with Maximum Principle Stress Plotted

The stress concentrations for each specimen detail were found by dividing the stress at the end of the weld estimated by the extrapolation by then nominal stress in the angle. The nominal stress range in the fatigue tests was multiplied by the stress concentration to estimate the hot spot stress at the crack tip. The hot spot stresses were then plotted on the S-N curve against the same number of cycles. A good model should reorient the data points so that the scatter of the data is reduced and the best fit slope of the data is close to negative three.

The stress concentrations and the calculated hot spot stresses are listed in Table 9. The hot spot stresses are plotted versus the fatigue lives in S-N, Figure 79. The results of the angles tested using test setup 2 and the angles that failed at the end weld were not included because their stress concentration could not be reliably calculated and compared to the rest of the results. The graphs show that the data does not look like the scatter has reduced very much but the data lines up with a slope very close to minus three. The data is lying on the A category line which is the category that corresponds to base metal without a weld or hole. The stress concentration calculations do not include notch effects that occur in the weld so the fatigue performance of the specimens should be less than a category A. The T line in Figure 79 is the line that IIW recommends for estimating fatigue life from hot spot stresses. This discrepancy is probably due to the fact that using a mesh thickness equal to one fourth of the angle thickness instead of equal to angle thickness caused the stress concentration to rise and in turn reflected a higher fatigue performance. However, since the mesh thickness is the same for each specimen the relative difference between their fatigue performances should be the same. The discrepancy could also be due to the fact the weld was not modeled.

Name	Nominal Stress Range	Hot Spot Stress	Stress Concentration Factor	Cycles	A
44b3	8	28	3.50	2924774	6.36E+10
44b4	8	28	3.50	3801386	8.26E+10
53Le3	8	34	4.25	1655604	6.63E+10
53Le4	8	34	4.25	2314378	9.26E+10
53Se1	8	29	3.63	1104311	2.79E+10
53Se6	8	29	3.63	1070376	2.70E+10
53Sb1	8	24	3.00	1764362	2.36E+10
53Sb6	8	24	3.00	1764362	2.36E+10
53Se2	11	40	3.64	824273	5.41E+10
53Se3	11	40	3.64	310191	2.04E+10
44e2	12	47	3.92	231174	2.36E+10
44b1	12	42	3.50	997143	7.32E+10
44b2	12	42	3.50	1025453	7.52E+10
53Le1	12	51	4.25	300052	4.05E+10
53Le2	12	51	4.25	318805	4.31E+10
53Sb4	12	36	3.00	963607	4.35E+10
53Sb5	12	36	3.00	963607	4.35E+10

Table 9. Modified Fatigue Performance Summary

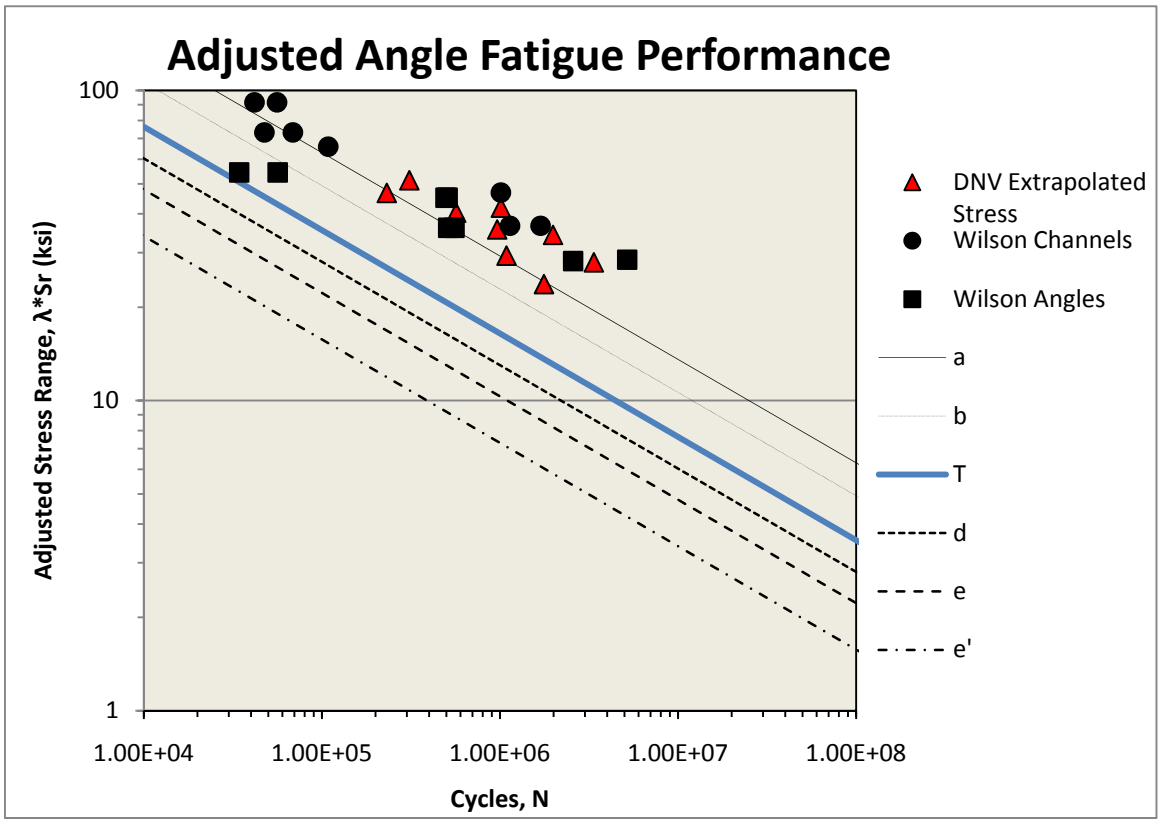

Figure 79. S-N Curve with Modified Stress Ranges

4.3 Summary of FEM Method

The results of the modeling investigation are as follows:

- The hot spot stresses were not sensitive to the element type. Linear reduced integration solid elements were chosen as the element used for the rest of the study.

- A mesh size of one quarter the thickness of the angle was chosen as the optimum element size for this study. The was stress concentration factor calculated with a mesh size of one half the thickness and one quarter the thickness of the angle were essentially equal indicating convergence of the solution.

- DNV extrapolation was chosen as the extrapolation method for this study because it did a better job of capturing the bending and membrane stresses without capturing the nonlinear geometric effects. The AWS method captured some of the nonlinear effects, while the Dong method showed sensitivity to the point at which equilibrium was calculated.

- The modeling of the weld geometry did not have a significant effect upon the stress concentration so it was not included in other models in this study. Also, the complicated

geometry associated weld length was difficult to analyze without changing other important variables.

- All of the models analyzed in the parametric study were modeled and analyzed using the methods described in the preceding chapter unless otherwise noted. This was done to ensure that no mesh sensitivity was induced in the analysis process.

CHAPTER 5

Parametric Study

5.1 Discussion of Parametric Variable Study

A finite element program was used to compare the effects of different geometric variables upon the stress concentration factor at the weld connecting the angle to the connection plate. The geometric variables considered in the study were: connection plate length, width, and thickness; the angle length, thickness, outstanding leg length, inside leg length, back weld length, and front weld length. Figure 80 and Figure 81 depict the geometric variables considered in the study. In the first stage of the parametric study, the effect of each variable was considered individually by holding the other variables constant and the comparing the stress concentration results. The 4x4 angle with equal length welds was used as the base geometry from which all other models were derived. For instance, the short plate model uses a 4x4 angle with equal length welds and the same plate thickness and width, but the plate length is shortened to 15 in. The base geometry can be seen below in Table 10.

Dimension Name	Dimension (in)
Plate Thickness	1 1/2
Plate Width	7 1/8
Plate Length	18 1/4
Angle Length	39 1/2
Outstanding Leg Length	4
Inside Leg Length	4
Angle Thickness	3/8
Front Weld Length	7 3/4
Back Weld Length	7 3/4
End Weld Length	4
Weld Size	3/8

Table 10. Base Model Dimensions

In the following section only one variable was changed for each new model. A table of the various geometries studied in this initial work and their values is given in Table 11. In the second stage of the parametric study, each geometry included in the initial study was used as its own base geometry and all other variables were changed one at a time to produce a full factorial of the geometric variables. This was done to determine the correlation between the geometric variables in the design and will be discussed in the next chapter.

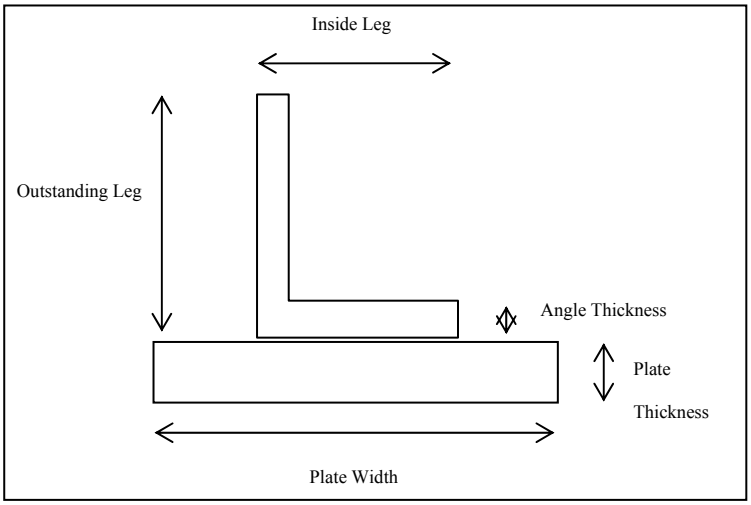

Figure 80. Specimen Cross Section View with Parameter Labels

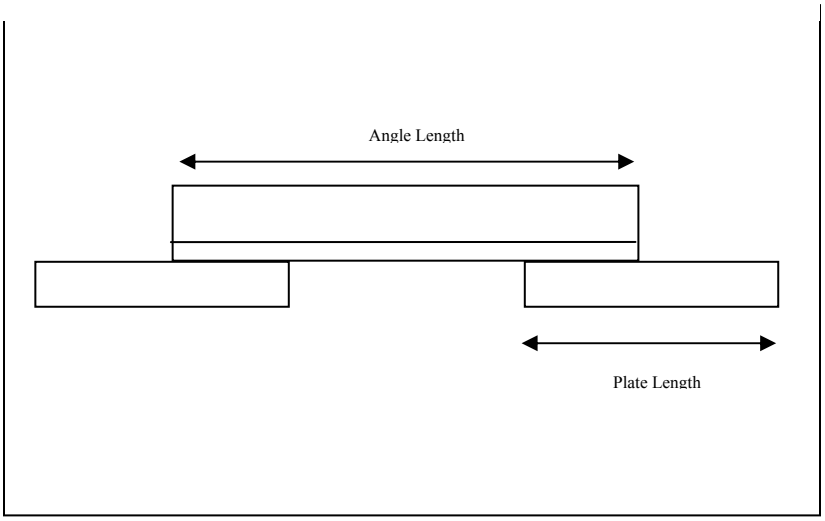

Figure 81. Specimen Side View with Parameter Labels

Geometric Variables	Value 1	Value 2	Value 3
Plate Length	15 in	18.25 in	21 in
Plate Thickness	0.75 in	1.5 in	2.5 in
Plate Width	5 in	7.125 in	9 in
Angle Length	30 in	39.5 in	50 in
Angle Thickness	0.4 in	.75 in	1 in
Outstanding Leg Length	2 in	3.94 in	6 in
Inside Leg Length	2 in	3.94 in	6 in
Front Weld Length	2 in	5 in	7.75 in
Back Weld Length	13.5 in	10.5 in	7.75 in

Table 11. Parametric Variables

The elements used for this analysis were solid linear reduced integration elements and the mesh size for each model was one fourth of the angle thickness in the angle. The stress concentration for each model was computed using DNV method but with the finer one quarter thickness mesh. The traditional DNV method uses a mesh thickness equal to the thickness of the member. Two maximum principal stresses were selected from two nodes on the surface of the angle at distances equal to t and $1.5*t$ away from the weld toe. The stress at the weld toe was then calculated by using a linear extrapolation from the two selected stresses to the weld toe. A more detailed discussion of the analysis methods used can be found in the Chapter 4 on finite element modeling.

5.2 Discussion of Initial Parametric Study

In the following section each variable will be plotted against the stress concentration factor and discussed. An analysis of the behavior and implications of each plot will be included.

Below, in Figure 82, the stress concentration factor plotted against the connection plate thickness. As the thickness of the plate increases the stress concentration decreases, and the relationship appears linear. Three plate thicknesses were evaluated .75, 1.5, and 2.5 inches. The stress concentration factor decreased from 4 and 3 as the plate thickness was increased. A linear best fit line of this plot yields a slope of approximately negative 0.5. The out of plane stiffness of the plate is increasing relative to the out of plane stiffness of the angle which reduces the bending of the angle.

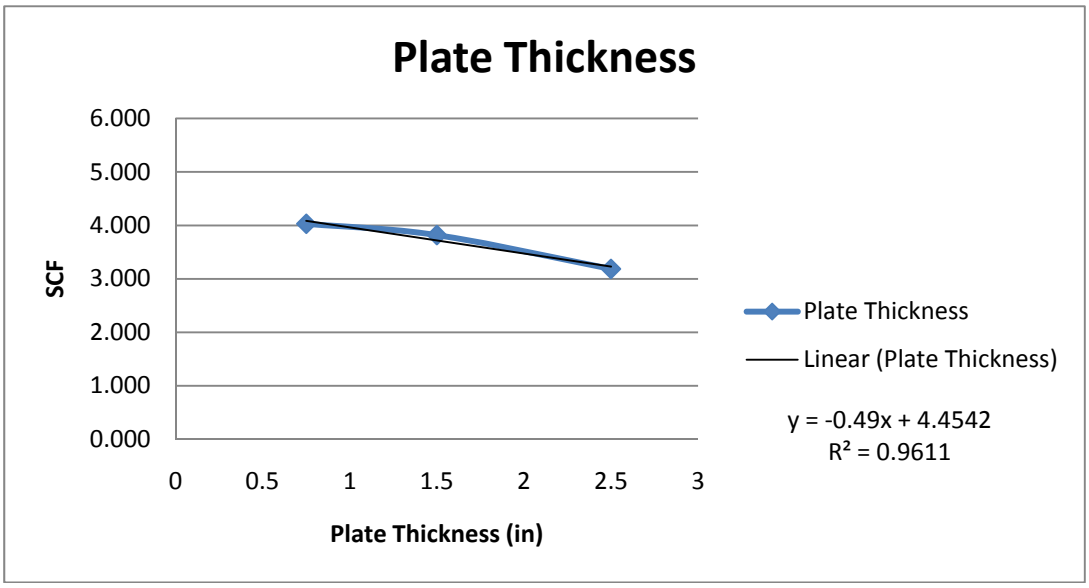

Figure 82. Plate Thickness vs. Stress Concentration Factor

In Figure 83, the stress concentration factor is plotted against the plate width. According to the plot, the plate width does not seem to influence the stress concentration factor at all. The plate width varies between 5 and 9 inches and the stress concentration factor is almost constant at 3.75. A linear best fit line yields a slope of negative 0.03, but the correlation coefficient is low and the variation may be attributed to error in the finite element analysis. As the plate width increases the in plane stiffness of the plate increases relative to the angle, but the plate is so stiff in each case that the stress concentration is not affected. The small influence of plate width relative to plate thickness seems reasonable since out of plane bending stiffness of the plate is a linear function of the width and a cubic function of the thickness so the plate thickness.

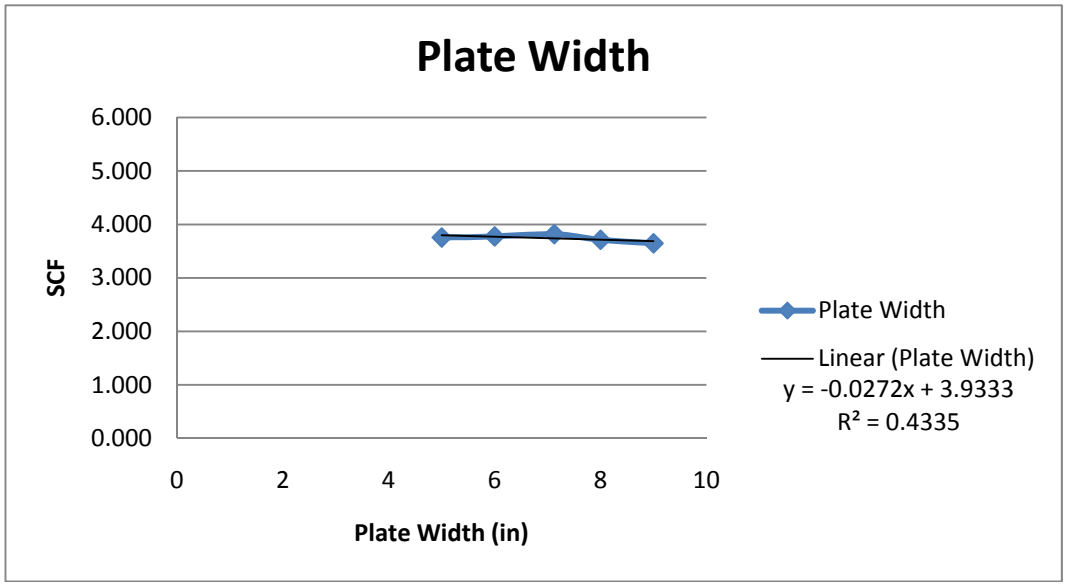

Figure 83. Plate Width vs. Stress Concentration Factor

In Figure 86, the stress concentration factor is plotted against the plate length. As the plate length increases the stress concentration increases linearly. The plate length increases from 15 and 21 inches and the stress concentration factor increases from 3.75 and 4.1. A linear best fit line yields a slope of 0.06. Figure 84 and Figure 85 show the deformations of a 15 inch plate and a 21 inch plate respectively with the same deformation scale. Notice how the longer plate deflects much more than the shorter plate at the toe of the weld. As the plate length increases and deflects more, the eccentricity of the plate force at the angle is reduced. However, the stress concentration factor is increasing as the plate length increases, so there must be some other effect that is increasing the stress.

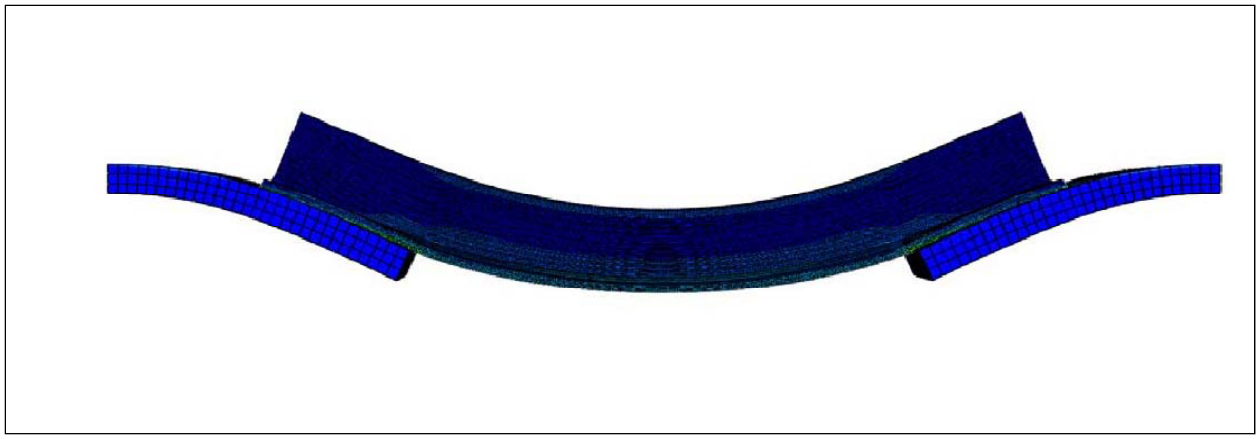

Figure 84. Short Plate Deformation

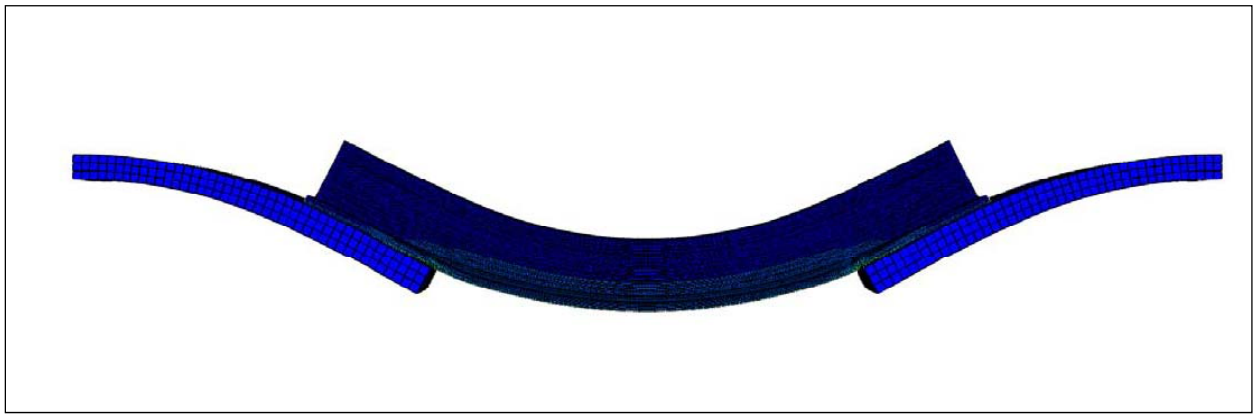

Figure 85. Long Plate Deformation

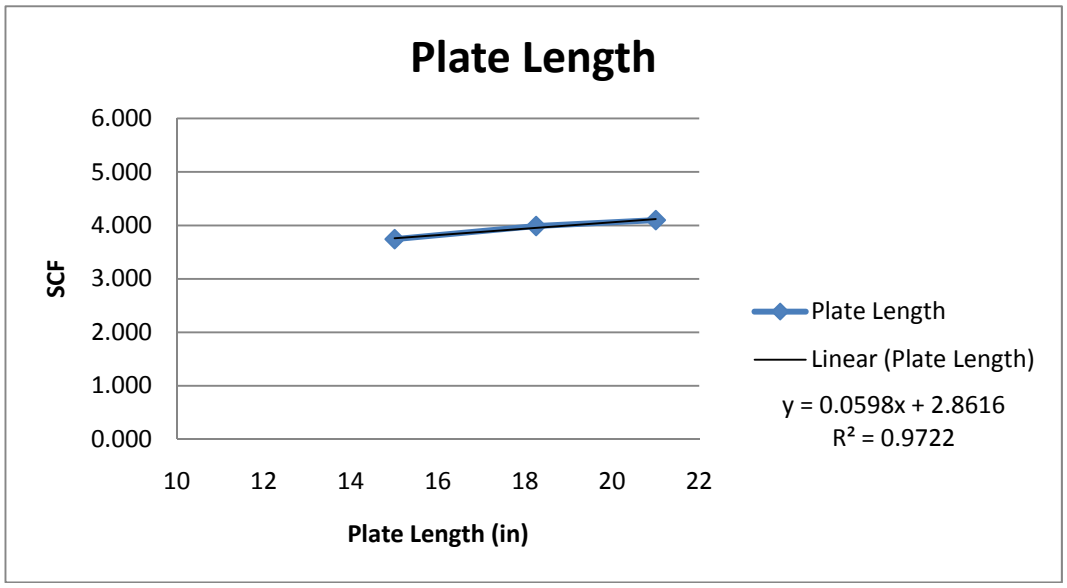

Figure 86. Plate Length vs. Stress Concentration Factor

In Figure 89, the stress concentration factor is plotted against the angle length. As the angle length increases the stress concentration factor decreases linearly. The angle length varies between 30 and 50 inches and the stress concentration varies between 3.6 and 4.1. A linear best fit line yields a slope of negative 0.02. As the angle length increases the angle deflects more which reduces the stress concentration at the weld. This can be seen below in Figure 87 and Figure 88 where the deformations of a 30 inch long angle and a 50 inch long angle are compared using the same base model, load and deformation scale. The angle deflects much more abruptly at the weld toe in the short angle model while the long angle model has a much more smooth transition at the connection.

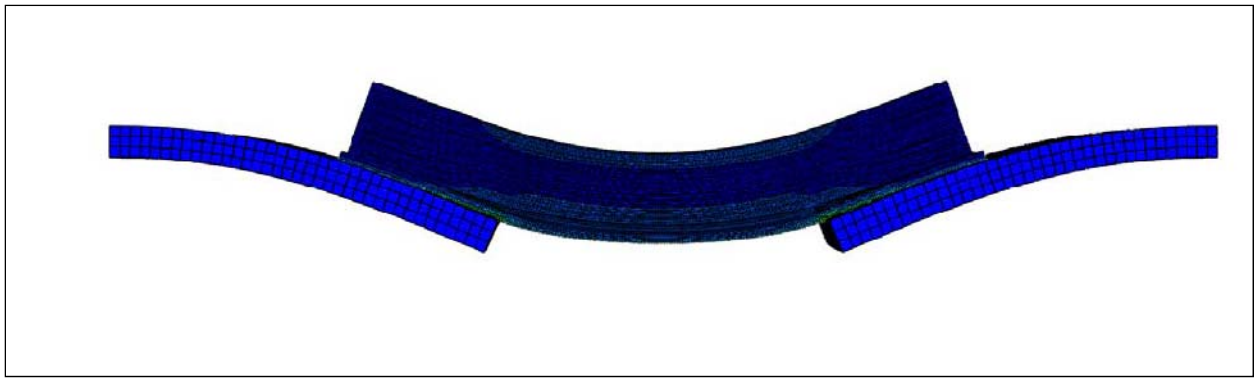

Figure 87. Short Angle Deformation

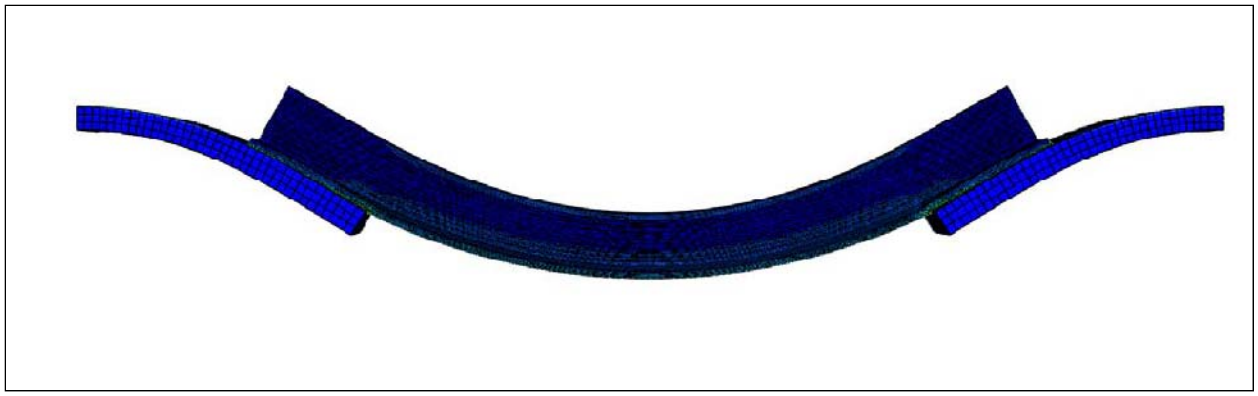

Figure 88. Long Angle Deformation

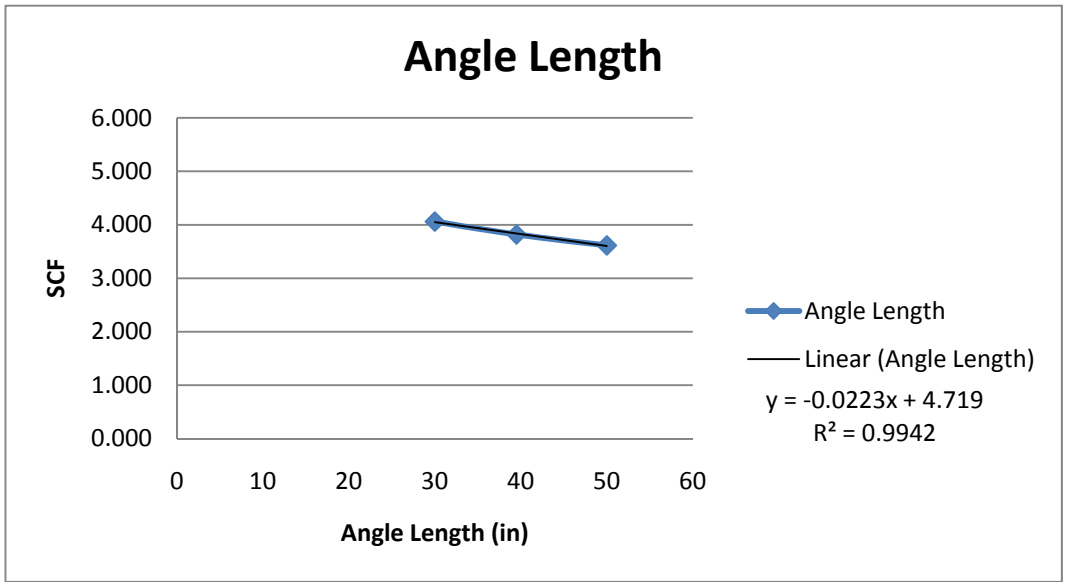

Figure 89. Angle Length vs. Stress Concentration Factor

In Figure 90, the stress concentration factor is plotted against the angle thickness. As the thickness of the angle increases the stress concentration factor decreases. The angle thickness increases from 0.4 and to 1 inch and the stress concentration factor decreases from 4.0 to 3.8. A linear best fit line yields a slope of negative 0.5. As the angle thickness increases the angle becomes stiffer, but the eccentricity of the load is increased as well. The increase in stiffness of the angle when the angle thickness is increased has a greater effect on the stress concentration factor than the eccentricity of the angle relative to the line of action of the force that occurs with the increase in thickness.

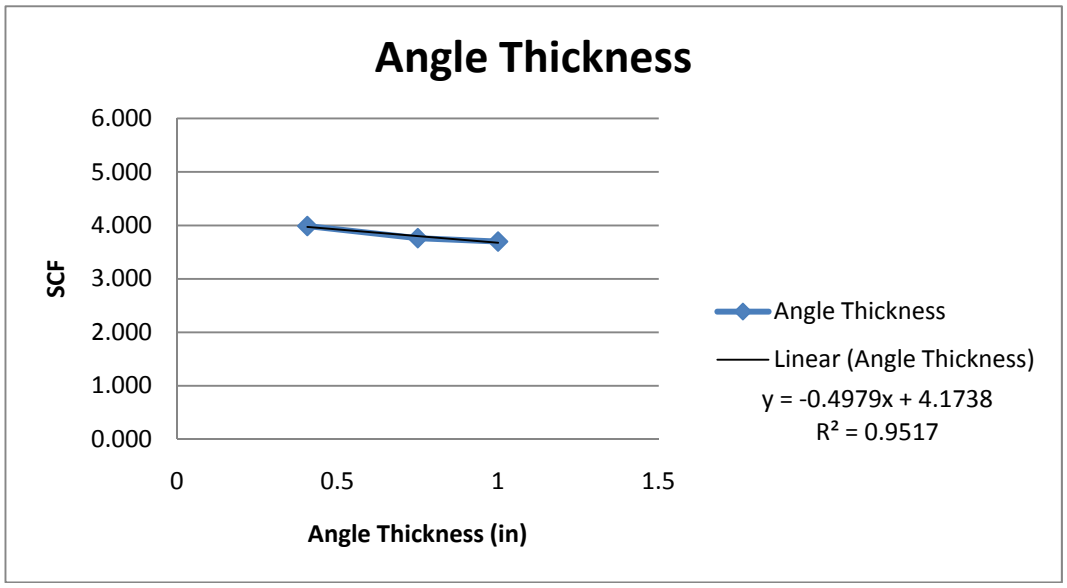

Figure 90. Angle Thickness vs. Stress Concentration Factor

In Figure 91, the outstanding leg length of the angle is plotted against the stress concentration factor. As the outstanding leg length is increased the stress concentration factor increases linearly. The outstanding leg length varies between 2 and 6 inches and the stress concentration factor varies between 2.6 and 4.7. This parameter produces the largest variation in stress concentration among the variables examined in the first stage of the study. A linear best fit line yields a slope of 0.5. As the outstanding leg length increases the eccentricity of the load increases, but the stiffness of the angle also increases. The eccentricity of the load has a greater effect on the stress concentration factor than the angle stiffness.

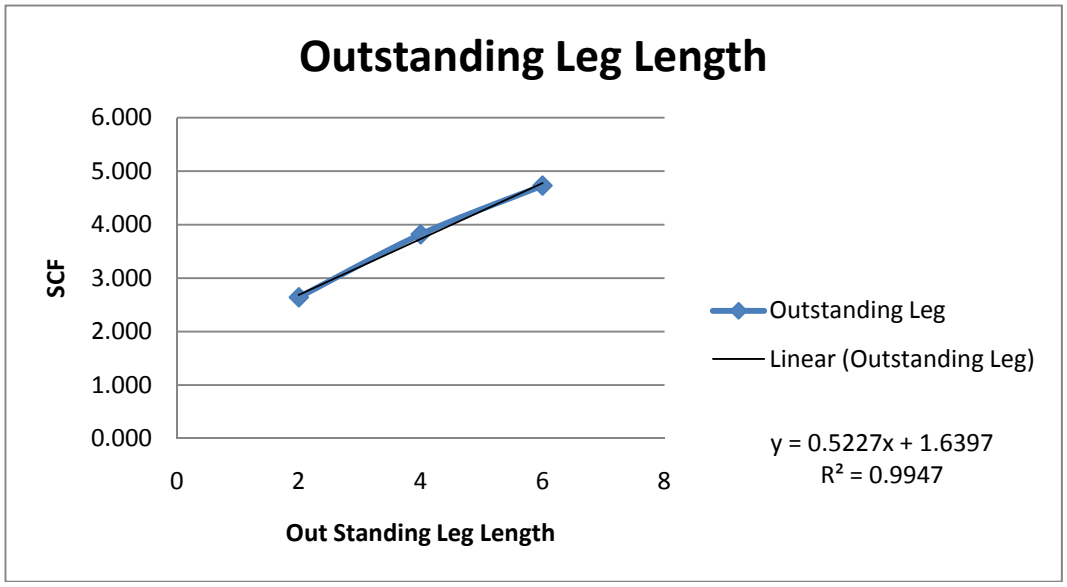

Figure 91. Outstanding Leg Length vs. Stress Concentration Factor

In Figure 92, the inside leg length of the angle is plotted against the stress concentration factor. The values of the inside leg length do not seem to give any real trend in the values. There is a lot of scatter in the data and the cause of this was not determined. It may be due to the fact that changing the inside leg length changes other variables that affect the stress concentration factor such as the changing eccentricity of the angle.

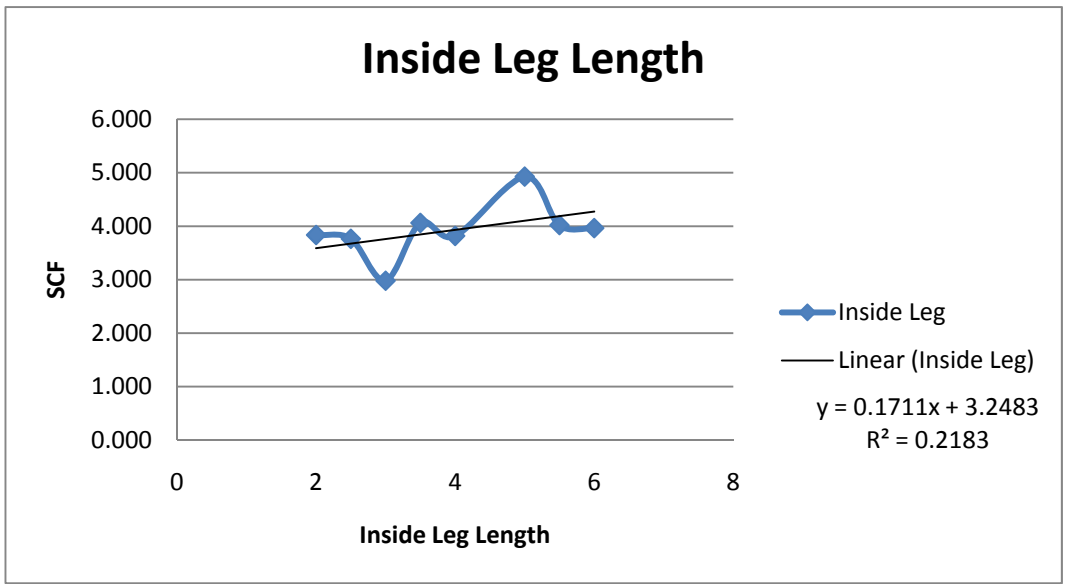

Figure 92. Inside Leg Length vs. Stress Concentration Factor

5.3 WELD STUDY

Studying the effect of weld geometry upon the stress concentration factor was more difficult because it was difficult to isolate the weld length and change it without changing other parameters. The effect of weld geometry was examined in three different methods. Each weld geometry model used the same base 4x4 angle with equal length weld model. In the first method, the length of the front weld was changed without changing the end or back welds. The second method kept the total weld length equal while varying the back and front welds. However, when the back weld was lengthened, the distance between the end of the plate and the end of the weld was shortened. The effect of changing the distance from the end of the plate to the end of the weld was investigated in a third study. In the thirds study, the total weld length kept constant while changing the length of the back and front welds and plate was lengthened to keep the distance from the end of the plate to the end of the weld constant.

In Figure 93 below, the front weld length is varied between 0 inches and 7.75 inches. A front weld length of 0 inches represents no weld on the front side of the angle so that there is only the end weld and back weld. The stress concentration factor for this case is taken at the weld toe of the end weld where the front weld would have intersected. The maximum stress concentration factor located at either the end of the back weld or front weld does not change very much between the different lengths, and does not have any discernable trend. The stress concentration could be changing because the in plane eccentricity is changing and the total weld

length is changing. Figure 94 below shows the variation in the stresses computed at the weld to in the front and back of the angle. As the front weld length increases the maximum stress moves from the weld toe at the back of the angle to the front of the angle.

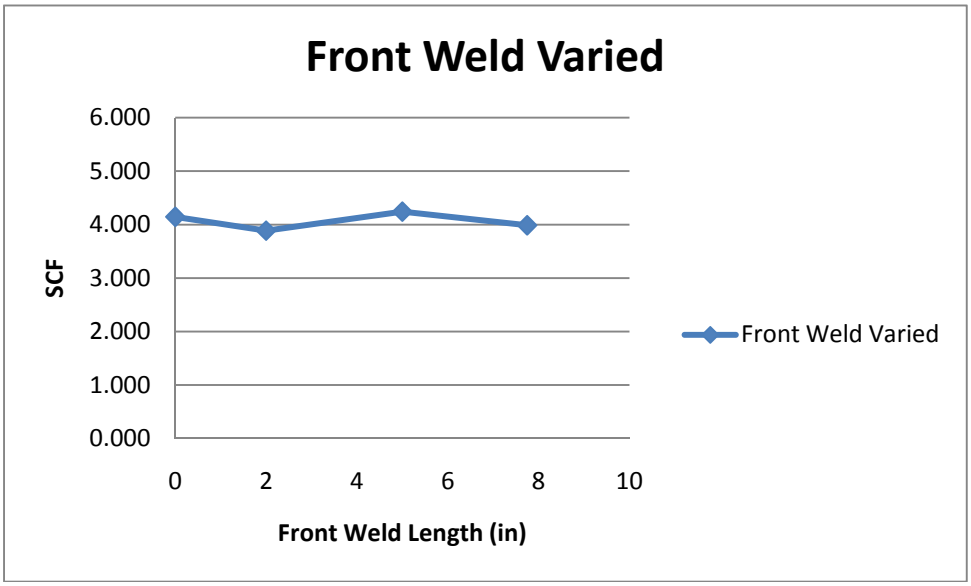

Figure 93. Front Weld Length vs. Maximum Stress Concentration Factor

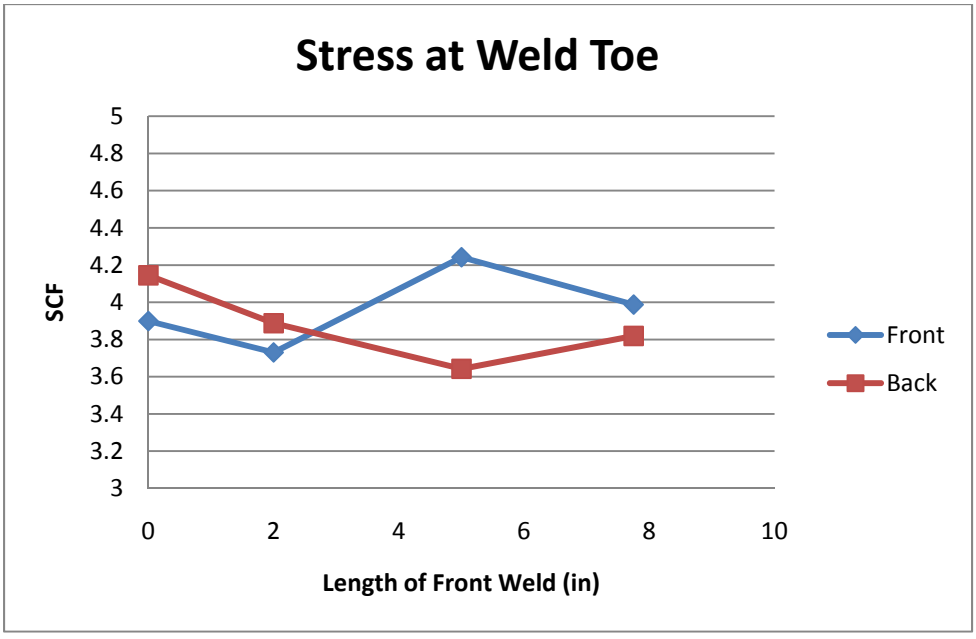

Figure 94. Front and Back Stress with Varying Weld Length

Figure 95 below shows the variation in the maximum stress concentration factor located at either the end of the front weld or back weld when the length of the front and back welds lengths are changed to keep a constant total weld length. The stress concentration factor does not vary significantly with the change in front weld length. This indicates that the in plane eccentricity is not very significant in determining the stress concentration. It is interesting to note that in this model the back stress always controls. The relationship between the front stress and the back stress can be seen in Figure 96 below.

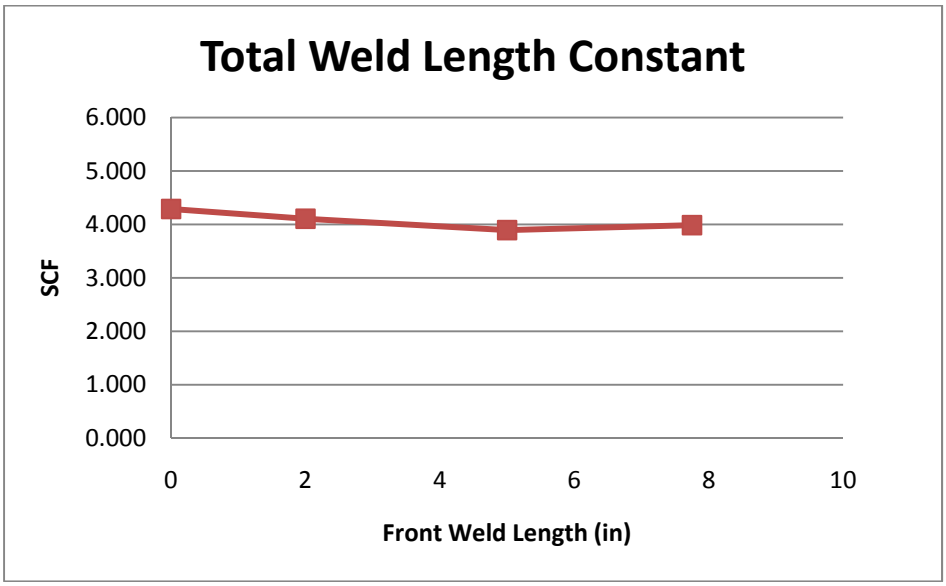

Figure 95. Front Weld Length vs. Stress Concentration Factor with Constant Total Weld Length

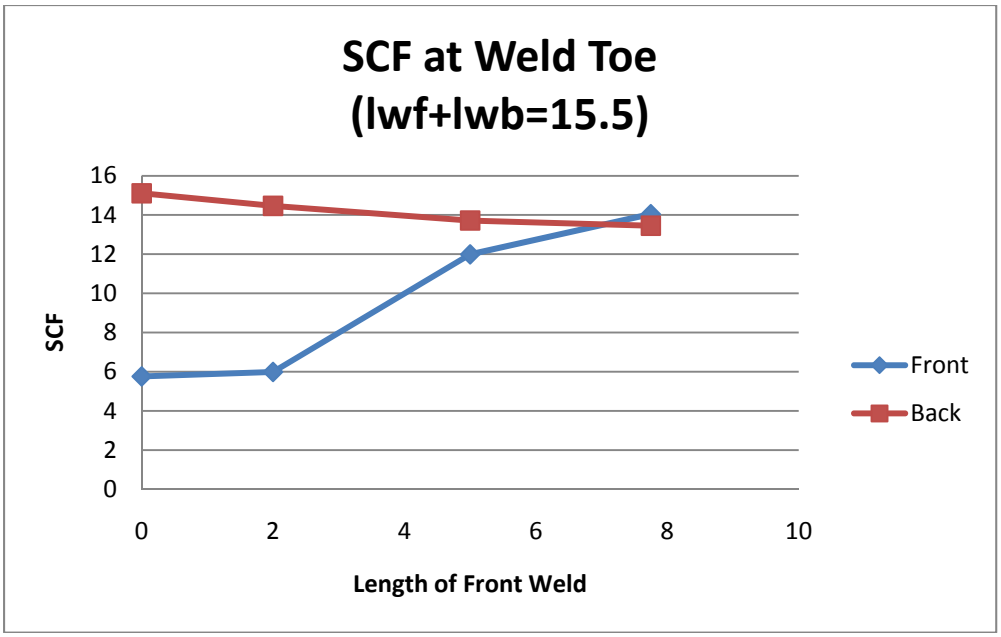

Figure 96. Front and Back Stress with Constant Total Weld Length

Figure 97 below shows the variation in stress concentration factor with respect to the front weld length, but with a constant total weld length and a varying plate length. The plate length was varied in order to keep the distance from the end of the angle to the end of the plate constant. The stress concentration factor varies more than in the previous model. The change in stress concentration is probably due to the effect of lengthening the plate which has been discussed earlier in this section. As the weld length gets longer and the plate length approaches the original plate length used for the previous model, the stress concentrations become almost equal. The relationship between the front stress and the back stress also remains the same as can be seen in Figure 98 below.

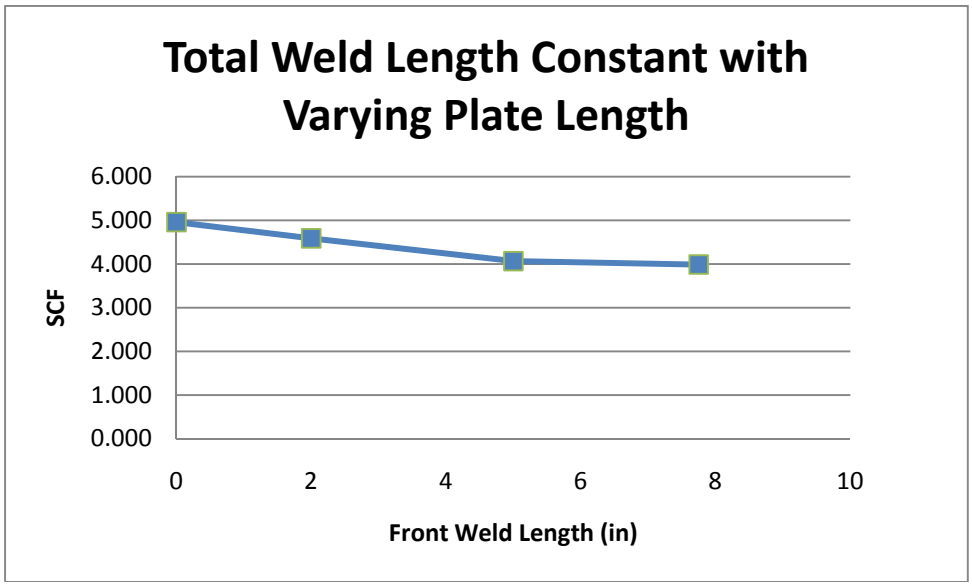

Figure 97. Front Weld Length vs. Stress Concentration Factor with Constant Total Weld Length and Varying Plate Length

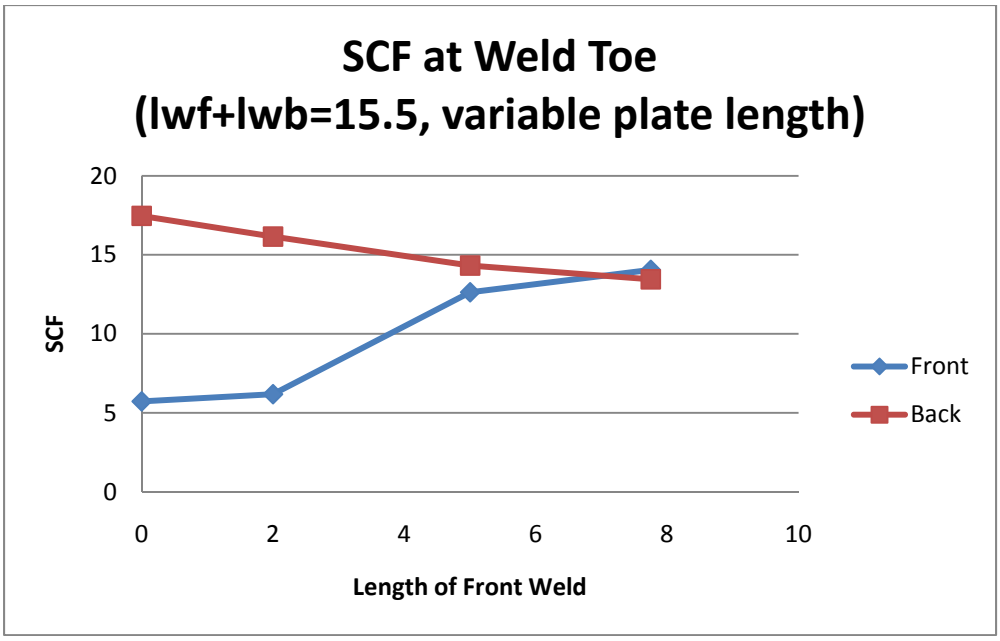

Figure 98. Front and Back Stress with Constant Total Weld Length and Varying Plate Length

In conclusion, the weld length does not seem to have a very large effect upon the stress concentration of the angle, even for the extreme examples that were used in this study. Other geometric effects such as the outstanding leg length, plate thickness, angle length and plate length have much larger effects on the stress concentration factor.

5.4 Parametric Study Second Stage Discussion

In Figure 99 below, the plate thickness is varied for three different angle lengths. As the plate thickness increases the stress concentration factor decreases and as the angle length increases the stress concentration factor decreases. As the plate thickness increases the correlation between the angle length and the plate thickness actually reverses. For small plate thicknesses the longer angle has a higher stress concentration but for the larger plate thicknesses the longer angle has a lower stress concentration. However, the difference in stress concentrations for the thin plate is very small. It may be that there is a small error associated with the finite element model and those stress concentrations should be equal. As the plate gets thinner the angle length seems to have little effect upon the stress concentration of the angle. As the plate gets thicker the angle length increasingly changes the stress concentration.

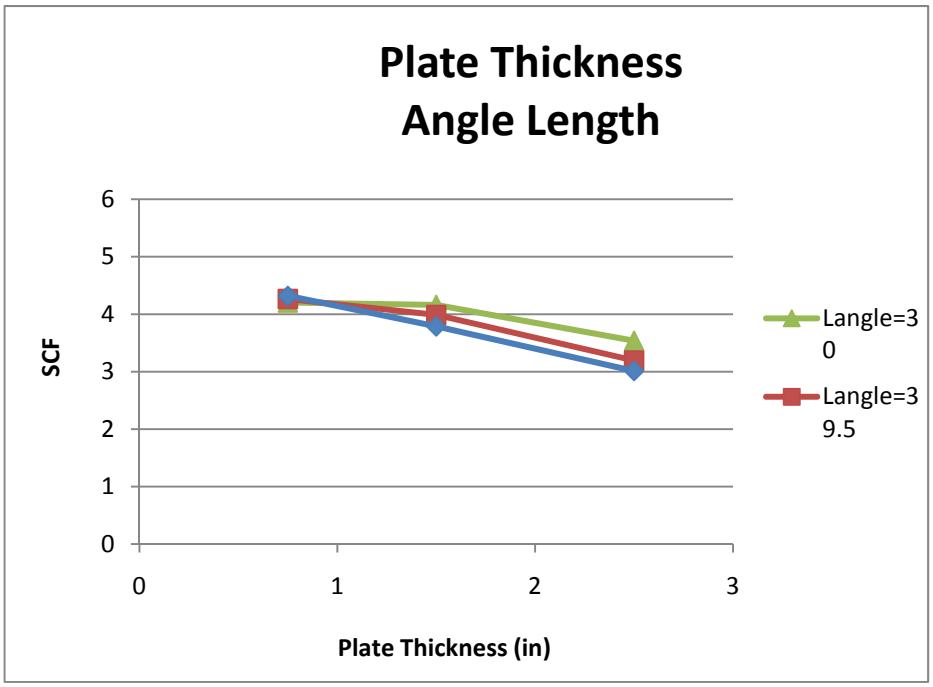

Figure 99. Plate Thickness and Angle Length vs. Stress Concentration Factor

In Figure 100 below, the plate thickness is varied for three different angle thicknesses. As the plate thickness increases the stress concentration decreases and the effect of the angle thickness upon the stress concentration decreases. The reduction of the effect of the angle thickness maybe a result of the plate is getting stiffer relative to the angle reducing the effect of the angle thickness. Increasing the angle stiffness also increases the eccentricity of the load and a stiffer plate would not be affected as much by a higher moment. Increasing the angle thickness decreases the stress concentration factor.

Figure 100. Plate Thickness and Angle Thickness vs. Stress Concentration Factor

In Figure 101 below, the plate thickness is varied for three different outstanding angle leg lengths. As the plate thickness increases the stress concentration factor decreases and as the outstanding leg length increases the stress concentration factor increases. As the outstanding leg length increases, the eccentricity increases, which causes a higher SCF. However, when the plate thickness is changed the outstanding leg length has little effect upon the stress concentration factor. This may be because the thin plate is able to bend more and does not cause such high stress concentrations despite the added bending of a larger outstanding leg.

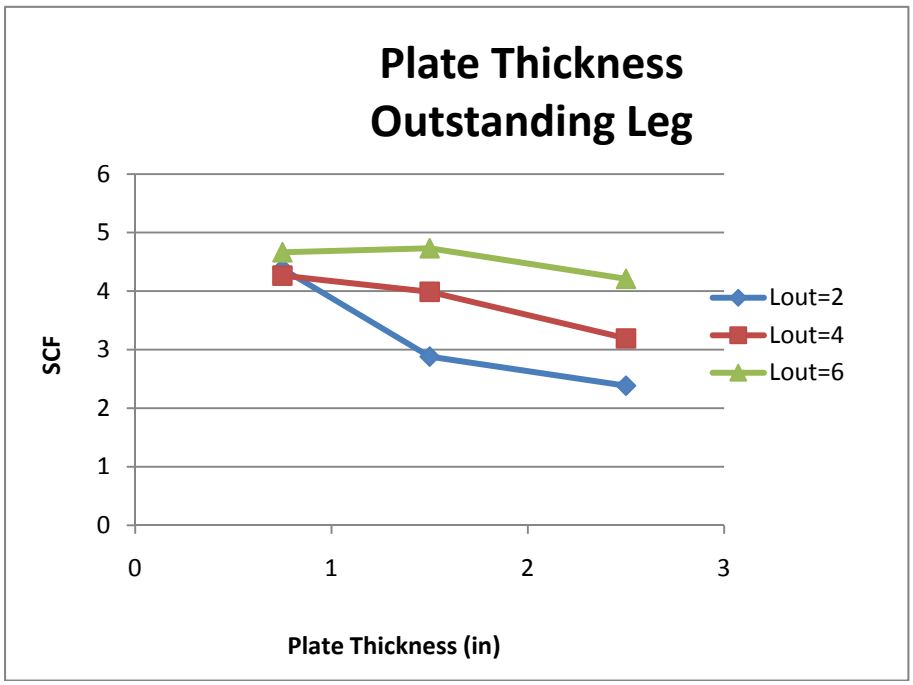

Figure 101. Plate Thickness and Outstanding Leg Length vs. Stress Concentration Factor

In Figure 102 below, the plate thickness is varied for three different inside angle leg lengths. As the plate thickness increases the stress concentration factor decreases and as the inside leg length increases the stress concentration factor increases but only slightly. There is little or no correlation between these two parameters. When the inside leg length equals two inches the stress concentration actually increases and then decreases as the plate thickness is increased. The effect of the inside leg length upon the stress concentration appears to be small.

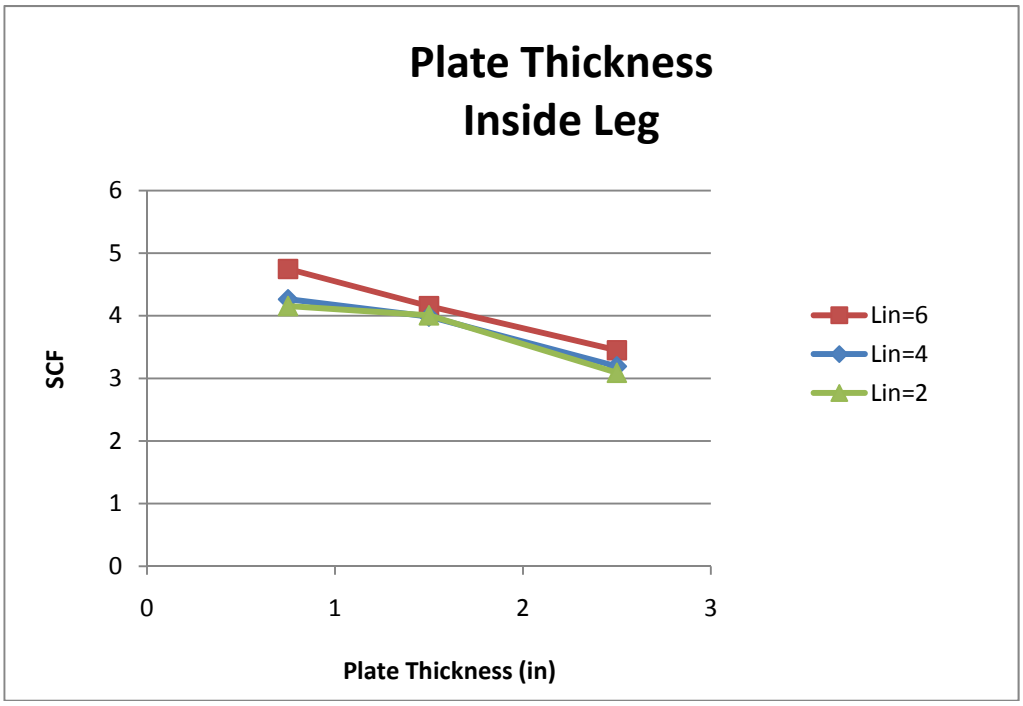

Figure 102. Plate Thickness and Inside Leg Length vs. Stress Concentration Factor

In Figure 103 below, the angle length is varied for three different inside angle leg lengths. As the angle length increases the stress concentration factor decreases and the effect of the length of the inside leg is very small. As the angle length increases the effect of the inside leg length upon the stress concentration factor increases. However, these are very small changes compared to other parameters.

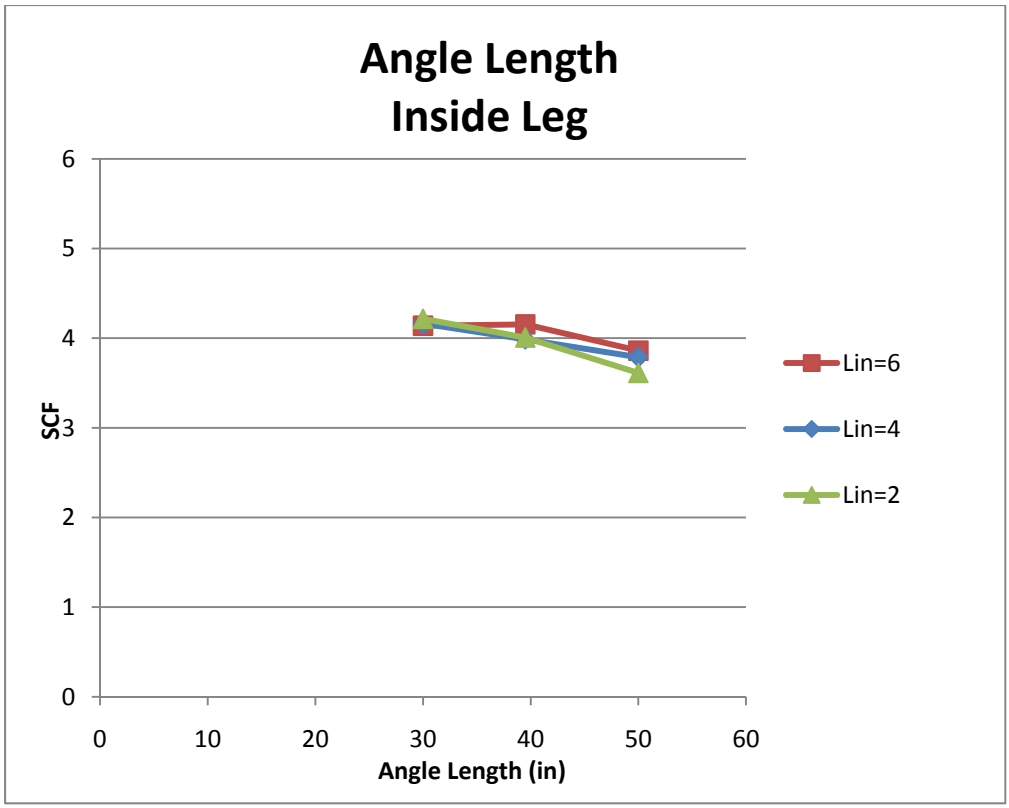

Figure 103. Angle Length and Inside Leg Length vs. Stress Concentration Factor

In Figure 104 below, the angle length is varied for three different outstanding angle leg lengths. The stress concentration factor decreases as the angle length is increased and increases as the outstanding leg length increases. Changing the outstanding leg length does not affect the relationship between angle length and stress concentration. This indicates that there is no correlation between the two variables.

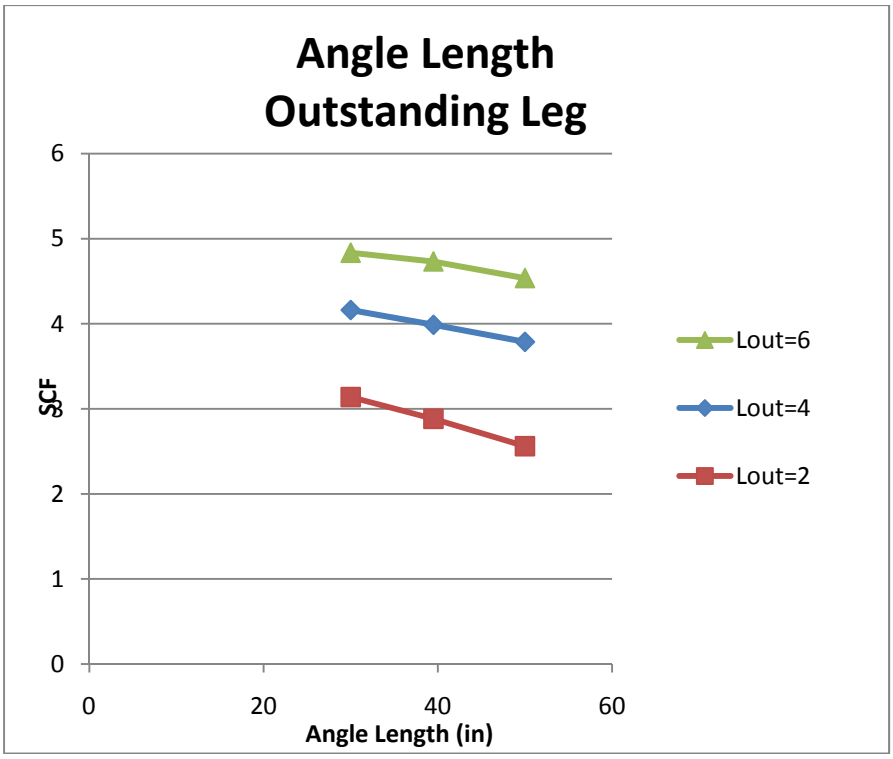

Figure 104. Angle Length and Outstanding Leg Length vs. Stress Concentration Factor

In Figure 105 below, the angle length is varied for three different angle thicknesses. As the angle length increases the stress concentration factor decreases and as the angle thickness increases the stress concentration factor decreases. Increasing the angle thickness causes the out of plane eccentricity to increase and the stiffness of the angle to increase, while increasing the angle length decreases the stiffness of the angle. As the angle thickness increases, the effect of the thickness upon the stress concentration factor is less. This may be because the effect of the thickness upon the stiffness of the angle becomes more significant as the outstanding leg becomes shorter.

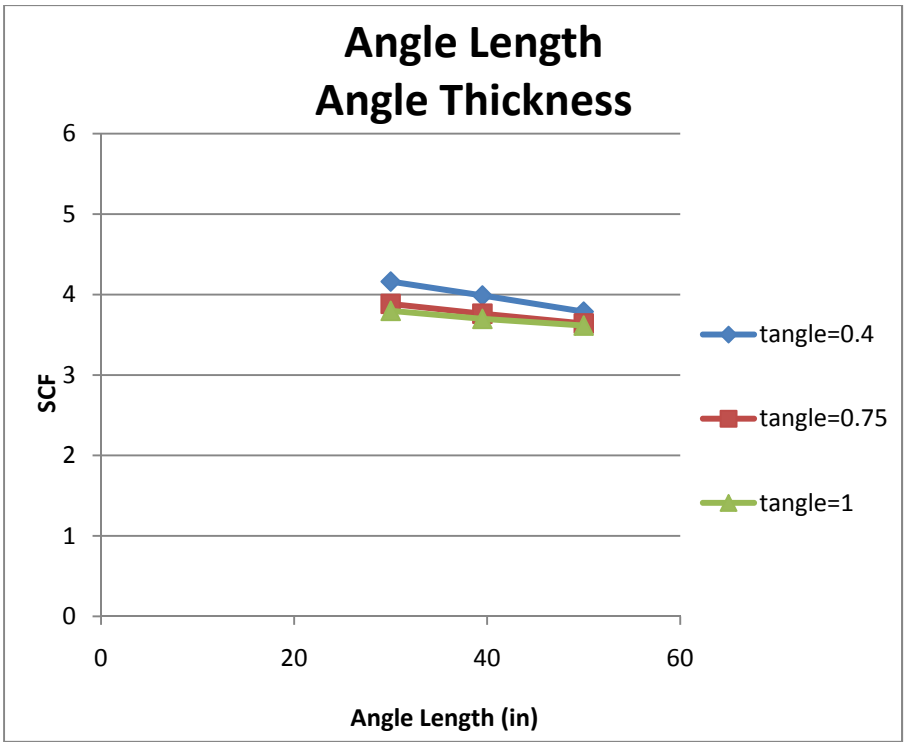

Figure 105. Angle Length and Angle vs. Stress Concentration Factor

In Figure 106 below, the outstanding angle leg length is varied for three different angle thicknesses. As the outstanding leg length increases the stress concentration factor increases and as the angle thickness increases the stress concentration factor decreases. Increasing the outstanding leg length increases in the out of plane eccentricity and increases the out of plane stiffness of the angle. Increasing the angle thickness increases the out of plane eccentricity and increases the stiffness of the angle. When the outstanding leg length is small the thickness of the angle has very little effect upon the stress concentration. However, when the outstanding leg length is large, the thickness of the angle has a larger effect upon the stress concentration. Also, as the angle thickness is increased the stress concentration is reduced.

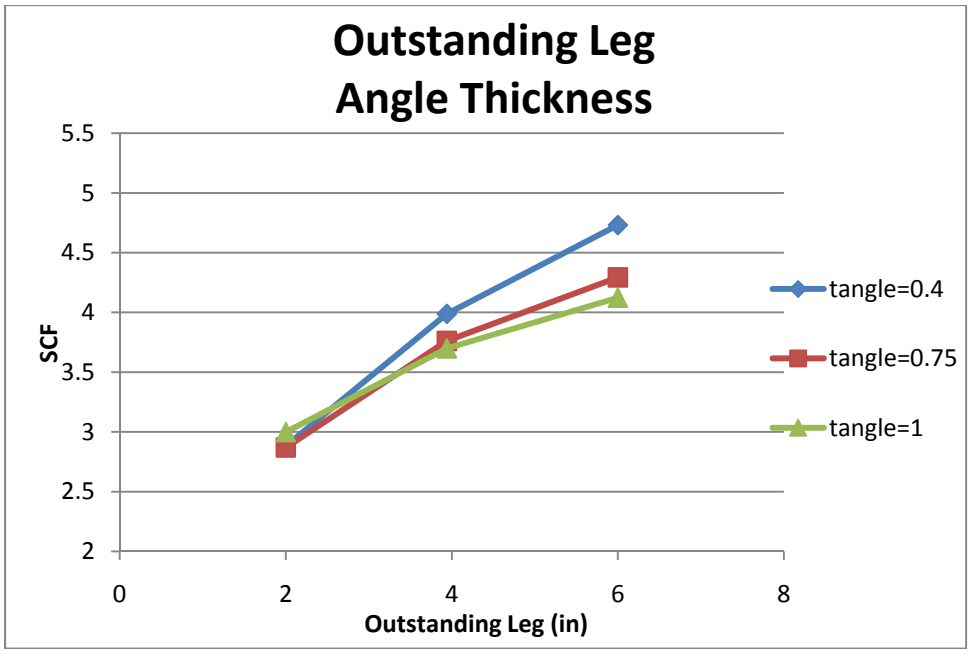

Figure 106. Outstanding Leg Length and Angle Thickness vs. Stress Concentration Factor

In Figure 107 below, the inside leg length is varied for three different angle thicknesses. As the inside angle leg length increases the stress concentration increases slightly and as the angle thickness increases the stress concentration factor decreases. Larger inside leg length decreases the eccentricity and increases the stiffness of the angle. The effect of the angle thickness upon the stress concentration was very small for varying leg lengths.

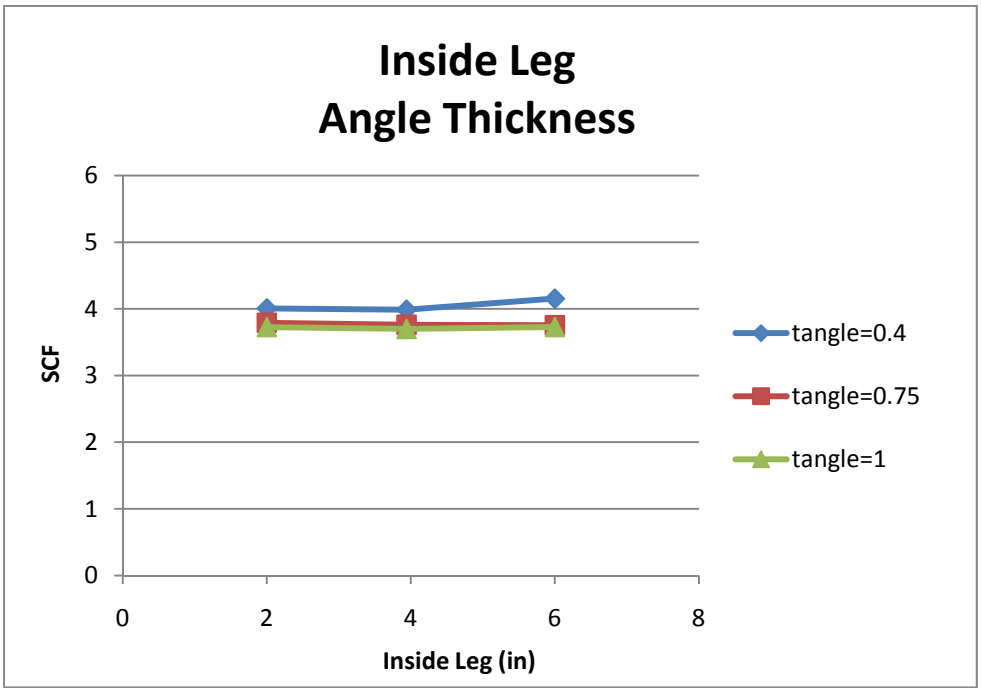

Figure 107. Inside Leg Length and Angle Thickness vs. Stress Concentration Factor

In Figure 108 below, the plate length is varied for three different plate widths. As the plate length increases the stress concentration factor increases and as the plate width increases the stress concentration factor decreases. Increasing the plate length increases the flexibility of the specimen. Increasing the plate width increases the in-plane stiffness of the plate. There is little correlation between the two parameters.

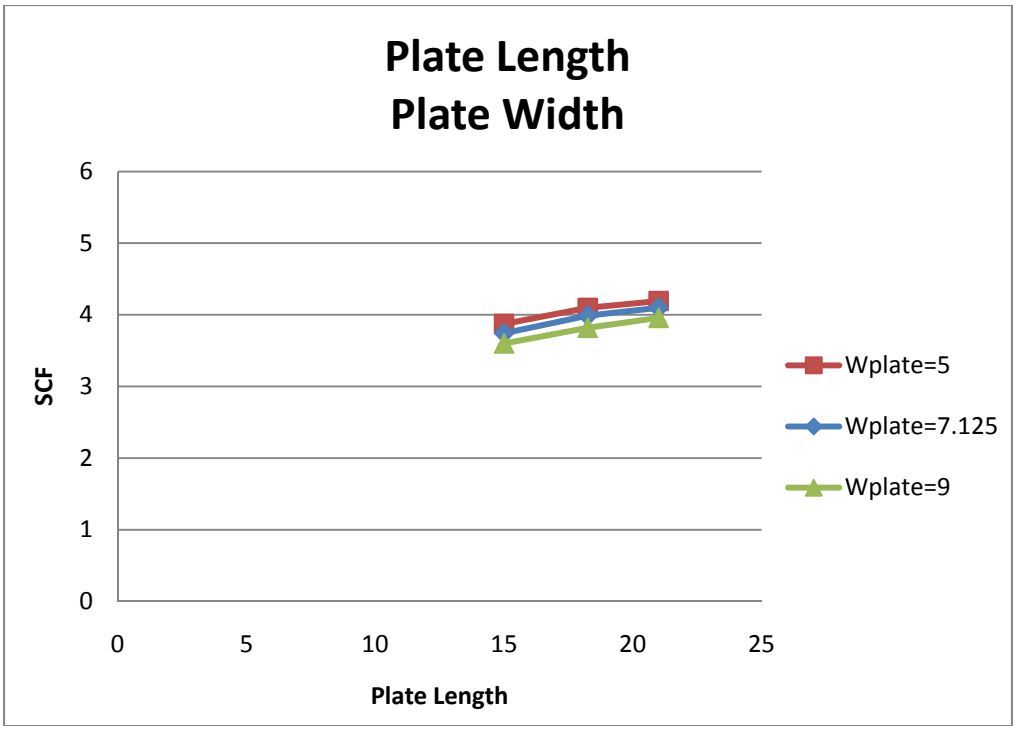

Figure 108. Plate Length and Plate Width vs. Stress Concentration Factor

In Figure 109 below, the plate length is varied for three different angle thicknesses. As the plate length increases the stress concentration factor increases and as the angle thickness increases the stress concentration factor decreases. Increasing the plate length increases the flexibility of the connection. Increasing the angle thickness increases the out of plane eccentricity, deceases the in plane eccentricity, and increases the stiffness of the angle. The plate length does not seem to affect the relationship between the angle thickness and the stress concentration factor.

Figure 109. Plate Length and Angle Thickness vs. Stress Concentration Factor

In Figure 110 below, the plate length is varied for three different angle lengths. As the plate length increases the stress concentration increases and as the angle length increases the stress concentration decreases. Increasing the plate length increases the flexibility of the plate and increasing the angle length increases the flexibility of the angle. As the plate length is increased the effect of the length of the angle length is slightly less.

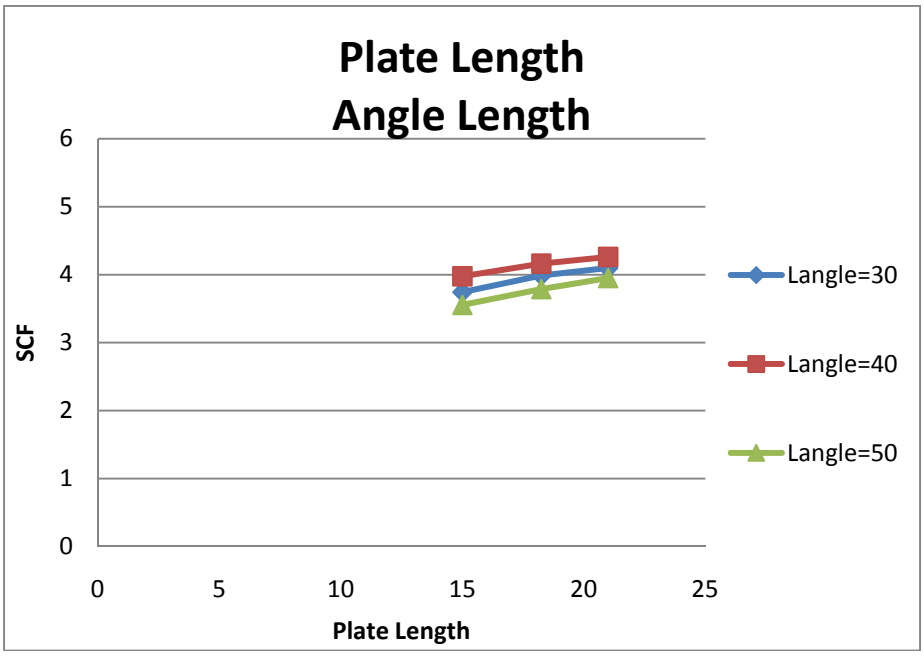

Figure 110. Plate Length and Angle Length vs. Stress Concentration Factor

In Figure 111 below, the plate length is varied for three different outstanding leg lengths. As the plate length and the outstanding leg length are increased the stress concentration factor increases. Increasing the outstanding leg increases the out of plane eccentricity and stiffness of the angle and increasing the plate length increases the flexibility and deflection of the plate. It does not appear as if there is any significant correlation between these two parameters. The outstanding leg length has the greatest effect upon the stress concentration factor.

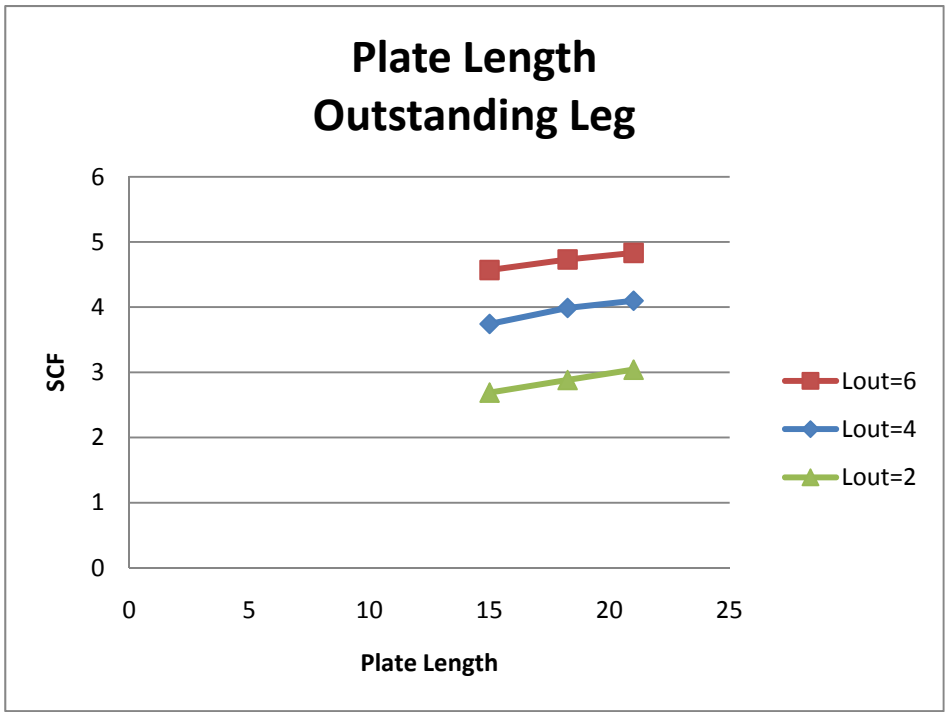

Figure 111. Plate Length and Outstanding Leg Length vs. Stress Concentration Factor

In Figure 112 below, the plate length is varied for three different inside angle leg lengths. As the plate length increases the stress concentration factor increases. As the inside leg length increases the stress concentration factor increases, but only when the inside leg length becomes very large relative to the plate width. As the plate length increases the flexibility and deflection of the plate increases and as the inside leg length increases the in plane eccentricity and stiffness of the angle increases. However, the effect of the plate length upon the relationship between the inside leg length and the stress concentration factor is very small.

Figure 112. Plate Length and Inside Leg Length vs. Stress Concentration Factor

In Figure 113 below, the plate length is varied for three different plate thicknesses. As the plate length increases the stress concentration factor increases and as the plate thickness increases the stress concentration factor decreases. Increasing the plate length increases the flexibility and deflection of the plate. Increasing the plate thickness increases the out of plane eccentricity and the stiffness of the plate. As the plate length decreases the plate thickness is more effective at changing the stress concentration for thinner plates. The shapes of the curves are very similar for plate thicknesses of 1.5 in. and 2.5 in., but the stress concentration factor is not affected by plate length with a plate thickness of 0.75 in. This may be because as the plate becomes more flexible, the less effect the length has upon the stress concentration factor.

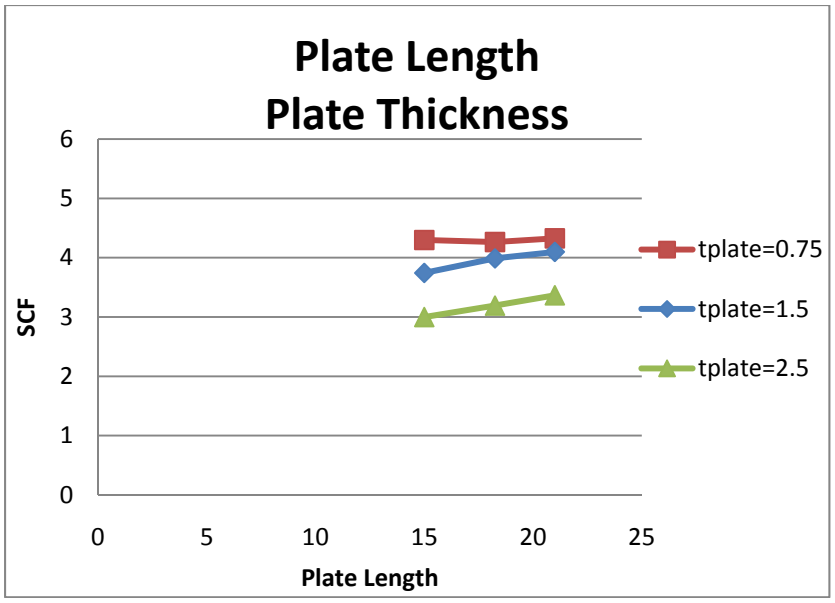

Figure 113. Plate Length and Plate Thickness vs. Stress Concentration Factor

5.5 Summary of Parametric Study

The first part of the parametric study illustrated how much each geometric variable affected the stress concentration factor of a 4x4 angle with equal leg welds. The variables that showed a significant effect upon the stress concentration were the outstanding leg length, angle length, plate length, plate thickness and angle thickness. The outstanding leg length showed the largest effect upon the stress concentration factor. The plate width and weld length did not have a large effect upon the stress concentration factor, and the inside leg length did not have a consistent effect upon the stress concentration indicating that there were multiple factors being affected or that the model was not performing correctly.

The second part of the parametric study determined which variables correlated with one another. These variables were the basis for the parametric variable selection which is discussed in the next chapter. The plate thickness, angle thickness, inside leg length all showed correlation with one another. The stress concentration was also correlated with plate and angle length. The plate length, angle length and inside leg length did not show a significant interaction with the other variables.

CHAPTER 6

Discussion of Data Analysis

6.1 Discussion Overview

Various properties of the specimen were considered in order to find a method of estimating the stress concentration factor. The variables considered are presented below along with discussions of their effects and implications.

6.2 Effect of Outstanding Leg

One of the most influential variables on the magnitude of the stress concentration was the outstanding leg length. The out-of-plane eccentricity of the angle is proportional to the size of the outstanding leg. The eccentricity, *ey*, about the face of the connection plate for each angle was computed and plotted against the stress concentration factor. The definition of out-of-plane eccentricity of the angle is shown in Figure 114. A plot of the stress concentration versus the eccentricity of the angle is shown in Figure 115. The stress concentration factor increases as the eccentricity of the angle increases although there is considerable scatter in the results.

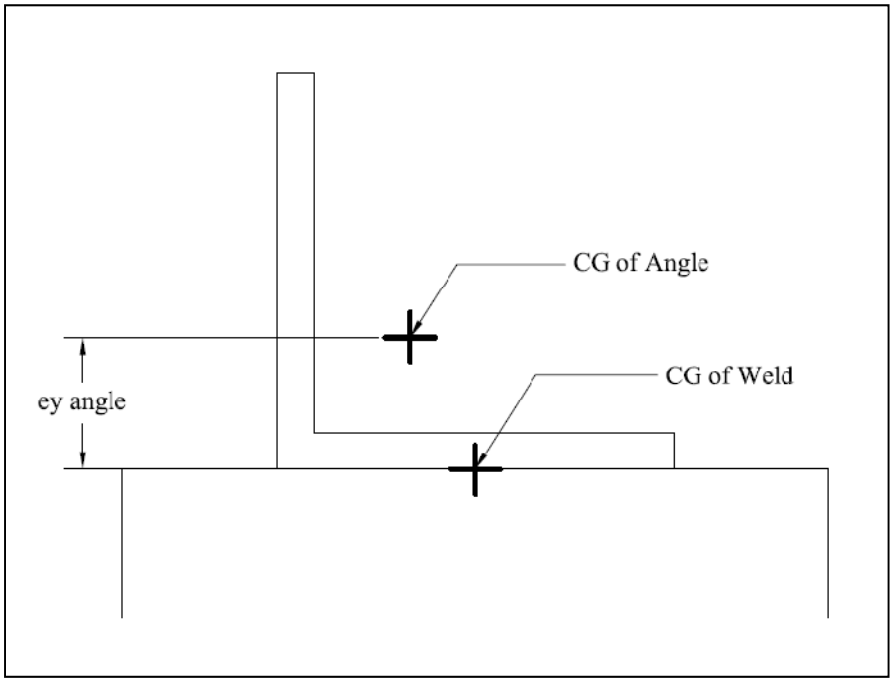

Figure 114. Out-of-plane Eccentricity of Angle

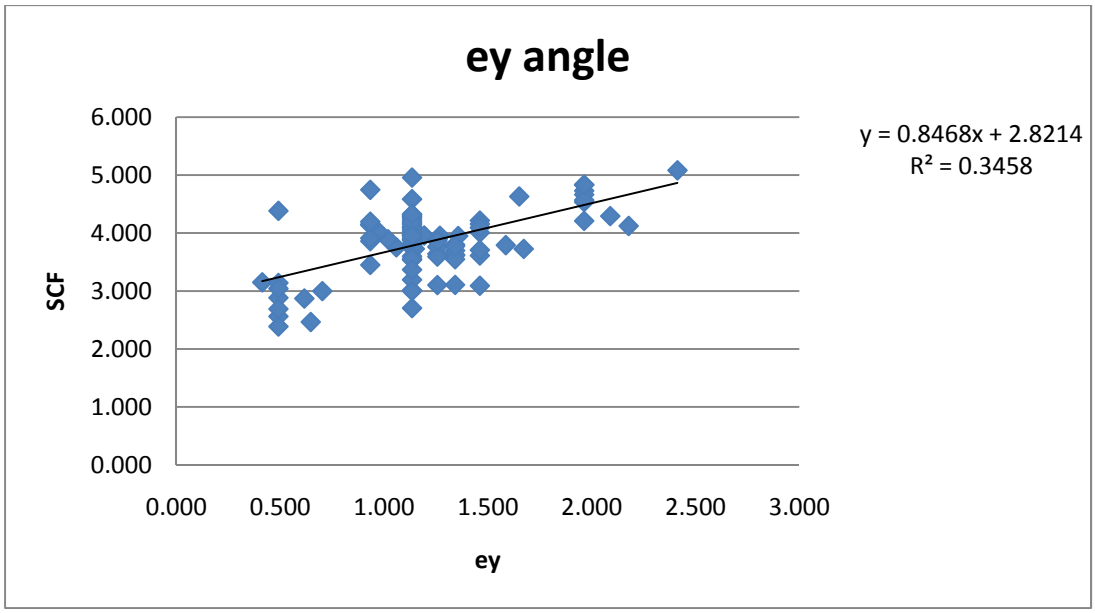

Figure 115. ey of Angle vs. Stress Concentration Factor

6.3 Effect of In-Plane Eccentricity of Angle

The eccentricity of the angle in-plane was not found to be as influential as the eccentricity out-of-plane, but it was still considered to see if any relationship could be found. The in-plane eccentricity of the angle is defined in Figure 116. CG of Weld represents the CG of the weld group so an equal length weld will have a CG of Weld that coincides with the CG of the end weld. In Figure 117 below, the stress concentration factor trends downward as the eccentricity gets larger. However there seems to be a lot more scatter than the eccentricity out-of-plane.

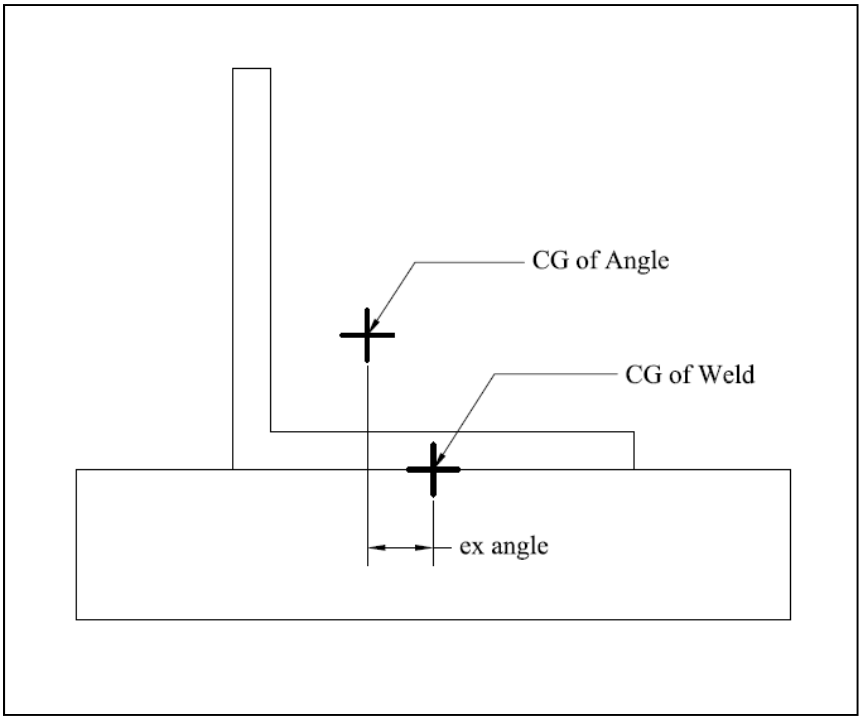

Figure 116. In-plane Eccentricity of Angle

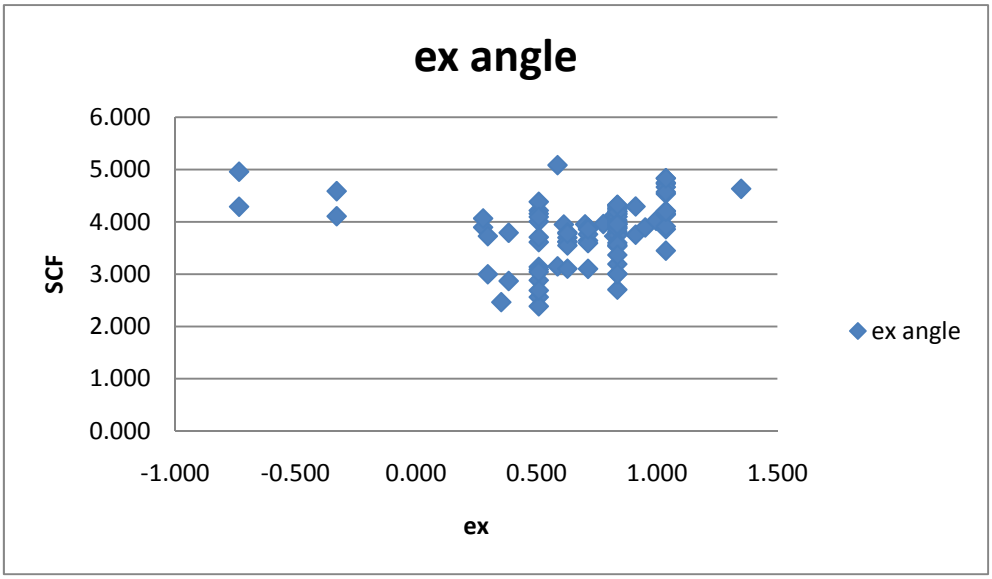

A

Figure 117. ex of Angle vs. Stress Concentration Factor

6.4 Effect of In-Plane Eccentricity of Plate

The eccentricity of the centroid of the plate to the centroid of the weld group was also investigated. Models with equal length welds will have no eccentricity with respect to the plate. Therefore, only models with balanced welds will create this eccentricity. The in-plane

eccentricity of the plate can be seen below in Figure 118. In Figure 119 below, the eccentricity in-plane of the plate is plotted against the stress concentration factor. As the eccentricity of the plate increases the stress concentration factor increases. This eccentricity can only be changed by changing the weld geometry to impose an eccentricity in the plate or by attaching the angle away from the centerline of the plate. This variable seems to have a fairly high effect upon the stress concentration factor.

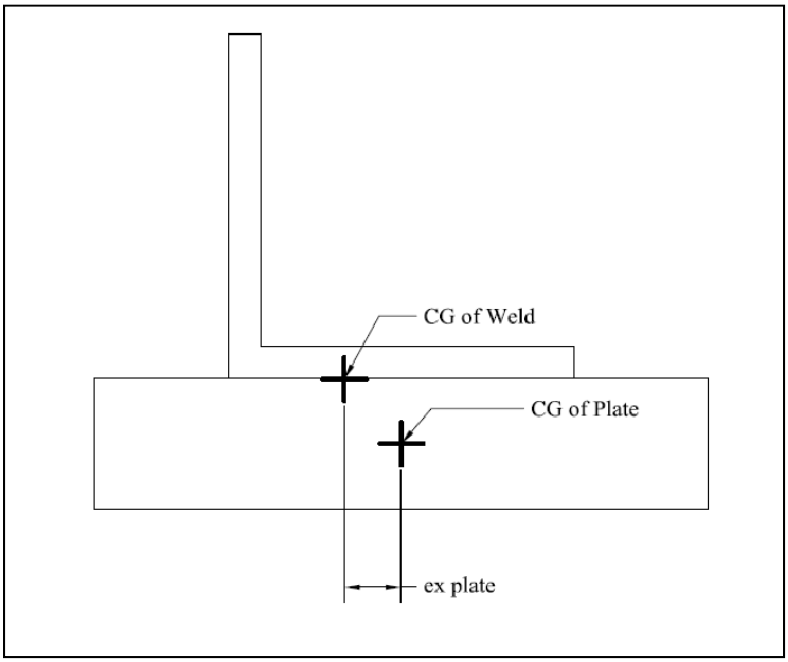

Figure 118. In-plane Eccentricity of Plate

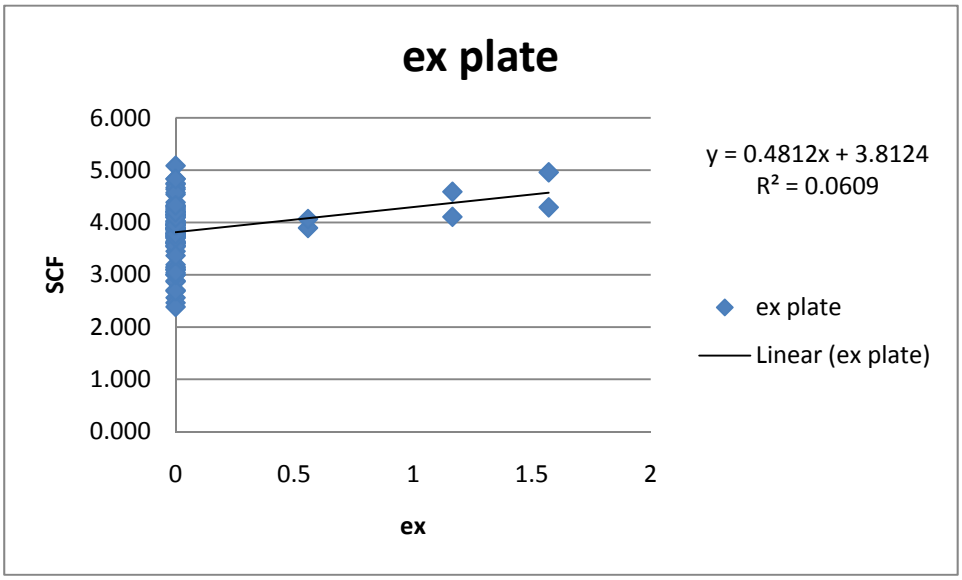

Figure 119. ex of Plate vs. Stress Concentration Factor

6.5 EFFECT OF OUT-OF-PLANE ECCENTRICITY OF PLATE

As the plate thickness increases the eccentricity out-of-plane of the plate increases and the stress concentration factor decreases. The out-of-plane eccentricity of the plate -is defined in Figure 120. This effect can be seen below in Figure 121. There is high variability but the effect of the eccentricity seems to be important.

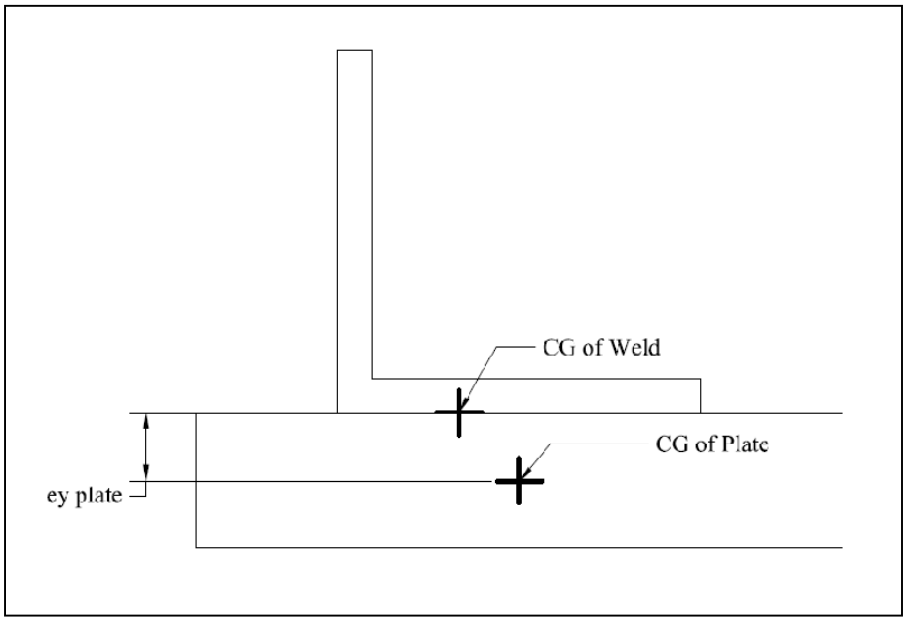

Figure 120. Out-of-plane Eccentricity of Plate

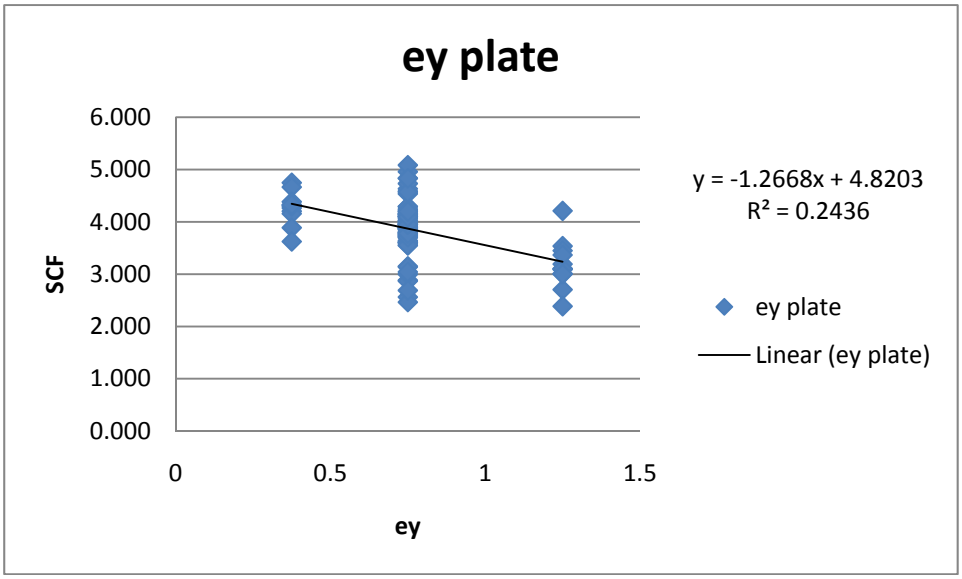

Figure 121. ey of Plate vs. Stress Concentration Factor

The value of the square of correlation coefficient values indicates the correlation of each variable upon the stress concentration factor. The out-of-plane eccentricity of each part had the highest coefficient of correlation with the out-of-plane eccentricity of the angle having the highest coefficient of correlation. This indicates that the out-of-plane eccentricity of the angle has the largest effect on the stress concentration factor.

6.6 Effect of Out-of-Plane Moment of Inertia of Angle

The moments of inertia of the angle and connection plate upon the stress concentration factor were considered. The moment of inertia of the angle about the center of gravity of the angle, Ixx, in the out-of-plane direction will be the first variable considered. In Figure 123 below, as the moment of inertia increases the stress concentration factor increases, although the graph trend is not linear. When the moment of inertia is very large the increase in stress concentration begins to reduce. However the scatter in data indicates other variables influence the stress concentration.

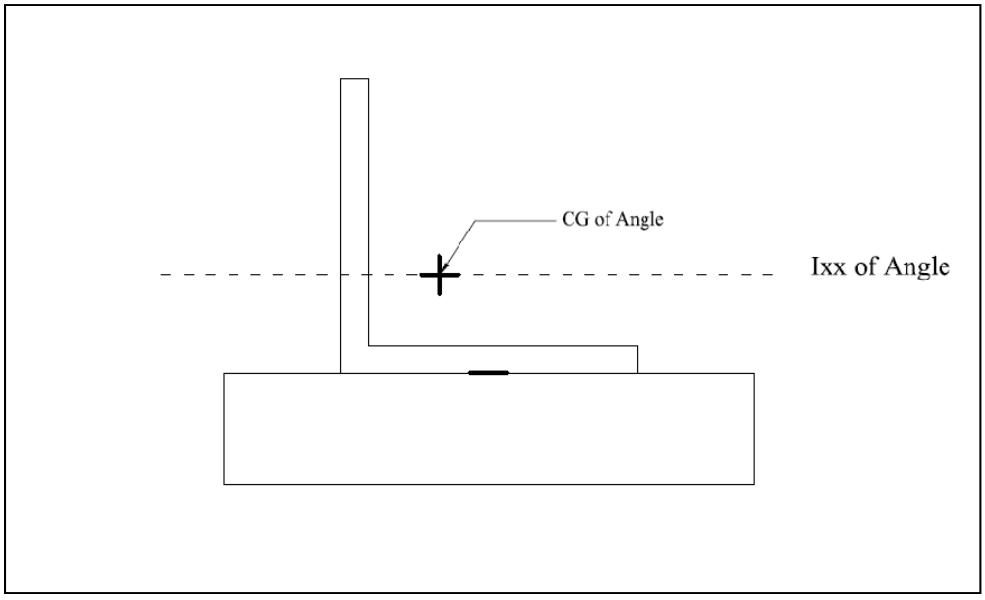

Figure 122. Ixx of Angle Diagram

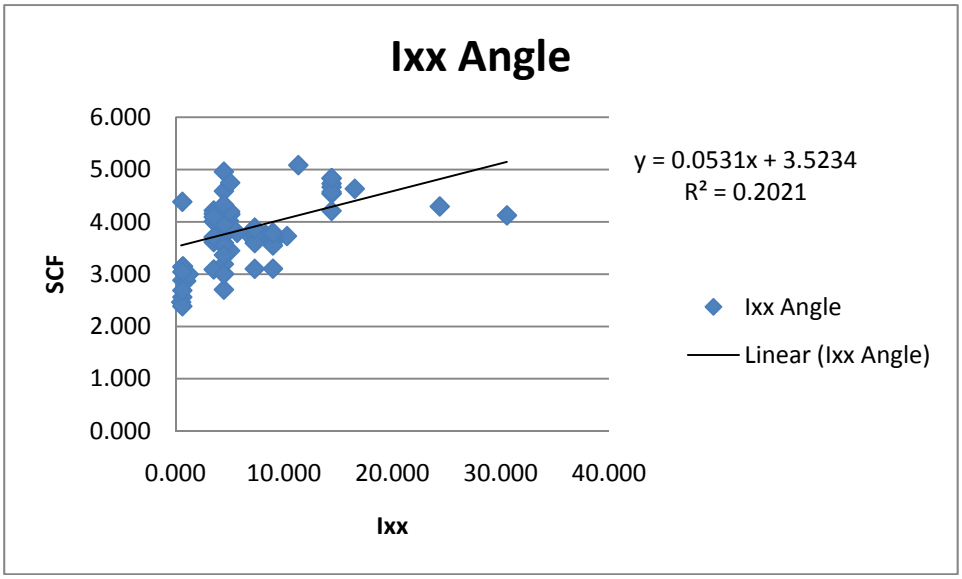

Figure 123. Ixx of Angle vs. Stress Concentration Factor

6.7 Effect of In-Plane Moment of Inertia of Angle

The effect of the moment of inertia of the angle about a vertical axis through the center of gravity of the angle, I_{yy}, was evaluated. In Figure 125 below, the data does not seem to have any real trend. Also, the low coefficient of correlation indicates that there is not a strong correlation between the stiffness of the angle and the stress concentration factor. This indicates that the stress concentration is not affected by the stiffness of the angle about this axis.

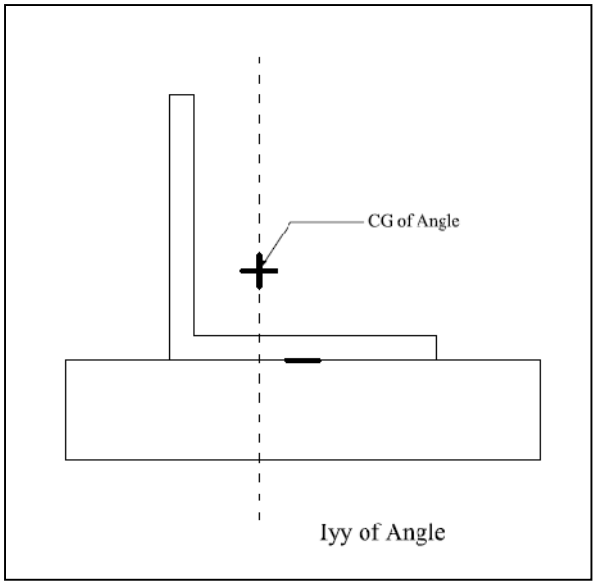

Figure 124. Iyy of Angle Diagram

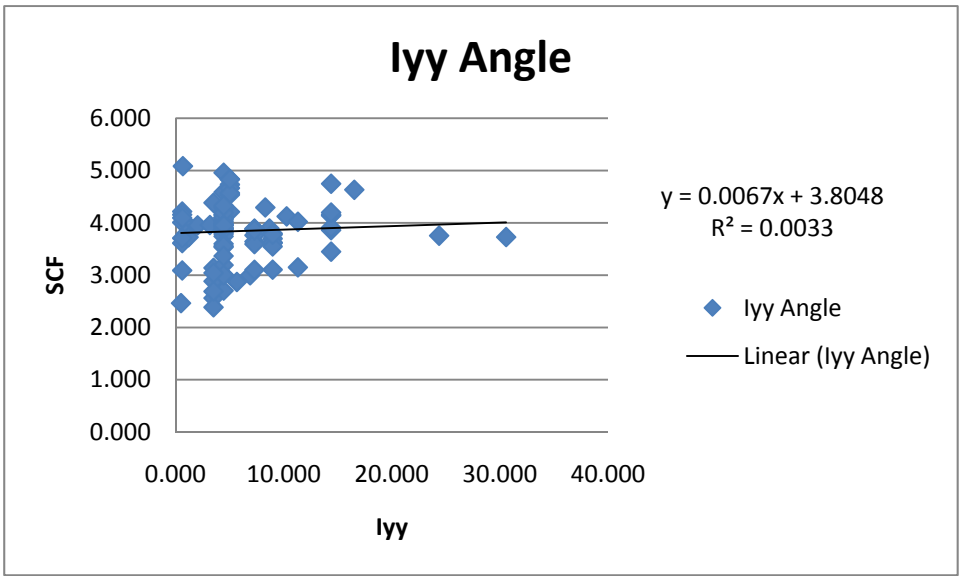

Figure 125. Iyy of Angle vs. Stress Concentration Factor

6.8 Effect of Out-of-Plane Moment of Inertia of Plate

The moment of inertia of the plate about the center of gravity of the plate in the out-of-plane direction was also considered. In Figure 127 below, the stress concentration factor decreases as the moment of inertia of the plate increases. There is some scatter in the plot but there is a fairly high coefficient of correlation indicating that this variable has some correlation with the stress concentration factor. The moment of inertia of the plate increases with increases in the thickness or width of the plate. It was found in the parametric study that the changing the thickness had the largest effect upon the stress concentration factor.

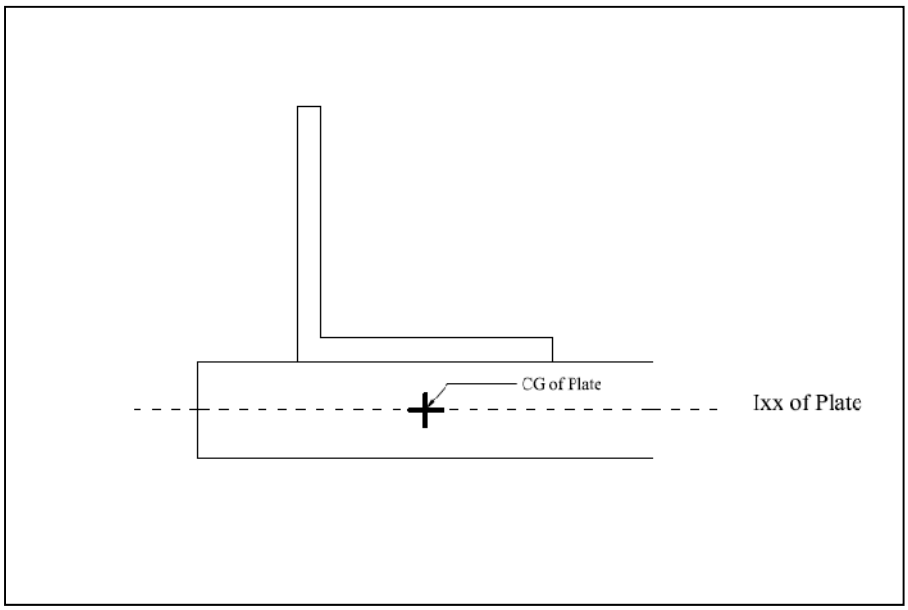

Figure 126. Ixx of Plate Diagram

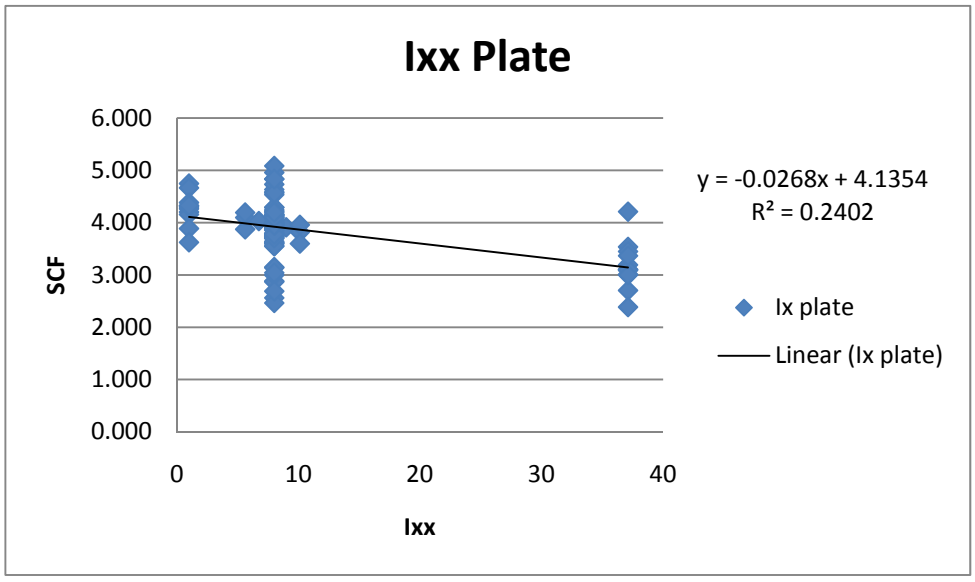

Figure 127. Ixx of Plate vs. Stress Concentration Factor

6.9 Effect of In-Plane Moment of Inertia of Plate

In Figure 129 below, as the moment of inertia of the plate about the vertical axis through its center of gravity increases, the stress concentration factor decreases. The coefficient of correlation of 0.18 is less than those for the out-of-plane quantities, but it is much higher than the in-plane moment of inertia of the angle which had a coefficient of correlation of 0.003. This

relationship indicates that the stress concentration factor is correlated more to the in-plane plate stiffness than the in-plane angle stiffness.

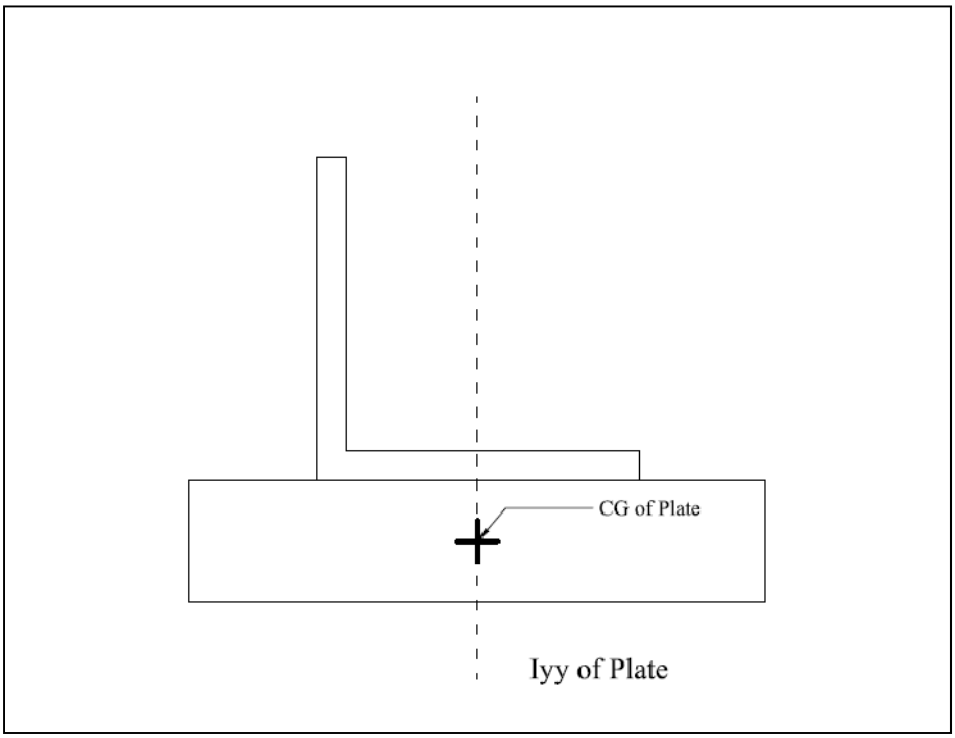

Figure 128. Iyy of Plate Diagram

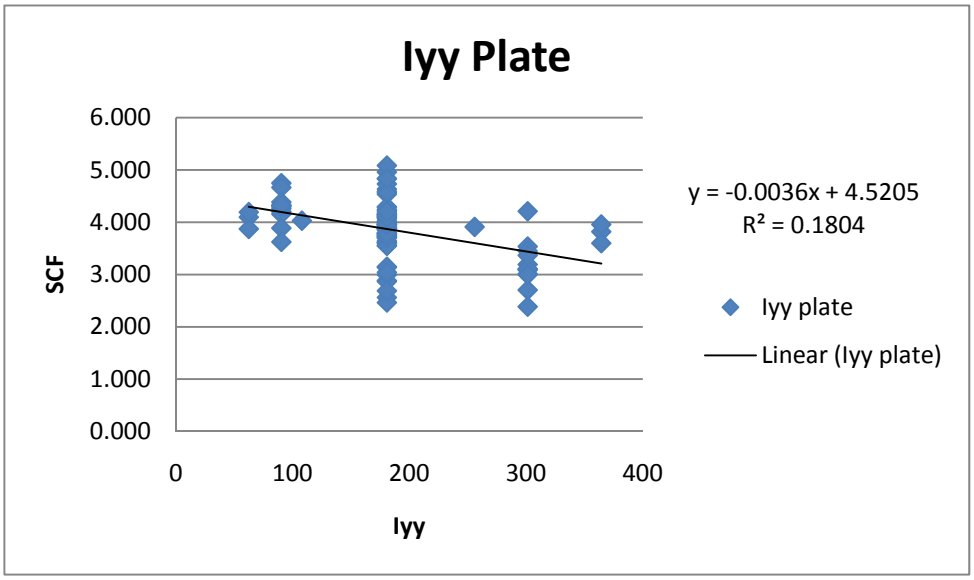

Figure 129. Iyy of Plate vs. Stress Concentration Factor

6.10 DEVELOPMENT OF PARAMETRIC VARIABLES

A free body diagram was taken below to determine the approximate moments of an idealized specimen. In Figure 130 below, if the load is assumed to completely pass through the weld at the end of the plate then the moment in the plate would be equal to $P*ey_{plate}$ where ey_{plate} is half the plate thickness. Also the moment in the angle will be equal to $P*ey_{angle}$ where ey_{angle} is the distance from the base of the angle to the center of gravity. This can be seen in Figure 131.

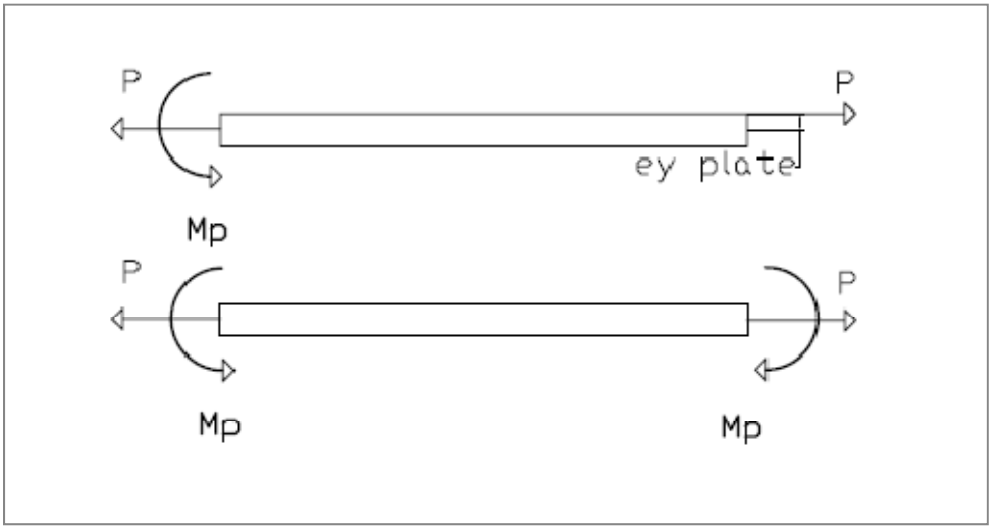

Figure 130. Plate Free Body Diagram

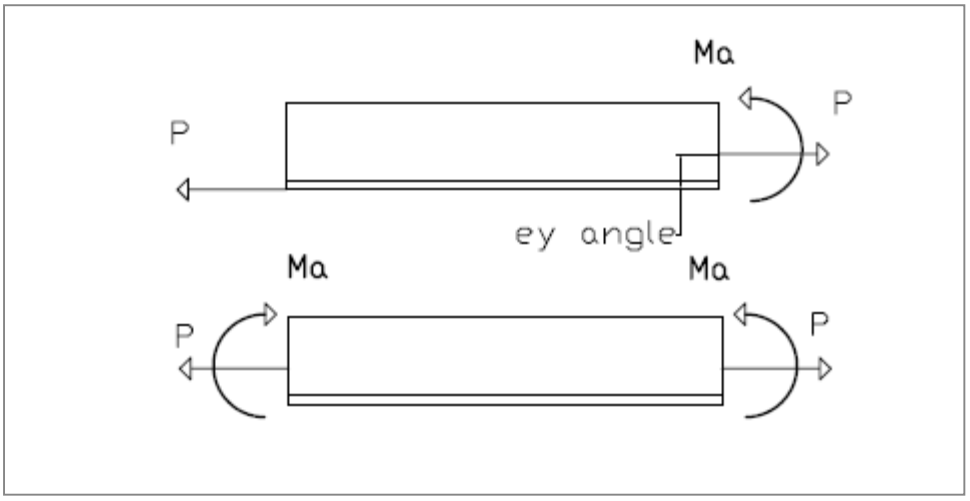

Figure 131. Angle Free Body Diagram

The two moments *M1* and *M2* depicted in Figure 132 will be opposite of each other due to the different eccentricities. If the load is assumed to pass directly into the plate at the toe of the weld towards the center of the specimen, then the moment diagram will immediately change from one moment to the other. However, in reality a much of the load will pass through the weld

at that point but some of the load will be distributed to the rest of the weld. In order to reflect this distribution a linear distribution of load was selected to approximate the change in moment in the section. The moment diagram for an idealized angle specimen can be seen in Figure 133. The moments *M1* and *M2* are indeterminate due to the interaction between the plate and the angle and can be seen below in Figure 132. If *M1* is taken to zero, then the maximum possible moment for *M2* is *Mp* + *Ma*. This value is used as the moment for the parametric equation.

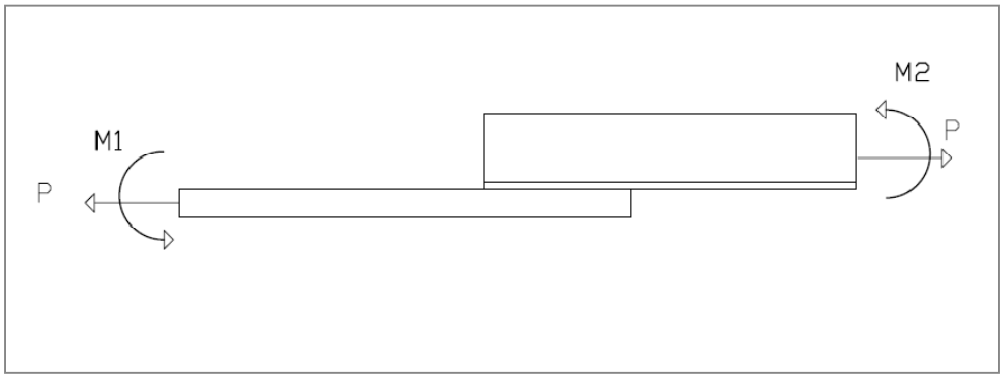

Figure 132. Specimen Free Body Diagram

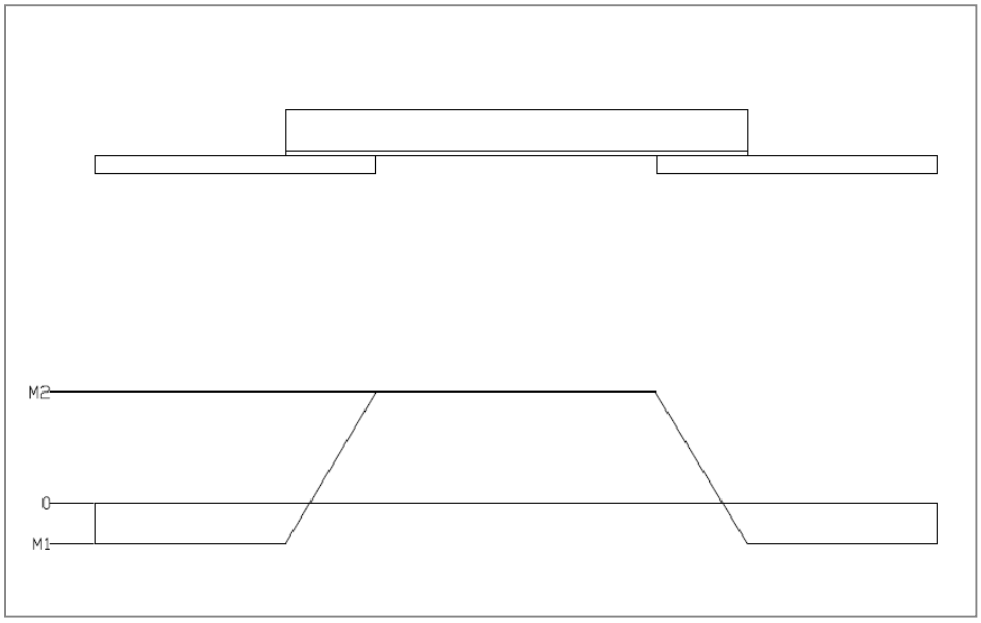

Figure 133. Moment Diagram

The stiffness of the specimen will be affected by the length of the plates, the length of the angle, the length of the welds, the moment of inertia of the plate and the moment of inertia of the angle. The moment diagram can be divided by the moment of inertia of the specimen at each point to reflect the curvature of the specimen. In the welded region the angle and plate were assumed to act uniformly as one element so the second moment of inertia was taken for the whole section.

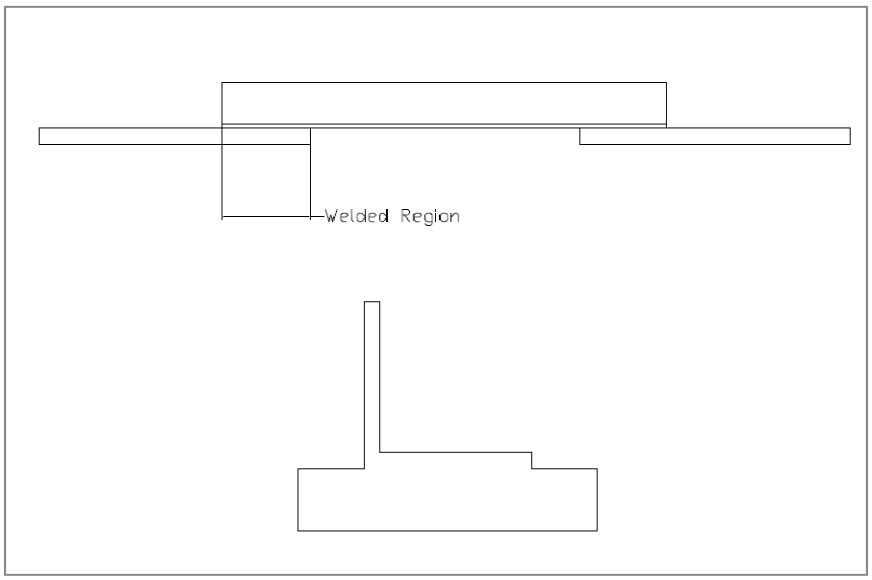

Figure 134. Assumed Welded Region Cross-Section

6.11 STRESS RATIO AS FIRST PARAMETRIC VARIABLE

The bending stress can then be calculated as a linear distribution of stress along the height of the cross-section, described by the equation Mc/I, where M is the moment, c is the distance of the point of interest from the neutral axis and I is the stiffness. In order to normalize the data, the bending stress at the weld toe was divided by the nominal axial stress in the angle, P/A. The resulting variable was a ratio of the bending stress to the axial stress. The equation for this stress ratio is shown below where c is the centroid of the combined plate and angle, A is the area of the angle, I_{xx} is the moment of inertia of the combined plate and angle about the centroid about the horizontal, x-axis and ey_{angle} and ey_{plate} are the out-of-plane eccentricities of the angle and plate respectively.

$$\sigma_{ratio} = \frac{\left(ey_{angle} + ey_{plate}\right) * c * A}{I_{xx}}$$

In Figure 135 below, the stress ratio is plotted against the stress concentration factor for each parametric specimen. There was good correlation between the data with an angle thickness of 3/8 in ($r^2 = 0.732$) but the thicker angles did not follow the same trend. A line has been fitted to the data with 3/8 in angle thickness to show the trend and correlation of the data. Also, it is important to note that there are lines of data that are stacked on top of each other, indicating that there is another variable that is not being accounted for.

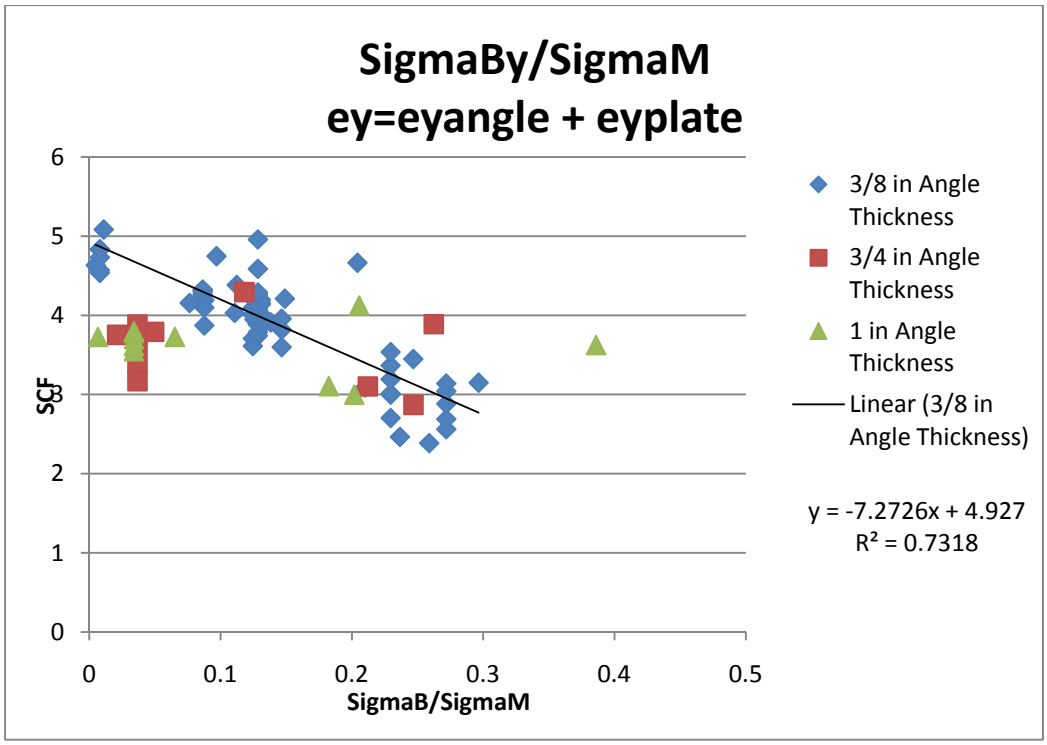

Figure 135. Stress Ratio vs. Stress Concentration Factor

Further study indicated that there may be some mesh sensitivity related to the thickness of the angle. A separate mesh thickness study was conducted using a 4x4 angle base model with a ¾ inch angle thickness. Three different mesh densities were used for the analysis and then compared. Figure 136 below shows the change in stress concentration with the change in mesh density. The stress concentration steadily increases as the mesh density increases indicating that there is still some mesh sensitivity. Because only specimens with a 3/8 inch angle thickness were tested, it is difficult to tell whether the effect of angle thickness is being accurately predicted by the model.

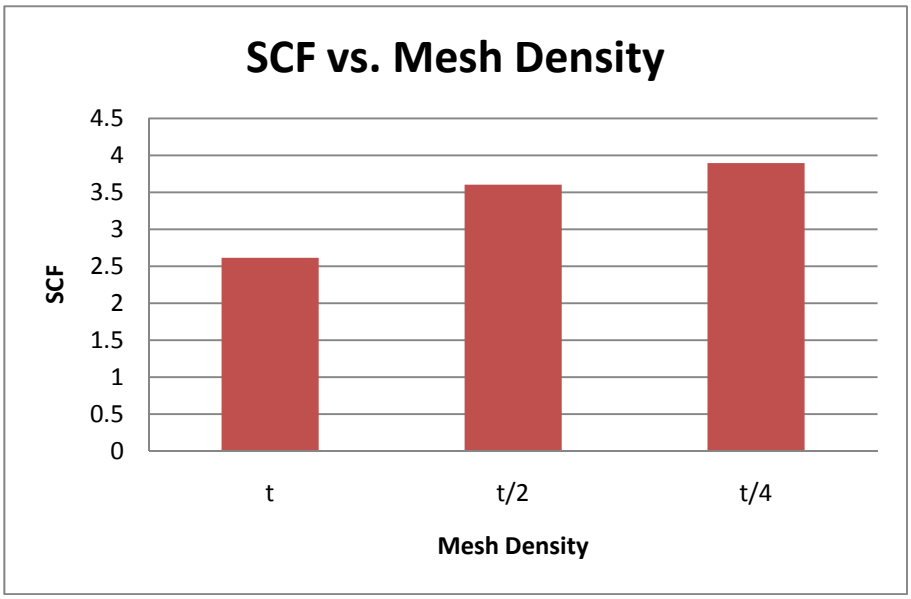

Figure 136. Stress Concentration Factor vs. Mesh Density for Thick Angle Model

6.12 Length Ratio as Second Parametric Variable

For each stress ratio value with a range stress concentrations in the previous figure, the length of the angle and connection plate was different. Another variable was needed to account for the change in stress concentration with the change in length of the angle and connection plate. The variable used was the length of the angle over the total length of the gripped specimen, taken as the distance from one grip to the other. Figure 138 compares stress concentration with the length ratio for the models which used the base 4x4x3/8 angle model with equal length welds only varied plate lengths or angle lengths. The correlation of this variable with the stress concentration is very good and became the second variable considered for the multivariable linear regression. The equation for the length ratio can be seen below where L_a is the angle length, L_p is the plate length and L_w is the length of the longest longitudinal weld.

$$L_{ratio} = \frac{L_a}{L_a + 2 * L_p - 2 * L_w}$$

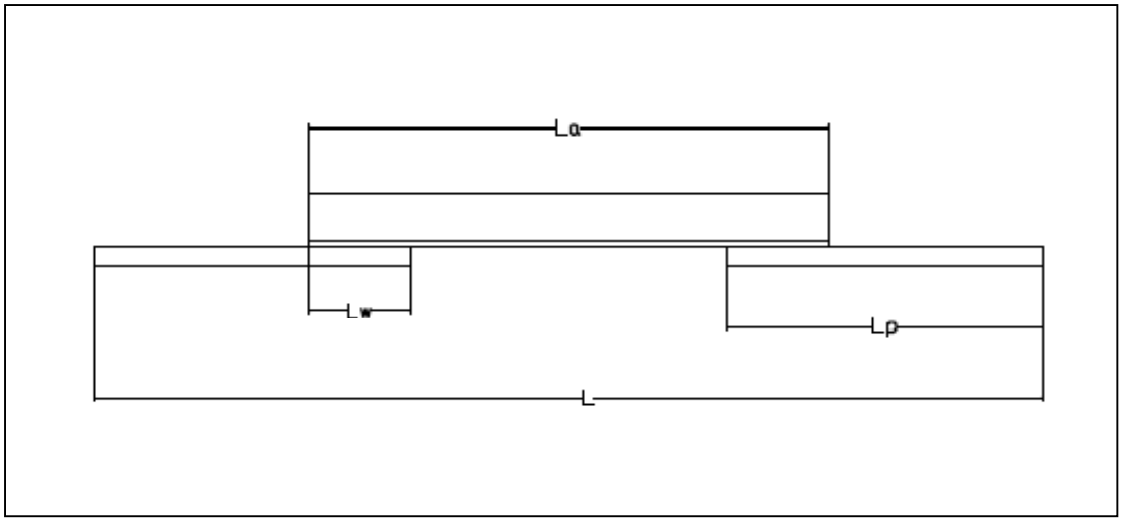

Figure 137. Lratio Diagram

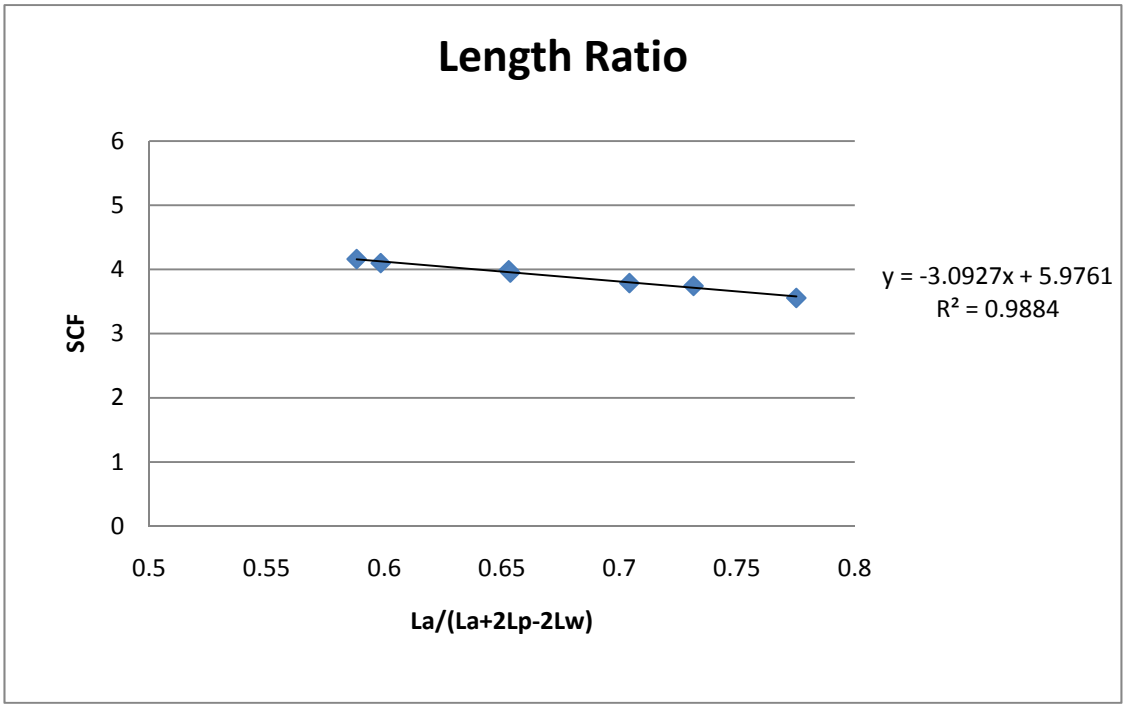

Figure 138. Length Ratio vs. Stress Concentration Factor

6.13 Parametric Equation and Comparison with Data

The multivariable linear regression was performed using the method described in the Experimental Statistics Handbook 91 of the United States Department of Commerce (United States Department of Commerce National Bureau of Standards, 1963). All of the data was used except those parametric models with variable thickness. These thicknesses were not used because it did not correlate well with the other data and could not be verified using the fatigue

specimens because only one thickness was tested. The parametric equation resulting from the regression is as follows:

$$SCF = 6.71 - 4.22 * \sigma_{ratio} - 3.55 * L_{ratio}$$

The standard deviation of the data from the regression is 0.375 indicating that for 98% of the data the stress concentration varies at most 0.75 above or below the calculated stress concentration.

The parametric stress concentration factors were calculated for each of the original six welded angle details and the S-N fatigue data was then modified to reflect the new stresses. Figure 139 below compares the data modified by the elastic method with the data modified by the parametric equation. The parametric method shows a much smaller amount of scatter and is very close to the category A-line from the AASHTO specification.

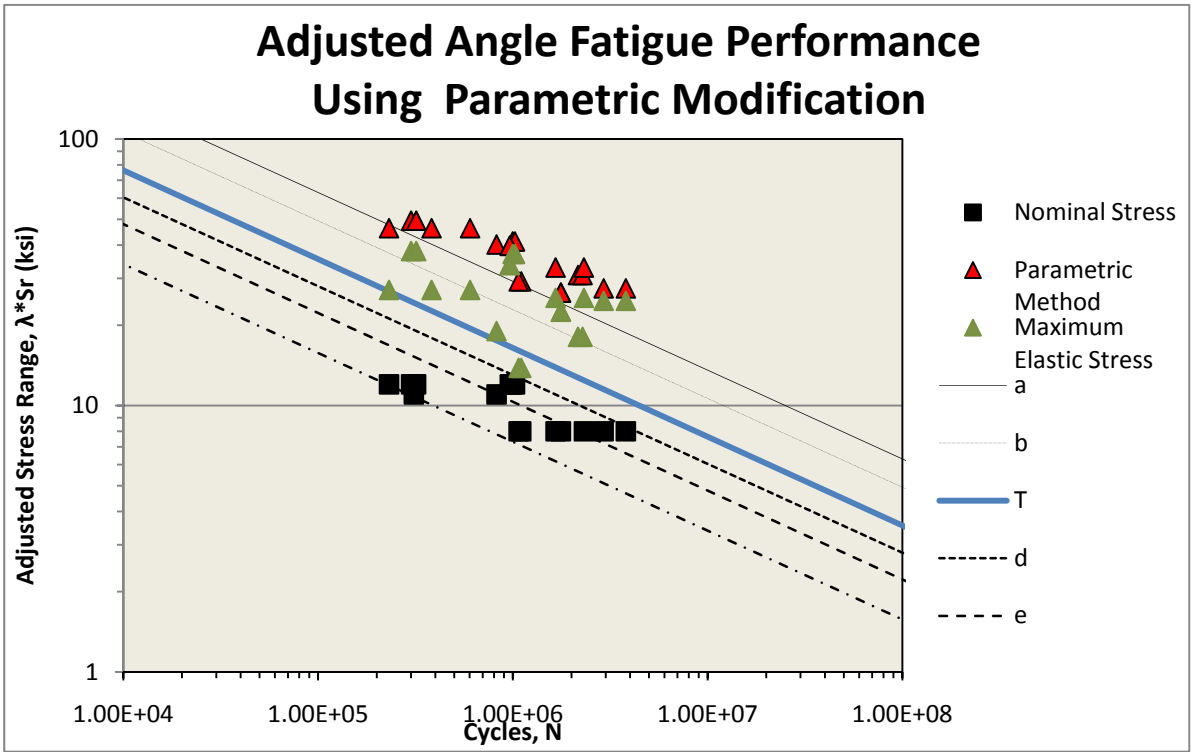

Figure 139. Comparison Between Elastic Method and Parametric Method

When compared to the DNV extrapolated stresses, the data modified by the parametric equation approximates the original extrapolated stress very well. The biggest difference between two estimated SCF and the value from the DNV method was 10 percent for the 53SB detail. The parametric stress concentration was conservative, it over estimated the value. This indicates that the parametric equation derived is internally consistent and can reasonably estimate stress concentrations for similar welded angle details.

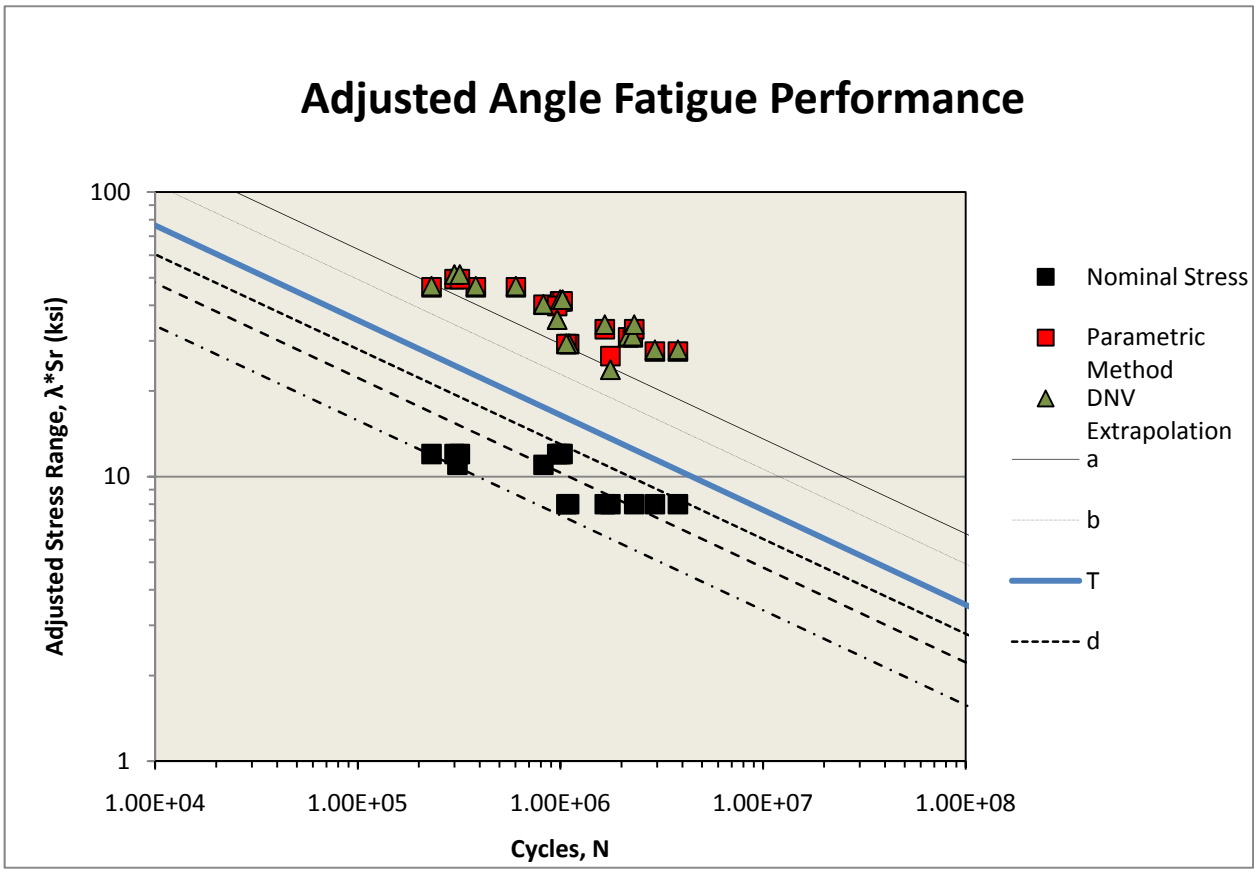

Figure 140. Comparison Between DNV Method and Parametric Method

The stress concentration factors calculated for the fatigue specimens using the DNV method and the derived parametric equation are plotted in Figure 141. Perfect correlation between the two points and a slope of one would indicate that there is no error between the two methods. A fitted line to the data gives a slope of 0.9995 and a coefficient of correlation of 0.95. These numbers indicate that the parametric equation is very accurate for these specimens.

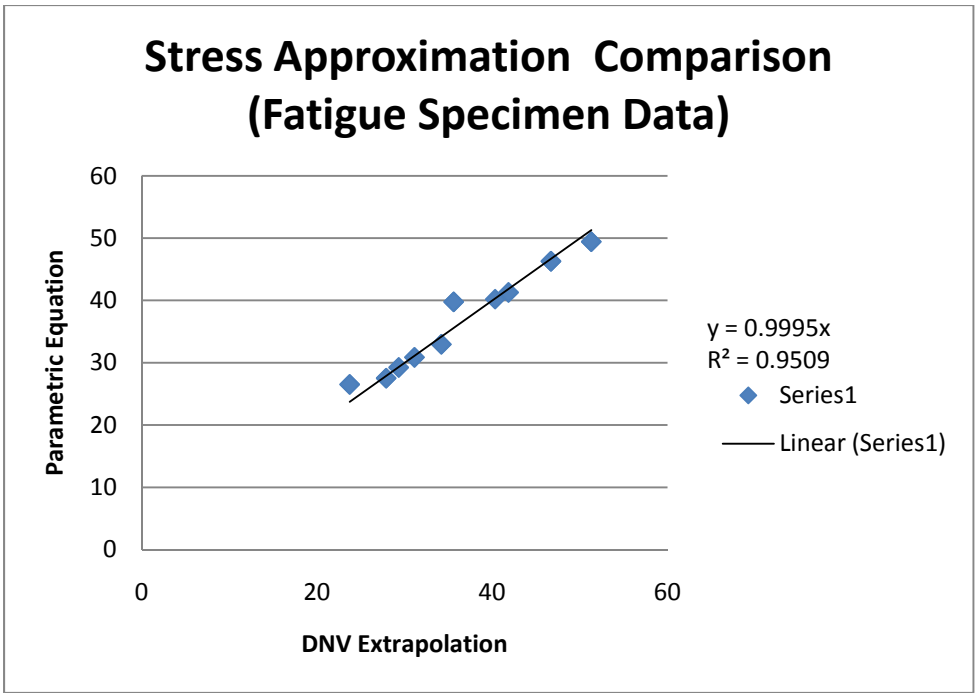

Figure 141. Stress Approximation Comparison for Fatigue Specimen Data

In Figure 142, data from all of the models is used in the comparison including fatigue specimen models and models with varying angle thickness. A fitted line for this data has a slope of 1.01 and coefficient of correlation of 0.195. The slope is very close to one but the correlation coefficient is very low indicating that while the equation approximates the fatigue specimen models very well, the equation does not approximate models that are very different from the base model. If the models that had angle thicknesses other than 3/8 in are removed, then the correlation becomes much better, with a slope of 1.04 and a correlation coefficient of 0.45 as indicated in Figure 143. The largest differences between the parametric equation and the DNV extrapolation were found mostly in models with balanced welds.

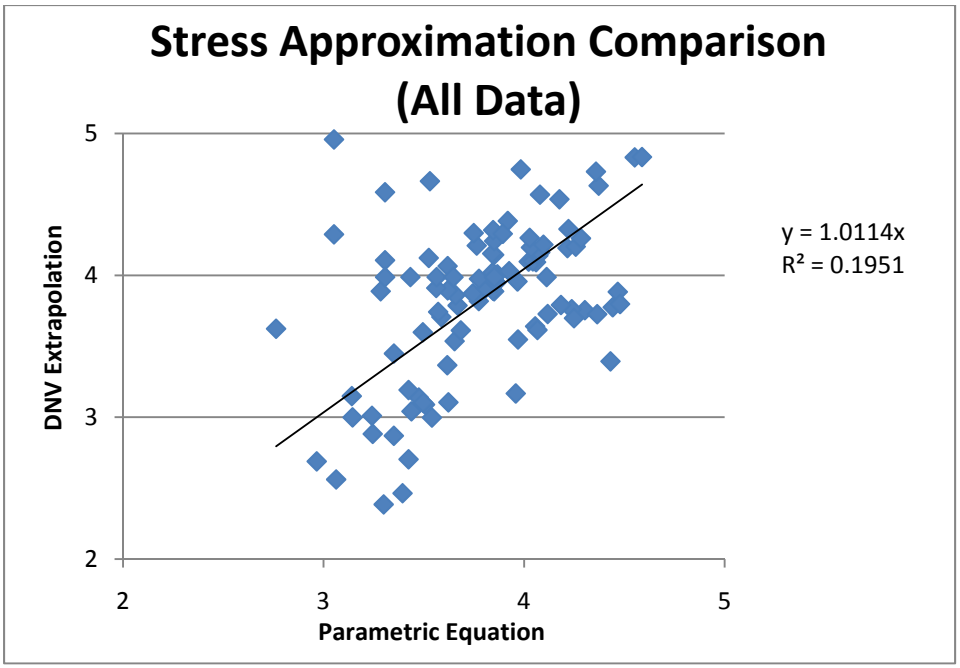

Figure 142. Stress Approximation Comparison for All Data

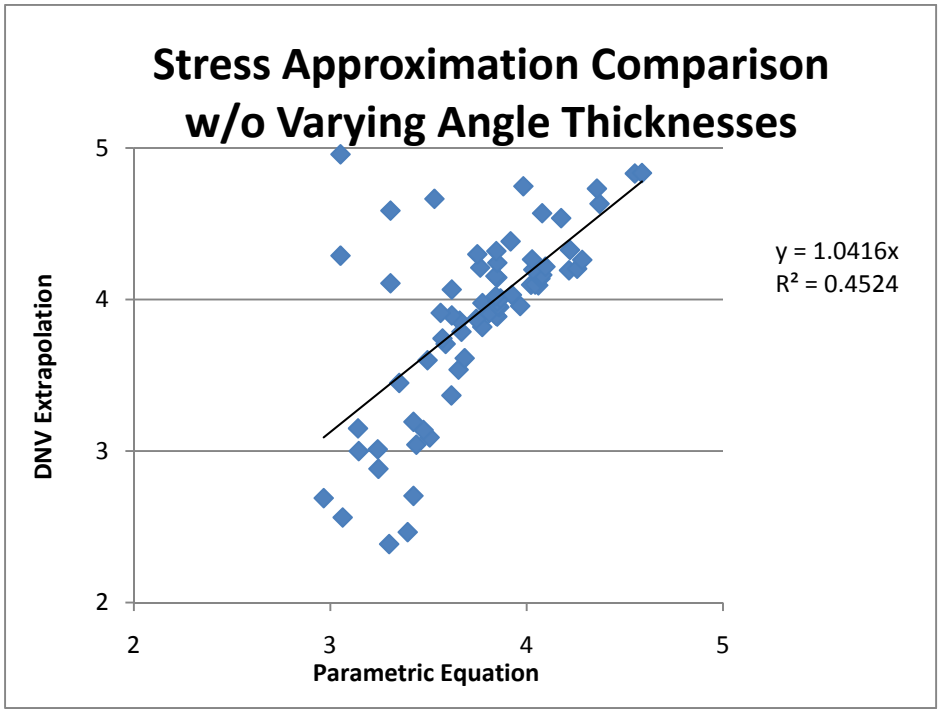

Figure 143. Stress Approximation Comparison w/o Varying Angle Thicknesses

CHAPTER 7

Conclusions and Recommendations

7.1 SUMMARY

Fatigue data was collected for 25 different welded angle connections with 6 different geometries. Each geometry was then modeled by the finite element analysis program ABAQUS and each detail's stress concentration were then calculated using the DNV method. A parametric study of the welded angle detail was then performed illustrate the effect of each parameter upon the stress concentration and to develop an equation that approximates the stress concentration factor of realistic welded angle designs. Also, six static tests of each detail were performed along with coupon testing to determine the shear lag effects.

7.2 FATIGUE TESTING RESULTS

All specimens failed within the E or E' categories delineated by the AASHTO specification (AASHTO, 2007) using the stress range calculated on the gross section. This was consistent with the recommendation given by the LRFD Design Manual for Highway Bridge Superstructures (Grubb, Corven, Wilson, Bouscher, & Volle, 2007). However, the details used for physical testing were differed from the typical details used in the field. Most cross frames have longer angles and thinner gusset plates then the test specimens which may affect the stress concentrations and the subsequent fatigue life. The effect of a thinner gusset plate and longer angle was examined using the hot spot stress approach calculated from a finite element analysis.

7.3 FINITE ELEMENT ANALYSIS RESULTS

Each welded angle detail was analyzed using a finite element program, ABAQUS, and the stress concentrations were calculated using the DNV method. The hot spot stress range at the weld toe was computed by taking the stress concentration factor and multiplying it by the nominal stress. The hot spot stresses resulted in a fatigue category A classification which was higher than expected. High stress concentrations resulting from the finite element analysis method used are probably responsible for this result. However, the high stresses are not important as long as the meshing and analysis methods are kept consistent. The modified data yielded an acceptable correlation and the method used to calculate the stress concentrations for a given detail was used to extend the range of the geometries beyond the geometries tested in the fatigue tests.

7.4 PARAMETRIC STUDY RESULTS

The first order parametric study showed that the variables with the most influence on the stress concentration factor were the outstanding leg length, angle length, plate length and plate thickness. The least influential variables were the plate width and inside leg length. Weld length and balancing of the weld showed little change in the stress concentration. The fatigue tests indicated that balancing of the weld increased the fatigue life of the angles, but other variables changed which affected the stress concentration and fatigue life such as the angle length. A second order parametric study was undertaken to examine the interaction between the variables.

The second order parametric study showed that most variables have a correlative effect on the stress concentration except for the longitudinal lengths such as the angle length, plate length and weld length. Some of the correlated effects were so small that they were not included in the variable study.

After considering many variable combinations, the ratio between the bending stress of the welded cross-section at the weld toe and the membrane stress of the angle provided a reasonable correlation to the estimated stress concentration. The ratio of the angle length to the total length was determined to be the second variable that included the effects of longitudinal length. A multivariable linear regression was performed to determine the parametric equation for the stress concentration factor based upon the stress ratio and the length ratio. The following equation was the result:

$$SCF = 6.71 - 4.22 * \sigma_{ratio} - 3.55 * L_{ratio}$$

The fatigue life predicted by multiplying the nominal stress by the calculated stress concentration yielded provided a better estimate than the elastic method used by Grubb (Grubb, Corven, Wilson, Bouscher, & Volle, 2007). There was much less scatter when the data was manipulated using the parametric equation versus the elastic method which indicates that the parametric equation is a more accurate approximation of the stress concentration. The r^2 value was increased from 0.303 for the original data to 0.649 using the parametric equation compared to 0.445 for the extrapolated stress. The stress concentrations derived by the extrapolation method were almost exactly the same as stress concentrations calculated from the equation. The largest error between the extrapolated stress and the stress calculated using the parametric equation was 12 percent with the average error being 3 percent. These two comparisons indicate that, according to the current data, this parametric equation is correct.

The fatigue life of a welded cross-frame can now be calculated by taking the A value associated with the A-line provided in the AASHTO specifications (AASHTO, 2007) and multiplying it by the stress concentration factor raised to the negative third power. The calculation of this modified A value or A' can be seen below the parametric equation provided above. The fatigue life

$$N = A * (SCF * S_r)^{-3}$$

$$A' = A * SCF^{-3}$$

7.5 DESIGN RECOMMENDATIONS

The design of an angle cross-frame connection should start with the calculation of the required fatigue life. This is done by multiplying the average daily truck traffic for a single lane (ADTTSL) by the required life, typically 50 years or 18250 days.

$$N = ADTT_{SL} * 18250$$

An initial cross-frame design should then be selected. The recommended angles provided by the AASHTO/NSBA guidelines for design details would be appropriate initial designs (AASHTO/NSBA, 2006). The stress concentration factor can then be calculated using the parametric equation derived in this report and can be seen below.

$$SCF = 6.71 - 4.22 * \sigma_{ratio} - 3.55 * L_{ratio}$$

The equation for this stress ratio (σ_{ratio}) can be seen below where c is the centroid of the combined plate and angle, A is the area of the angle, I_{xx} is the moment of inertia of the combined plate and angle at the centroid about the x-axis and ey_{angle} and ey_{plate} are the out-of-plane eccentricities of the angle and plate respectively.

$$\sigma_{ratio} = \frac{(ey_{angle} + ey_{plate}) * c * A}{I_{xx}}$$

The equation for the length ratio can be seen below where L_a is the angle length, L_p is the plate length and L_w is the length of the longest longitudinal weld.

$$L_{ratio} = \frac{L_a}{L_a + 2 * L_p - 2 * L_w}$$

After the stress concentration factor (SCF) is determined the detail category (A) can be modified to create a new detail category (A') that will determine the fatigue life of the connection. The new detail category is determined by multiplying the value of the AASHTO detail category A by the stress concentration factor raised to the negative third power. This modification can be seen below.

$$A' = A * SCF^{-3}$$

Then the nominal stress range of the angle must then be calculated using the fatigue design truck loads. Theses stresses can be found using a refined structural model that includes the cross-frame members in the design. Current AASHTO specifications allow for the nominal stress to be 75 percent of the factored axial strength of the member without determining the true stress (AASHTO, 2007). This stress is much higher than the typical stresses observed in field tests and would probably make the fatigue design overly conservative. The fatigue life can then be determined by multiplying the modified detail category (A') by the nominal stress range raised to the negative third power (Sr^{-3}).

$$N = A' * {S_r}^{-3}$$

Finally compare the required fatigue life with the design fatigue life to determine whether the angle connection is adequate. If necessary, modify the angle geometry to increase the fatigue life.

In lieu of the complex procedure outlined above, the influence of angle geometry upon the fatigue strength can be estimated using the effective net area of the angle to calculate the fatigue strength of the angle. The fatigue life is calculated using Category E and the stress range calculated on the net area of the angle.

7.6 RECOMMENDATIONS FOR FURTHER STUDY

The model used for this study displayed some mesh sensitivity when investigating other angle thicknesses. Because only one angle thickness was used for fatigue testing, it was difficult to ascertain whether the model was showing signs of mesh sensitivity or if the model is inconsistent for other angle thicknesses. More fatigue testing should be conducted using multiple angle thicknesses in order to better understand the effect of angle thickness on the stress concentration factor.

Appendix A

MEASURED SPECIMEN DIMENSIONS

4X4X3/8 WITH EQUAL WELD

Name	Outstanding Leg Length	Inside Leg Length	Angle Length	Gusset Plates						Distance Between Plates
				Left			Right			
				L	W	D	L	W	D	
44E1	3.94	3.94	39.5	24	7.125	1.5	24	7.125	1.5	24.125
44E2	3 15/16	3 15/16	39 1/2	24	7.125	1.5	24	7.125	1.5	24
44E3	3 15/16	3 15/16	39 1/2	24	7.125	1.5	24	7.125	1.5	24
44E4	3 15/16	3 15/16	39 1/2	24	7.125	1.5	24	7.125	1.5	24
44E5	3 15/16	3 15/16	39 1/2	24	7.125	1.5	24	7.125	1.5	24
44E6	3 15/16	3 15/16	39 1/2	24	7.125	1.5	24	7.125	1.5	24
Average	4	4	39 1/2	24	7 1/8	1 1/2	24	7 1/8	1 1/2	24
Stdev	0	0	0	0	0	0	0	0	0	0

Table 12. 4x4x3/8 with Equal Weld Measured Dimensions

Name	Front Weld		Back Weld		End Weld		Distance Between Welds	
	L	R	L	R	L	R	Back	Front
44E1	7.00	7.06	7.25	7.31	4.75	4.75	25	25
44E2	7 7/8	7 1/2	7 5/8	7 1/2	4 3/4	4 3/4	24 1/4	24 3/4
44E3	7 5/16	7 5/16	7	7 5/16	4 3/4	4 3/4	25	24
44E4	7 1/4	7 1/16	7 1/8	7 5/16	4 3/4	4 3/4	25	25 3/16
44E5	7 1/4	7 1/8	7 1/4	7 1/4	4 3/4	4 3/4	25 5/16	25 1/4
44E6	7 1/4	7 1/16	7 3/16	7 7/16	4 3/4	4 3/4	25 3/16	25
Average	7 1/3	7 1/5	7 1/4	7 1/3	4 3/4	4 3/4	25	24 5/6
Stdev	2/7	1/6	1/5	0	0	0	2/5	1/2

Table 13. 4x4x3/8 with Equal Weld Measured Weld Dimensions

Name	Outstanding Leg Thickness				Inside Leg Thickness			
	Left	Middle	Right	Average	Left	Middle	Right	Average
44E1	0.405	0.408	0.406	0.406	0.405	0.405	0.407	0.406
44E2	0.402	0.408	0.405	0.405	0.410	0.406	0.408	0.408
44E3	0.406	0.406	0.406	0.406	0.409	0.404	0.406	0.406
Average	0.404	0.407	0.406	0.406	0.408	0.405	0.407	0.407
Stdev	0.002	0.001	0.001		0.003	0.001	0.001	

Table 14. 4x4x3/8 Measured Angle Thicknesses

4X4X3/8 WITH BALANCED WELD

Name	Outstanding Leg Length	Inside Leg Length	Angle Length	Gusset Plates						Distance Between Plates
				Left			Right			
				L	W	D	L	W	D	
44B1	3 15/16	3 15/16	47	24	7.125	1.5	24	7.125	1.5	23
44B2	3 15/16	3 15/16	47	24	7.125	1.5	24	7.125	1.5	23.25
44B3	3 15/16	3 15/16	47	24	7.125	1.5	24	7.125	1.5	24
44B4	3 15/16	3 15/16	47	24	7.125	1.5	24	7.125	1.5	24
44B5	3 15/16	3 15/16	47	24	7.125	1.5	24	7.125	1.5	23
44B6	3 15/16	3 15/16	47	24	7.125	1.5	24	7.125	1.5	23
Average	4	4	47	24	7 1/8	1 1/2	24	7 1/8	1 1/2	23 3/8
Stdev	0	0	0	0	0	0	0	0	0	1/2

Table 15. 4x4x3/8 with Balanced Weld Measured Dimensions

Name	Front Weld		Back Weld		End Weld		Distance Between Welds	
	L	R	L	R	L	R	Back	Front
44B1	3 5/16	3 1/4	11 1/4	11 1/4	4 3/4	4 3/4	24 1/4	40 1/4
44B2	3 1/4	3 1/4	11 1/4	11 1/4	4 3/4	4 3/4	24 1/4	40 1/2
44B3	3 1/2	3	11 1/4	11 3/8	4 3/4	4 3/4	24 1/4	40 1/4
44B4	3 1/2	3 5/16	11 9/16	11 1/2	4 3/4	4 3/4	24 1/4	40 1/4
44B5	3 1/4	3 7/16	11 1/4	11 3/8	4 3/4	4 3/4	24	40 1/8
44B6	3 3/8	3 1/4	11 15/16	11 1/2	4 3/4	4 3/4	24 1/4	40 1/4
Average	3 3/8	3 1/4	11 2/5	11 3/8	4 3/4	4 3/4	24 1/5	40 2/7
Stdev	1/9	1/7	2/7	1/9	0	0	1/9	1/7

Table 16. 4x4x3/8 with Balanced Weld Measured Weld Dimensions

5X3X3/8 WITH 5 INCH LEG OUTSTANDING AND EQUAL WELD

Name	Outstanding Leg Length	Inside Leg Length	Angle Length	Gusset Plates						Distance Between Plates
				Left			Right			
				L	W	D	L	W	D	
53LE1	5	2 15/16	40 1/2	24	7.125	1.5	24	7.125	1.5	24
53LE2	5	2 15/16	40 1/2	24	7.125	1.5	24	7.125	1.5	24
53LE3	5	2 15/16	40 1/2	24	7.125	1.5	24	7.125	1.5	24
53LE4	5	2 15/16	40 1/2	24	7.125	1.5	24	7.125	1.5	24
53LE5	5	2 15/16	40 1/2	24	7.125	1.5	24	7.125	1.5	24
53LE6	5	2 15/16	40 1/2	24	7.125	1.5	24	7.125	1.5	24
Average	5	3	40.50	24	7 1/8	1 1/2	24	7 1/8	1 1/2	24
Stdev	0	0	0	0	0	0	0	0	0	0

Table 17. 5x3x3/8 with Long Leg Outstanding and Equal Weld Measured Dimensions

Name	Front Weld		Back Weld		End Weld		Distance Between Welds	
	L	R	L	R	L	R	Back	Front
53LE1	7 7/8	7 5/8	7 3/4	7 3/4	3 3/4	3 3/4	25	25
53LE2	7 5/8	7 3/8	7 9/16	7 5/8	3 3/4	3 3/4	25 1/4	25 1/4
53LE3	7 13/16	7 1/2	7 11/16	7 3/4	3 3/4	3 3/4	25	25
53LE4	7 3/4	7 1/2	7 1/2	7 11/16	3 3/4	3 3/4	25 1/4	25 1/4
53LE5	7 13/16	7 1/2	7 3/4	7 3/4	3 3/4	3 3/4	25	25
53LE6	7 5/8	7 7/8	7 5/8	7 3/4	3 3/4	3 3/4	25	25
Average	7 3/4	7 4/7	7 2/3	7 5/7	3 3/4	3 3/4	25.08	25.08
Stdev	1/9	1/6	1/9	0	0	0	1/8	1/8

Table 18. 5x3x3/8 with Long Leg Outstanding and Equal Weld Measured Weld Dimensions

Name	Outstanding Leg Thickness				Inside Leg Thickness			
	Left	Middle	Right	Average	Left	Middle	Right	Average
53LE1	0.405	0.392	0.398	0.398	0.384	0.385	0.382	0.384
53LE2	0.399	0.398	0.395	0.397	0.383	0.384	0.385	0.384
53LE3	0.394	0.395	0.398	0.396	0.385	0.383	0.385	0.384
Average	0.399	0.395	0.397	0.397	0.384	0.384	0.384	0.384
Stdev	0.006	0.003	0.002		0.001	0.001	0.002	

Table 19. 5x3x3/8 with Long Leg Outstanding Measured Angle Thicknesses

5X3X3/8 WITH 5 INCH LEG OUTSTANDING AND BALANCED WELD

Name	Outstanding Leg Length	Inside Leg Length	Angle Length	Gusset Plates						Distance Between Plates
				Left			Right			
				L	W	D	L	W	D	
53LB1	5	2 15/16	50	24	7.125	1.5	24	7.125	1.5	24
53LB2	5	2 15/16	50	24	7.125	1.5	24	7.125	1.5	24
53LB3	5	2 15/16	50	24	7.125	1.5	24	7.125	1.5	24
53LB4	5	2 15/16	50	24	7.125	1.5	24	7.125	1.5	24
53LB5	5	2 15/16	50	24	7.125	1.5	24	7.125	1.5	24
53LB6	5	2 15/16	50	24	7.125	1.5	24	7.125	1.5	24
Average	5	3	50	24	7 1/8	1 1/2	24	7 1/8	1 1/2	24
Stdev	0	0	0	0	0	0	0	0	0	0

Table 20. 5x3x3/8 with Long Leg Outstanding and Balanced Weld Measured Dimensions

Name	Front Weld		Back Weld		End Weld		Distance Between Welds	
	L	R	L	R	L	R	Back	Front
53LB1	2 3/4	2 11/16	12 5/16	12 5/8	3 3/4	3 11/16	25	44 1/2
53LB2	3	2 1/2	12 1/4	12 1/2	3 3/4	3 3/4	25 1/8	44 1/8
53LB3	2 11/16	2 5/8	12 3/16	12 9/16	3 3/4	3 11/16	25 1/8	44 1/2
53LB4	2 7/8	2 7/8	12 3/8	12 3/8	3 3/4	3 3/4	25 1/4	44 1/8
53LB5	2 15/16	2 7/8	12 5/16	12 7/16	3 3/4	3 3/4	25 1/4	44.25
53LB6	2 7/8	2 7/8	12 1/4	12 1/2	3 3/4	3 11/16	25 1/4	44.25
Average	2 6/7	2 3/4	12 2/7	12 1/2	3 3/4	3 5/7	25 1/6	44 2/7
Stdev	1/9	1/6	0	0	0	0	1/9	1/6

Table 21. 5x3x3/8 with Long Leg Outstanding and Balanced Weld Measured Weld Dimensions

5X3X3/8 WITH 3 INCH LEG OUTSTANDING AND EQUAL WELD

Name	Outstanding Leg Length	Inside Leg Length	Angle Length	Gusset Plates						Distance Between Plates
				Left			Right			
				L	W	D	L	W	D	
53SE1	2 15/16	4 7/8	38 1/4	24	7.125	1.5	24	7.125	1.5	24
53SE2	2 15/16	4 7/8	38 1/4	24	7.125	1.5	24	7.125	1.5	24
53SE3	2 15/16	4 7/8	38 1/4	24	7.125	1.5	24	7.125	1.5	24
53SE4	2 15/16	4 7/8	38 1/4	24	7.125	1.5	24	7.125	1.5	24
53SE5	2 15/16	4 7/8	38 1/4	24	7.125	1.5	24	7.125	1.5	24
53SE6	2 15/16	4 7/8	38 1/4	24	7.125	1.5	24	7.125	1.5	24
Average	3	4 7/8	38 1/4	24	7 1/8	1 1/2	24	7 1/8	1 1/2	24
Stdev	0	0	0	0	0	0	0	0	0	0

Table 22. 5x3x3/8 with Short Leg Outstanding and Equal Weld Measured Dimensions

Name	Front Weld		Back Weld		End Weld		Distance Between Welds	
	L	R	L	R	L	R	Back	Front
53SE1	7 9/16	7 1/2	6 5/16	6 7/16	5 3/4	5 11/16	25	25
53SE2	7 1/2	7 1/2	6 5/16	6 5/8	5 3/4	5 3/4	25	25
53SE3	7 9/16	7 1/2	6 7/16	6 5/8	5 3/4	5 3/4	25	25
53SE4	7 9/16	7 5/16	6 1/2	6 9/16	5 3/4	5 3/4	25	25
53SE5	7 1/2	7 7/16	6 1/2	6 5/8	5 3/4	5 11/16	25	25
53SE6	7 9/16	7 1/4	6 7/16	6 5/8	5 3/4	5 3/4	25	25
Average	7 1/2	7 3/7	6 3/7	6 4/7	5 3/4	5 3/4	25	25
Stdev	0	1/9	0	0	0	0	0	0

Table 23. 5x3x3/8 with Short Leg Outstanding and Equal Weld Measured Weld Dimensions

Name	Outstanding Leg Thickness				Inside Leg Thickness			
	Left	Middle	Right	Average	Left	Middle	Right	Average
53SE1	0.382	0.380	0.382	0.381	0.392	0.395	0.392	0.393
53SE2	0.384	0.384	0.383	0.384				
53SE3	0.383	0.384	0.383	0.383				
Average	0.383	0.383	0.383	0.383				

Table 24. 5x3x3/8 with Short Leg Outstanding Measured Angle Thicknesses

5X3X3/8 WITH 3 INCH LEG OUTSTANDING AND BALANCED WELD

Name	Outstanding Leg Length	Inside Leg Length	Angle Length	Gusset Plates						Distance Between Plates
				Left			Right			
				L	W	D	L	W	D	
53SB1	2 15/16	4 15/16	44	18	7.125	1.5	18	7.125	1.5	24
53SB2	2 15/16	4 15/16	44	18	7.125	1.5	18	7.125	1.5	24
53SB3	2 15/16	4 15/16	44	18	7.125	1.5	18	7.125	1.5	24
53SB4	2 15/16	4 15/16	44	18	7.125	1.5	18	7.125	1.5	24
53SB5	2 15/16	4 15/16	44	18	7.125	1.5	18	7.125	1.5	24
53SB6	2 15/16	4 15/16	44	18	7.125	1.5	18	7.125	1.5	24
Average	3	5	44	18	7 1/8	1 1/2	18	7 1/8	1 1/2	24
Stdev	0	0	0	0	0	0	0	0	0	0

Table 25. 5x3x3/8 with Short Leg Outstanding and Balanced Weld Measured Dimensions

Name	Front Weld		Back Weld		End Weld		Distance Between Welds	
	L	R	L	R	L	R	Back	Front
53SB1	3 7/8	3 3/4	9 1/4	9 1/2	5 3/4	5 3/4	25	44.5
53SB2	4	3 1/13	9 1/2	9 3/16	5 3/4	5 3/4	25	44.5
53SB3	3 3/4	3 3/4	9 7/16	9 5/8	5 3/4	5 3/4	25	44.5
53SB4	3 13/16	3 9/16	9 7/16	9 5/16	5 3/4	5 3/4	25	44.5
53SB5	3 11/16	3 11/16	9 1/2	9 7/16	5 3/4	5 3/4	25	44.5
53SB6	3 13/16	3 11/16	9 1/4	9 3/8	5 3/4	5 3/4	25	44.5
Average	3 5/6	3 3/5	9 2/5	9 2/5	5 3/4	5 3/4	25	44 1/2
Stdev	1/9	1/4	1/9	1/7	0	0	0	0

Table 26. 5x3x3/8 with Short Leg Outstanding and Balanced Weld Measured Weld Dimensions

Appendix B

FATIGUE TESTING SUMMARY

Angle	Sr	Min Stress	N	A	Failure Location	Test Configuration	Notes
44e1	12	4	231,174	4.E+08	Front	1st	Single Test
44e3	12	4	602,830	1.E+09	Front	2nd	Unspaced
44e4	8	4	2,158,038	1.E+09	Front	2nd	Unspaced
44e5	12	4	382,325	7.E+08	Front	2nd	Unspaced
44e6	8	4	2,278,038	1.E+09	Front	2nd	Unspaced
44b1	12	4	997,143	2.E+09	Back	3rd	
44b2	12	4	1,025,453	2.E+09	Back	3rd	
44b3	8	4	2,924,774	1.E+09	Back	3rd	
44b4	8	4	3,801,386	2.E+09	Back	3rd	

Table 27. 4x4 Angle Testing Summary

Angle	Sr	Min Stress	N	A	Failure Location	Test Configuration	Notes
53Le1	12	4	300,052	5.E+08	Back	3rd	
53Le2	12	4	318,805	6.E+08	Front	3rd	2 Cracks
53Le3	8	4	1,655,604	8.E+08	Back	3rd	
53Le4	8	4	2,314,378	1.E+09	Front	3rd	
53Lb1	8	4	3,080,034	2.E+09	End	4th	Uncharacteristic Failure Mode
53Lb2	8	4	3,080,034	2.E+09	End	4th	Uncharacteristic Failure Mode
53Lb3	12	4	505,290	9.E+08	End	4th	Uncharacteristic Failure Mode
53Lb4	12	4	505,290	9.E+08	End	4th	Uncharacteristic Failure Mode
53Se1	8	4	1,104,311	6.E+08	Front	3rd	
53Se2	11	4	824,273	1.E+09	Front	3rd	
53Se3	11	4	310,191	4.E+08	Front	3rd	Uncharacteristically Low
53Se6	8	4	1,070,376	5.E+08	Front	3rd	2 Cracks
53Sb1	8	4	1,764,362	9.E+08	Front	4th	
53Sb4	12	4	963,607	2.E+09	Front	4th	
53Sb5	12	4	963,607	2.E+09	Front	4th	
53Sb6	8	4	1,764,362	9.E+08	Front	4th	

Table 28. 5x3 Angle Testing Summary

Appendix C

FINITE ELEMENT MODEL DIMENSIONS

Name	Plate Thickness	Plate Width	Plate Length	Plate Area	Angle Length	Outstanding Length	Inside Length	Angle Thickness	Angle Area	Front Weld Length	Back Weld Length	End Weld Length
SALLI	1.5	7.125	18.25	10.6875	30	3.94	6	0.406	3.8708	7.75	7.75	6
SALLO	1.5	7.125	18.25	10.6875	30	6	3.94	0.406	3.8708	7.75	7.75	3.94
SASLI	1.5	7.125	18.25	10.6875	30	3.94	2	0.406	2.2468	7.75	7.75	2
SASLO	1.5	7.125	18.25	10.6875	30	2	3.94	0.406	2.2468	7.75	7.75	3.94
SAThickA	1.5	7.125	18.25	10.6875	30	3.94	3.94	0.75	5.3475	7.75	7.75	3.94
SAThickA1	1.5	7.125	18.25	10.6875	30	3.94	3.94	1	6.88	7.75	7.75	3.94
SAThickP	2.5	7.125	18.25	17.8125	30	3.94	3.94	0.406	3.03444	7.75	7.75	3.94
SAThinP	0.75	7.125	18.25	5.34375	30	3.94	3.94	0.406	3.03444	7.75	7.75	3.94
Short Angle	1.5	7.125	18.25	10.6875	30	3.94	3.94	0.406	3.03444	7.75	7.75	3.94
SPSA	1.5	7.125	15	10.6875	30	3.94	3.94	0.406	3.03444	7.75	7.75	3.94
LPSA	1.5	7.125	21	10.6875	30	3.94	3.94	0.406	3.03444	7.75	7.75	3.94
F0B15.5	1.5	7.125	18.25	10.6875	39.5	3.94	3.94	0.406	3.03444	0	15.5	3.94
F0B15.5P	1.5	7.125	18.25	10.6875	39.5	3.94	3.94	0.406	3.03444	0	15.5	3.94
F2B13.5	1.5	7.125	18.25	10.6875	39.5	3.94	3.94	0.406	3.03444	2	13.5	3.94
F2B13.5P	1.5	7.125	18.25	10.6875	39.5	3.94	3.94	0.406	3.03444	2	13.5	3.94
F5B10.5	1.5	7.125	18.25	10.6875	39.5	3.94	3.94	0.406	3.03444	5	10.5	3.94
F5B10.5P	1.5	7.125	18.25	10.6875	39.5	3.94	3.94	0.406	3.03444	5	10.5	3.94
FW0	1.5	7.125	18.25	10.6875	39.5	3.94	3.94	0.406	3.03444	7.75	7.75	3.94
FW2	1.5	7.125	18.25	10.6875	39.5	3.94	3.94	0.406	3.03444	7.75	7.75	3.94
FW5	1.5	7.125	18.25	10.6875	39.5	3.94	3.94	0.406	3.03444	7.75	7.75	3.94

Table 29. FEM Model Dimensions

Name	Plate Thickness	Plate Width	Plate Length	Plate Area	Angle Length	Outstanding Length	Inside Length	Angle Thickness	Angle Area	Front Weld Length	Back Weld Lengh	End Weld Length
LLILLO	1.5	7.125	18.25	10.6875	39.5	6	6	0.406	4.70716	7.75	7.75	6
LLISLO	1.5	7.125	18.25	10.6875	39.5	2	6	0.406	3.08316	7.75	7.75	6
LLIThickA	1.5	7.125	18.25	10.6875	39.5	3.94	6	0.75	6.8925	7.75	7.75	6
LLIThickA1	1.5	7.125	18.25	10.6875	39.5	3.94	6	1	8.94	7.75	7.75	6
LLIThickP	2.5	7.125	18.25	17.8125	39.5	3.94	3.94	0.406	3.03444	7.75	7.75	3.94
LLOThickA	1.5	7.125	18.25	10.6875	39.5	6	3.94	0.75	6.8925	7.75	7.75	3.94
LLOThickA1	1.5	7.125	18.25	10.6875	39.5	6	3.94	1	8.94	7.75	7.75	3.94
Long Leg Inside	1.5	7.125	18.25	10.6875	39.5	3.94	6	0.406	3.8708	7.75	7.75	6
Long Leg Inside 2.5	1.5	7.125	18.25	10.6875	39.5	3.94	2.5	0.406	2.4498	7.75	7.75	2.5
Long Leg Inside 3	1.5	7.125	18.25	10.6875	39.5	3.94	3	0.406	2.6528	7.75	7.75	3
Long Leg Inside 3.5	1.5	7.125	18.25	10.6875	39.5	3.94	3.5	0.406	2.8558	7.75	7.75	3.5
Long Leg Inside 5	1.5	7.125	18.25	10.6875	39.5	3.94	5	0.406	3.4648	7.75	7.75	5
Long Leg Inside 5.5	1.5	7.125	18.25	10.6875	39.5	3.94	5.5	0.406	3.6678	7.75	7.75	5.5
Long Leg Outstanding	1.5	7.125	18.25	10.6875	39.5	6	3.94	0.406	3.8708	7.75	7.75	3.94
Narrow Plate	1.5	5	18.25	7.5	39.5	3.94	3.94	0.406	3.03444	7.75	7.75	3.94
Narrow Plate 6	1.5	6	18.25	9	39.5	3.94	3.94	0.406	3.03444	7.75	7.75	3.94
Narrow Plate 8	1.5	8	18.25	12	39.5	3.94	3.94	0.406	3.03444	7.75	7.75	3.94
Normal	1.5	7.125	18.25	10.6875	39.5	3.94	3.94	0.406	3.03444	7.75	7.75	3.94
Short Leg Inside	1.5	7.125	18.25	10.6875	39.5	3.94	2	0.406	2.2468	7.75	7.75	2
Short Leg Outstanding	1.5	7.125	18.25	10.6875	39.5	2	3.94	0.406	2.2468	7.75	7.75	3.94

Table 29. FEM Model Dimensions Continued

Name	Plate Thickness	Plate Width	Plate Length	Plate Area	Angle Length	Outstanding Length	Inside Length	Angle Thickness	Angle Area	Front Weld Length	Back Weld Length	End Weld Length
SLILLO	1.5	7.125	18.25	10.6875	39.5	6	2	0.406	3.08316	7.75	7.75	2
SLISLO	1.5	7.125	18.25	10.6875	39.5	2	2	0.406	1.45916	7.75	7.75	2
SLIThickA	1.5	7.125	18.25	10.6875	39.5	3.94	2	0.75	3.8925	7.75	7.75	2
SLIThickA1	1.5	7.125	18.25	10.6875	39.5	3.94	2	1	4.94	7.75	7.75	2
SLOThickA	1.5	7.125	18.25	10.6875	39.5	2	3.94	0.75	3.8925	7.75	7.75	3.94
SLOThickA1	1.5	7.125	18.25	10.6875	39.5	2	3.94	1	4.94	7.75	7.75	3.94
Thick Angle	1.5	7.125	18.25	10.6875	39.5	3.94	3.94	0.75	5.3475	7.75	7.75	3.94
Thick Angle 1	1.5	7.125	18.25	10.6875	39.5	3.94	3.94	1	6.88	7.75	7.75	3.94
Thick Plate	2.5	7.125	18.25	17.8125	39.5	3.94	3.94	0.406	3.03444	7.75	7.75	3.94
ThickPLLI	2.5	7.125	18.25	17.8125	39.5	3.94	6	0.406	3.8708	7.75	7.75	6
ThickPLLO	2.5	7.125	18.25	17.8125	39.5	6	3.94	0.406	3.8708	7.75	7.75	3.94
ThickPSLI	2.5	7.125	18.25	17.8125	39.5	3.94	2	0.406	2.2468	7.75	7.75	2
ThickPSLO	2.5	7.125	18.25	17.8125	39.5	2	3.94	0.406	2.2468	7.75	7.75	3.94
ThickPThickA	2.5	7.125	18.25	17.8125	39.5	3.94	3.94	0.75	5.3475	7.75	7.75	3.94
ThickPThickA1	2.5	7.125	18.25	17.8125	39.5	3.94	3.94	1	6.88	7.75	7.75	3.94
Thin Plate	0.75	7.125	18.25	5.34375	39.5	3.94	3.94	0.406	3.03444	7.75	7.75	3.94
ThinPLLI	0.75	7.125	18.25	5.34375	39.5	3.94	6	0.406	3.8708	7.75	7.75	6
ThinPLLO	0.75	7.125	18.25	5.34375	39.5	6	3.94	0.406	3.8708	7.75	7.75	3.94
ThinPSLI	0.75	7.125	18.25	5.34375	39.5	3.94	2	0.406	2.2468	7.75	7.75	2
ThinPSLO	0.75	7.125	18.25	5.34375	39.5	2	3.94	0.406	2.2468	7.75	7.75	3.94
ThinPThickA	0.75	7.125	18.25	5.34375	39.5	3.94	3.94	0.75	5.3475	7.75	7.75	3.94
ThinPThickA1	0.75	7.125	18.25	5.34375	39.5	3.94	3.94	1	6.88	7.75	7.75	3.94
Wide Plate	1.5	9	18.25	13.5	39.5	3.94	3.94	0.406	3.03444	7.75	7.75	3.94

Table 29. FEM Model Dimensions Continued

Name	Plate Thickness	Plate Width	Plate Length	Plate Area	Angle Length	Outstanding Length	Inside Length	Angle Thickness	Angle Area	Front Weld Length	Back Weld Length	End Weld Length
Short Plate	1.5	7.125	15	10.6875	39.5	3.94	3.94	0.406	3.03444	7.75	7.75	3.94
Long Plate	1.5	7.125	21	10.6875	39.5	3.94	3.94	0.406	3.03444	7.75	7.75	3.94
SPNP	1.5	5	15	7.5	39.5	3.94	3.94	0.406	3.03444	7.75	7.75	3.94
SPWP	1.5	9	15	13.5	39.5	3.94	3.94	0.406	3.03444	7.75	7.75	3.94
SPThickA	1.5	7.125	15	10.6875	39.5	3.94	3.94	0.75	5.3475	7.75	7.75	3.94
SPThickA1	1.5	7.125	15	10.6875	39.5	3.94	3.94	1	6.88	7.75	7.75	3.94
SPSLO	1.5	7.125	15	10.6875	39.5	2	3.94	0.406	2.2468	7.75	7.75	3.94
SPLLO	1.5	7.125	15	10.6875	39.5	6	3.94	0.406	3.8708	7.75	7.75	3.94
SPSLI	1.5	7.125	15	10.6875	39.5	3.94	2	0.406	2.2468	7.75	7.75	2
SPLLI	1.5	7.125	15	10.6875	39.5	3.94	6	0.406	3.8708	7.75	7.75	6
SPThickP	2.5	7.125	15	17.8125	39.5	3.94	3.94	0.406	3.03444	7.75	7.75	3.94
SPThinP	0.75	7.125	15	5.34375	39.5	3.94	3.94	0.406	3.03444	7.75	7.75	3.94
LPNP	1.5	5	21	7.5	39.5	3.94	3.94	0.406	3.03444	7.75	7.75	3.94
LPWP	1.5	9	21	13.5	39.5	3.94	3.94	0.406	3.03444	7.75	7.75	3.94
LPThickA	1.5	7.125	21	10.6875	39.5	3.94	3.94	0.75	5.3475	7.75	7.75	3.94
LPThickA1	1.5	7.125	21	10.6875	39.5	3.94	3.94	1	6.88	7.75	7.75	3.94

Table 29. FEM Model Dimensions Continued

Name	Plate Thickness	Plate Width	Plate Length	Plate Area	Angle Length	Outstanding Length	Inside Length	Angle Thickness	Angle Area	Front Weld Length	Back Weld Length	End Weld Length
LPSLO	1.5	7.125	21	10.6875	39.5	2	3.94	0.406	2.2468	7.75	7.75	3.94
LPLLO	1.5	7.125	21	10.6875	39.5	6	3.94	0.406	3.8708	7.75	7.75	3.94
LPSLI	1.5	7.125	21	10.6875	39.5	3.94	2	0.406	2.2468	7.75	7.75	2
LPLLI	1.5	7.125	21	10.6875	39.5	3.94	6	0.406	3.8708	7.75	7.75	6
LPThickP	2.5	7.125	21	17.8125	39.5	3.94	3.94	0.406	3.03444	7.75	7.75	3.94
LPThinP	0.75	7.125	21	5.34375	39.5	3.94	3.94	0.406	3.03444	7.75	7.75	3.94
LALLI	1.5	7.125	18.25	10.6875	50	3.94	6	0.406	3.8708	7.75	7.75	6
LALLO	1.5	7.125	18.25	10.6875	50	6	3.94	0.406	3.8708	7.75	7.75	3.94
LASLI	1.5	7.125	18.25	10.6875	50	3.94	2	0.406	2.2468	7.75	7.75	2
LASLO	1.5	7.125	18.25	10.6875	50	2	3.94	0.406	2.2468	7.75	7.75	3.94
LAThickA	1.5	7.125	18.25	10.6875	50	3.94	3.94	0.75	5.3475	7.75	7.75	3.94
LAThickA1	1.5	7.125	18.25	10.6875	50	3.94	3.94	1	6.88	7.75	7.75	3.94
LAThickP	2.5	7.125	18.25	17.8125	50	3.94	3.94	0.406	3.03444	7.75	7.75	3.94
LAThinP	0.75	7.125	18.25	5.34375	50	3.94	3.94	0.406	3.03444	7.75	7.75	3.94
Long Angle	1.5	7.125	18.25	10.6875	50	3.94	3.94	0.406	3.03444	7.75	7.75	3.94
SPLA	1.5	7.125	15	10.6875	50	3.94	3.94	0.406	3.03444	7.75	7.75	3.94
LPLA	1.5	7.125	21	10.6875	50	3.94	3.94	0.406	3.03444	7.75	7.75	3.94

Table 29. FEM Model Dimensions Continued

FINITE ELEMENT MODEL RESULTS

Name	Load	Nominal Stress	Front Stress	Back Stress	Max Stress	SCF
SALLI	10.69	2.76	11.32	11.43	11.43	4.14
SALLO	10.69	2.76	13.35	13.09	13.35	4.83
SASLI	10.69	4.76	20.06	19.47	20.06	4.22
SASLO	10.69	4.76	14.93	13.76	14.93	3.14
SAThickA	10.69	2.00	7.76	7.24	7.76	3.88
SAThickA1	10.69	1.55	5.90	5.62	5.90	3.80
SAThickP	17.81	5.87	20.76	20.04	20.76	3.54
SAThinP	5.34	1.76	7.40	7.11	7.40	4.20
Short Angle	10.69	3.52	14.66	14.30	14.66	4.16
SPSA	10.69	3.52	14.00	13.32	14.00	3.98
LPSA	10.69	3.52	15.01	14.34	15.01	4.26
F0B15.5	10.69	3.52	5.76	15.11	15.11	4.29
F0B15.5P	10.69	3.52	5.72	17.46	17.46	4.96
F2B13.5	10.69	3.52	5.99	14.46	14.46	4.11
F2B13.5P	10.69	3.52	6.18	16.15	16.15	4.59
F5B10.5	10.69	3.52	11.99	13.72	13.72	3.89
F5B10.5P	10.69	3.52	12.63	14.32	14.32	4.07
FW0	10.69	3.52	13.73	14.60	14.60	4.15
FW2	10.69	3.52	13.14	13.69	13.69	3.89
FW5	10.69	3.52	14.94	12.83	14.94	4.24

Table 30. FEM Results

Name	Load	Nominal Stress	Front Stress	Back Stress	Max Stress	SCF
LLILLO	10.69	2.27	10.52	10.30	10.52	4.63
LLISLO	10.69	3.47	10.92	10.20	10.92	3.15
LLIThickA	10.69	1.55	5.82	5.61	5.82	3.75
LLIThickA1	10.69	1.20	4.46	4.40	4.46	3.73
LLIThickP	17.81	5.87	15.87	15.14	15.87	2.70
LLOThickA	10.69	1.55	6.66	6.09	6.66	4.29
LLOThickA1	10.69	1.20	4.93	4.55	4.93	4.12
Long Leg Inside	10.69	2.76	11.47	10.95	11.47	4.15
Long Leg Inside 2.5	10.69	4.36	17.23	16.43	17.23	3.95
Long Leg Inside 3	10.69	4.03	15.93	15.20	15.93	3.95
Long Leg Inside 3.5	10.69	3.74	14.81	14.08	14.81	3.96
Long Leg Inside 5	10.69	3.08	11.44	12.01	12.01	3.89
Long Leg Inside 5.5	10.69	2.91	11.54	11.72	11.72	4.02
Long Leg Outstanding	10.69	2.76	13.04	13.06	13.06	4.73
Narrow Plate	7.50	2.47	10.13	9.29	10.13	4.10
Narrow Plate 6	9.00	2.97	11.95	11.20	11.95	4.03
Narrow Plate 8	12.00	3.95	15.47	14.68	15.47	3.91
Normal	10.69	3.52	14.05	13.45	14.05	3.99
Short Leg Inside	10.69	4.76	19.06	18.25	19.06	4.01
Short Leg Outstanding	10.69	4.76	13.71	12.56	13.71	2.88

Table 30. FEM Results Continued

Name	Load	Nominal Stress	Front Stress	Back Stress	Max Stress	SCF
SLILLO	10.69	3.47	16.63	17.62	17.62	5.08
SLISLO	10.69	7.32	18.05	16.65	18.05	2.46
SLIThickA	10.69	2.75	10.41	9.90	10.41	3.79
SLIThickA1	10.69	2.16	8.06	7.88	8.06	3.73
SLOThickA	10.69	2.75	7.88	6.99	7.88	2.87
SLOThickA1	10.69	2.16	6.49	6.01	6.49	3.00
Thick Angle	10.69	2.00	7.52	6.80	7.52	3.76
Thick Angle 1	10.69	1.55	5.74	5.31	5.74	3.70
Thick Plate	17.81	5.87	18.74	18.71	18.74	3.19
ThickPLLI	17.81	4.60	15.87	15.14	15.87	3.45
ThickPLLO	17.81	4.60	19.05	19.37	19.37	4.21
ThickPSLI	17.81	7.93	23.21	24.49	24.49	3.09
ThickPSLO	17.81	7.93	18.91	17.69	18.91	2.39
ThickPThickA	17.81	3.33	10.33	9.37	10.33	3.10
ThickPThickA1	17.81	2.59	8.04	7.23	8.04	3.11
Thin Plate	5.34	1.76	7.51	7.10	7.51	4.26
ThinPLLI	5.34	1.38	6.55	5.30	6.55	4.75
ThinPLLO	5.34	1.38	6.44	5.12	6.44	4.66
ThinPSLI	5.34	2.38	9.88	8.81	9.88	4.16
ThinPSLO	5.34	2.38	10.43	8.81	10.43	4.38
ThinPThickA	5.34	1.00	3.89	3.25	3.89	3.89
ThinPThickA1	5.34	0.78	2.81	2.61	2.81	3.62
Wide Plate	13.50	4.45	16.99	16.23	16.99	3.82
Short Plate	10.69	3.52	13.18	12.40	13.18	3.74
Long Plate	10.69	3.52	14.43	13.50	14.43	4.10

Table 30. FEM Results Continued

Name	Load	Nominal Stress	Front Stress	Back Stress	Max Stress	SCF
SPNP	7.50	2.47	9.57	8.82	9.57	3.87
SPWP	13.50	4.45	16.01	15.34	16.01	3.60
SPThickA	10.69	2.00	6.33	5.68	6.33	3.17
SPThickA1	10.69	1.55	5.51	5.04	5.51	3.55
SPSLO	10.69	4.76	12.79	11.66	12.79	2.69
SPLLO	10.69	2.76	12.62	12.50	12.62	4.57
SPSLI	10.69	4.76	17.63	17.22	17.63	3.71
SPLLI	10.69	2.76	10.80	10.30	10.80	3.91
SPThickP	17.81	5.87	17.61	17.52	17.61	3.00
SPThinP	5.34	1.76	7.57	5.96	7.57	4.30
LPNP	7.50	2.47	10.36	9.59	10.36	4.19
LPWP	13.50	4.45	17.61	16.74	17.61	3.96
LPThickA	10.69	2.00	6.78	6.17	6.78	3.39
LPThickA1	10.69	1.55	5.86	5.47	5.86	3.78

Table 30. FEM Results Continued

Name	Load	Nominal Stress	Front Stress	Back Stress	Max Stress	SCF
LPSLO	10.69	4.76	14.47	13.03	14.47	3.04
LPLLO	10.69	2.76	13.34	13.08	13.34	4.83
LPSLI	10.69	4.76	19.47	18.95	19.47	4.09
LPLLI	10.69	2.76	11.59	11.24	11.59	4.20
LPThickP	17.81	5.87	19.76	19.14	19.76	3.37
LPThinP	5.34	1.76	7.62	5.96	7.62	4.33
LALLI	10.69	2.76	10.66	10.16	10.66	3.86
LALLO	10.69	2.76	12.53	12.39	12.53	4.54
LASLI	10.69	4.76	17.18	17.01	17.18	3.61
LASLO	10.69	4.76	12.18	10.85	12.18	2.56
LAThickA	10.69	2.00	7.28	6.46	7.28	3.64
LAThickA1	10.69	1.55	5.62	5.00	5.62	3.62
LAThickP	17.81	5.87	17.54	17.67	17.67	3.01
LAThinP	5.34	1.76	7.61	5.97	7.61	4.32
Long Angle	10.69	3.52	13.34	12.73	13.34	3.79
SPLA	10.69	3.52	12.52	11.87	12.52	3.56
LPLA	10.69	3.52	13.92	13.02	13.92	3.95

Table 30. FEM Results Continued

References

AASHTO. (2007). Bridge Design and Specification. *4th*. Washington, D.C.

AASHTO/NSBA. (2006). Guidelines for Design Details. Washington, D.C.: AASHTO.

ABAQUS/Explicit User's Manual. (2002). Hibbit, Karlsson, & Sorenson.

American Institute of Steel Construction. (2005). *Steel Construction Manual.*

American Society of Mechanical Engineers. (2007). API 579 Fitness for Service. *2nd*. Washington, D.C.: API Publishing Services.

Cheplak, B. A. (2001). *Field Measurements of Intermediate External Diaphragms on a Trapezoidal Steel Box Girder Bridge.* Austin: University of Texas at Austin.

Dong, P. (2001). A structural stress definition and numerical implementation for. *International Journal of Fatigue* , 12.

Douglas C. Montgomery, George C. Runger, Norma Faris Hubele. (2004). *Engineering Statistics.* New York: John Wiley & Sons Inc.

Duraisamy, R. (2005, December). Finite Element Study of Mast Arm Socket Welded Connections. University of Texas at Austin.

Grubb, M. A., Corven, J. A., Wilson, K. E., Bouscher, J. W., & Volle, L. E. (2007). Load and Resistance Factor Design (LRFD) for Highway Bridge Superstructures – Design Manual. *2* . Arlington, VA: Federal Highway Administration National Highway Institute.

Helwig, T. A., Wang, L., Deaver, J., & Romero, C. *Cross-Frame and Diaphragm Behavior in Bridges with Skewed Supports: Summary.* TxDOT.

Helwig, T. (2006). Bracing Systems for Straight and Curved Steel Bridge Girders. *CTR Symposium "Navigating Costs"*, (p. 41).

Kang, H. T., Dong, P., & Hong, J. (2006). Fatigue analysis of spot welds using a mesh insensitive structural. *International Journal of Fatigue* , 8.

Koenigs, M. T. (2003, May). Fatigue Resistance of Traffic Signal Mast-Arm Connection Details. University of Texas at Austin.

Mertz, D. R. (2001). Designers' Guide to Cross-Frame Diaphragms. American Iron and Steel Institute.

Munse, W. H. (1964). *Fatigue of Welded Steel Structures.* New York: Welding Research Council.

Ocel, J. M. (2006, October). The behavior of thin hollow structural section (HSS) to plate connections. University of Minnesota.

Segui, W. T. (2007). *Steel Design.* Toronto: Thompson.
TxDOT. (2007). Preferred Practices for Steel Bridge Deign, Fabrication, and Erection.
UEG. (1985). *Design of Tubular Joints for Offshore Structures* (Vol. 2). Norwich: UEG.
Warpinski, M. (2006, May). The Effect of Base Connection Geometry on the Fatigue Performance of Welded Socket Connections in Multi-sided High-mast Lighting Towers. Lehigh University.

Wilbur M. Wilson, Walter H. Bruckner, John E. Duberg, Howard C. Beede. (1944). Fatigue Strength of Fillet-Weld and Plug-Weld Connections in Steel Structural Members. *University of Illinois Bulletin , 41* (30).

Wilbur M. Wilson, William H. Munse, Walter H. Bruckner. (1949). Fatigue Strength of Fillet-Weld, Plug-Weld, and Slot-Weld Joints Connecting Steel Structural Members. *University of Illinois Bulletin , 46* (68).